Role of tetraspanin 15 in metabotropic glutamate receptor 5 signaling and extracellular vesicles docking at neurons from *mus musculus domesticus*

Submitted by

Daniele Stajano

Dissertation submitted to the University of Hamburg

To achieve a doctoral degree at the Faculty of
Mathematics, Informatics, and Natural Sciences. Department of Chemistry
of the University of Hamburg

Hamburg, Germany
1st September 2023

The present investigation was carried out in the research unit of Molecular Neurogenetics, led by Prof. Dr. Matthias Kneussel, in the Center of Molecular Neurobiology of Hamburg (ZMNH) at the Universitätsklinikum Hamburg-Eppendorf (UKE) (Hamburg, Germany), starting in April 2019.

dSTORM imaging was performed at the Bordeaux Neurocampus (Bordeaux, France) at the Institute for Interdisciplinary Neuroscience and the Bordeaux Imaging Center, led by Prof. Dr. Daniel Choquet.

Thesis Reviewers:

Prof. Dr. Matthias Kneussel

Prof. Dr. Wolfram Brune

Oral defense committee:

Prof. Dr. Wolfram Brune

Prof. Dr. Kay Grünewald

Priv.-Doz. Sabine Hoffmeister-Ullerich

Oral Dissertation: 1st September 2023

“Man cannot remake himself without suffering,

for he is both the marble and the sculptor”

Alexis Carrel

French biologist and surgeon, Nobel Prize in Physiology or Medicine 1912

List of publication

(Gromova et al., 2023. Accepted by Cell Reports)
"The kinesin Kif21b binds MyosinVa and mediates unconventional changes in actin dynamics underlying homeostatic synaptic downscaling. "
Kira V. Gromova, Edda Thies, Philipp C. Janiesch, Felix P. Lützenkirchen, Yipeng Zhu, Daniele Stajano, Céline D. Dürst, Michaela Schweizer, Anja Konietzny, Marina Mikhaylova, Christine E. Gee, Matthias Kneussel

(Stajano et al., 2023. Accepted by Journal of Extracellular Biology)
"**Tetraspanin 15 Depletion impairs Extracellular Vesicle Docking at Target Neurons"**
Daniele Stajano, Franco L. Lombino, Michaela Schweizer, Markus Glatzel, Paul Saftig, Kira V. Gromova, Matthias Kneussel

Table of content

List of Figures

List of Tables

List of abbreviations

2R,4R-APDC	2R,4R-4-Aminopyrrolidine-2,4-Dicarboxylate
3,5-DHPG	Dihydroxyphenylglycine
AA	Amino Acid
AAV	Adeno-Associated Virus
AC	Adenylate Cyclase
ACSF	Artificial Cerebrospinal Fluid
ADAM	A Disintegrin And Metalloprotease
AMPA	A-Amino-3-Hydroxy-A-Amino-3-Hydroxy-5-Methyl-4-Isoxazolepropionic Acid
AP4	Adaptor Protein Complex
APP	Amyloid Precursor Protein
Arc	Activity-Regulated Cytoskeleton-Associated Protein
ASD	Autistic Spectrum Disorder
BSA	Bovine Serum Albumine
CA	Cornu Ammonis
Ca2+	Calcium
CamKII	Ca2+/Calmodulin-Dependent Protein Kinase Ii
CD	Cluster Of Differentiation
CM	Conditioned Media
CNS	Central Nervous System
C-Terminus	Carboxyl-Terminus
DAB	3, 3'-Diaminobenzidine
DAG	Diacylglycerol
DAPI	4′ ,6-Diamidino-2-Phenylindole

DIV	Day In Vitro
DMEM	Delbucco´S Minimal Essential Medium
DNA	Deoxyribonucleic Acid
EEA1	Early Endosome Accociated Protein 1
EGTA	Ethylene Glycol-Bis (B-Aminoethyl Ether)-N, N, N′, N ′ - Tetraacetic Acid
ER	Endoplasmatic Reticulum
ERC	Endocytic Recycling Compartment
ERGIC	ER-Golgi Intermediate Compartment
ERKs	Extracellular Signal-Regulated Kinases
ESCRT	Endosomal Sorting Complexes Required For Transport Components
EtOH	Ethanol
EV	Extracellular Vesicles
FasL	Fas Ligand
FXS	Fragile X Syndrome
GA	Glutaraldehyde
GFP	Green Fluorescent Protein
GluA2	Glutamate Ionotropic Receptor Ampa Type Subunit 2
GM	Gangliosides
GPCR	G-Protein Coupled Receptor
GRK	G Protein-Coupled Receptor Kinase
GTP	Guanosine Triphosphate
HBSS	Hanks' Balanced Salt Solution
HRP	Horseradish Peroxidase

Hsc	Heat Shock Cognate
Hsp	Heat Shock Proteins
HSP	Heat-Shock Proteins
Ig	Immunoglobuline
iGluR	Ionotropic Receptors For The Glutamate
IP3	Inositol 1,4,5-Triphosphate
KAR	Kainic Acid Receptors
KO	Knock-Out
L-AP4	L-2-Amino-4-Phosphonobutyric Acid
LEL	Small Extracellular Loop
lncRNA	Long Non-Coding Rna
LTD	Long-Term Depression
LTP	Long-Term Potentiation
MeOH	Methanol
mGluR	Metabotropic Glutamate Receptor
MHC	Major Histocompatibility Complex
miRNA	Microrna
mRNA	Messenger Rna
MVB	Multivesicular Bodies
NMDAR	N-Methyl-D-Aspartate Receptor
NTA	Nano Tracking Analyisis
N-terminus	Amino-Terminus
p38 MAPK	P38 Mitogen-Activated Protein Kinase
PBS	Phosphate Buffer Saline
PC	Phosphatidylcholine

PCR	Polymerase Chain Reaction
PDVF	Polyvinylidene Difluoride
PE	Phosphatidylethanolamine
PFA	Paraformaldehyde
PI	Phosphatidylinositol
PI3K	Phosphoinositide 3-Kinase
PICK1	Protein-Interacting-With-C-Kinase-1
PIP2	Phosphatidylinositol 4,5-Bisphosphate
PKA	Protein Kinase A
PKC	Protein Kinase A
PLC	Phospholipase C
PNGM	Primary Neuron Growth Medium
PNS	Peripheral Nervous System
PP2A	Protein Phosphatase A
PP2B	Protein Phosphatase A
P/S	Penicillin/ Streptomycin
PS	Phosphatidylserine
PSD	Post-Synaptic Density
PTP	Protein Tyrosine Phosphatases
Rab GTPase	Ras-Related In Brain Gtpase
RBP	Ribosomal-Binding Proteins
RNA	Ribonucleic Acid
S.E.M.	Standard Error Of The Mean
S.O.C.	Super Optimal Broth
S1PR2	Sphingosine-1-Phosphate-Receptor-2

sAPPα	Soluble Amyloid Precursor Protein Alpha
SDS-PAGE	Sodium Dodecyl Sulphate - Polyacrylamide Gel Electrophoresis
SEL	Small Extracellular Loop
Ser	Serine
Shank	Sh3 And Multiple Ankyrin Repeat Domains
SN	Substantia Nigra
STEP	Striatal-Enriched Protein Phosphatase
Syn	Synapsin
TALEN	Transcription Activator-Like Effector Nucleases
TBS-T	Tris-Buffered Saline Supplied With Tween
TEM	Tetraspanin-Enriched Microdomains
TfR	Transferrin Receptor
TGF	Transforming Growth Factor
TNF	Tumor Necrosis Factor
TRAIL	TNF-Related Apoptosis-Inducing Ligand
TSG	Tumor Suspectibility Gene
TSG101	Tumor Susceptibility Gene 101
Tspan	Tetraspanin
UV	Ultraviolet
VTA	Ventral Tegmented Area
WB	Western Blot
WT	Wild-Type

German Abstract

Tetraspanine sind kleine Transmembranproteine, die auf biologischen Membranen Tetraspanin-angereicherte Mikrodomänen (TEMs) bilden und als molekulare Vermittler funktioneller Proteinkomplexe fungieren, die am synaptischen Rezeptortransport und an der Dynamik extrazellulärer Vesikel beteiligt sind. Tetraspanin 15 (Tspan15) ist im Gehirn angereichert und spielt als Regulator der ADAM10-Proteaseaktivität eine wesentliche Rolle in Hippocampus-Neuronen. Aktuelle Arbeiten zeigen, dass Tspan15 an der synapsen- und extrazellulären Vesikel-vermittelten interzellulären Kommunikation beteiligt ist. Bildgebende Verfahren in lebenden Zellen, Immunzytochemie und biochemische Tests weisen darauf hin, dass Tspan15 mit dem metabotropen Glutamatrezeptor 5 (mGLuR5) interagiert, der eine wesentliche Rolle bei der synaptischen Plastizität und der Modulation des Sozialverhaltens spielt. Das Fehlen der Tspan15-Expression korreliert mit einer abnormalen Invasion und Akkumulation von mGLuR5 in der postsynaptischen Dichte. Darüber hinaus bleiben in Tspan15-KO-Neuronen die mGluR5-Oberflächenspiegel nach Behandlung mit DHPG-Agonisten unverändert, und Tspan15-KO-Mäuse sind nicht in der Lage, eine mGLuR5-abhängige Langzeitdepression (LTD) aufrechtzuerhalten. CA1-Pyramidalneuronen zeigen morphologische Anomalien an den apikalen Dendriten und der dendritischen Stacheldichte. Schließlich zeigen Verhaltensdaten, dass Tspan15-KO-Mäuse im Vergleich zu WT-Kontrollmäusen einen dominanteren und aggressiveren Phänotyp zeigen. Insgesamt deuten unsere Daten darauf hin, dass die Ablation von Tspan15 mit einer mGluR5-Invasion in die PSD sowie mit mGluR5-vermittelten elektrophysiologischen, morphologischen und Verhaltensanomalien korreliert und einen Phänotyp nachahmt, der dem bei neurologischen Störungen wie dem Fragilen-X-Syndrom ähnelt. In einem parallelen Projekt wurde die durch extrazelluläre Vesikel (EV) vermittelte Kommunikation zwischen Neuronen untersucht. Obwohl EVs einen potenziellen Träger darstellen, der in der Diagnostik und/oder Therapie genutzt werden kann, sind die Mechanismen, die die Interaktion zwischen EVs und Zielzellen beeinflussen, noch nicht vollständig geklärt. Insbesondere kann die Aufnahme von EVs das Überleben und die Aktivität von Neuronen beeinflussen, und es wird vermutet, dass EVs an der Entwicklung

neurodegenerativer Erkrankungen beteiligt sind. Mehrere Tetraspanine wurden als EV-ansässige Proteine identifiziert; das Vorhandensein und die Rolle von Tspan15 in der EV-vermittelten Kommunikation zwischen Neuronen sind jedoch noch unklar. Aktuelle Daten zeigen, dass Tspan15 auf kortikalen EVs exprimiert wird. Außerdem trägt Tspan15, wenn es in Spenderzellen und EVs exprimiert wird, zur EV-vermittelten Kommunikation zwischen kortikalen Neuronen bei, indem es den Kontakt zwischen kortikalen EVs und Zielneuronen erleichtert.

Abstract

Tetraspanins are small transmembrane proteins that form tetraspanin-enriched microdomains (TEMs) on biological membranes and act as molecular facilitators of functional protein complexes involved in synaptic receptor trafficking and extracellular vesicle dynamics. Tetraspanin 15 (Tspan15), is enriched in the brain and plays an essential role in hippocampal neurons as the regulator of ADAM10 protease activity. Current work demonstrates that Tspan15 is involved in synapse- and extracellular vesicle-mediated intercellular communication. Live cell imaging, immunocytochemistry and biochemical assays indicate that Tspan15 interacts with metabotropic glutamate receptor 5 (mGLuR5), which plays an essential role in synaptic plasticity and modulation of social behavior. Lack of Tspan15 expression correlates with mGLuR5 abnormal invasion and accumulation in the postsynaptic density. In addition, in Tspan15 KO neurons mGluR5 surface levels remain unaltered after treatment with DHPG agonist and Tspan15 KO mice are not able to sustain mGLuR5-dependent long-term depression (LTD). CA1 pyramidal neurons present morphological abnormalities at the apical dendrites and the dendritic spine density. Finally, behavioral data demonstrate that Tspan15 KO mice express a more dominant and aggressive phenotype compared to the WT control. Altogether our data suggest that the ablation of Tspan15 correlates with mGluR5 invasion of the PSD, mGluR5-mediated electrophysiological, morphological and behavioral abnormalities, mimicking a phenotype similar to the one found in neurological disorders, such as the Fragile X Syndrome.

Extracellular vesicle (EV)-mediated communication among neurons has been investigated in a parallel project. Although EVs represent a potential carrier to be exploited in diagnostics and/or therapeutics, the mechanisms modulating EV-target cell interaction are yet to be fully elucidated. In particular, EV uptake can affect neuronal survival and activity, and EVs are thought to participate in the development of neurodegenerative pathologies. Several tetraspanins have been identified as EV-resident proteins; however, the presence and the role of Tspan15 in EV-mediated communication among neurons are still unclear. Current data demonstrate that Tspan15 is expressed on cortical EVs. Furthermore, when expressed in donor cells

and EVs, Tspan15 contributes to EV-mediated communication among cortical neurons by facilitating the contact between cortical EVs and target neurons.

1 Introduction

1.1 The Central Nervous System

The nervous system can be subdivided into the Central nervous system (CNS), represented by the encephalon and the spinal cord, and the Peripheral Nervous System (PNS), formed by the nerves and ganglia residing outside the CNS. The main computational element of the CNS is represented by neurons, which are structurally and metabolically supported by glial cells. Neurons are electrically excitable cells, highly specialized in cellular communication, and can receive, integrate and transmit information in the form of cellular signals. In general conditions, neuronal cells present a cell body (soma) from which multiple dendrites and an axon can depart, respectively receiving and transmitting the information. (Bruce Alberts, 2002)

1.2 Intercellular Communication

Cellular communication can be divided into intracellular (within the same cell) and intercellular signaling (mediated by external elements). The latter can be subdivided into (i) paracrine, where ligands cover a small distance to interact with their receptor (e.g. chemical synapses); (ii) autocrine, when a cell releases a biological element that can contact and interact with the same cell (e.g. cytokines); (iii) endocrine, when a ligand is released in low concentrations and can cover long distances until it targets a recipient cell (e.g. hormones, extracellular vesicles); (iv) cell-to-cell signaling, occurring via physical contact between cells (e.g. electrical synapses).

1.3 Synaptic Transmission

Synaptic transmission can be defined as the propagation of information between two neurons through specialized structures called synapses (from the Greek words “syn” together and “haptein” to clasp). Synapses can be electrical, when a structural continuity between the two cells allows the direct flow of electrically charged particles called ions. However, in vertebrates, chemical synapses represent the most diffused class of synapses. These present a synaptic cleft, a 20-30 nanometer (nm)

extracellular space, dividing the transmitting axon of the pre-synaptic cell from the receiving dendrite of post-synaptic neurons. (Dale Purves, 2001)

1.4 Chemical synaptic transmission

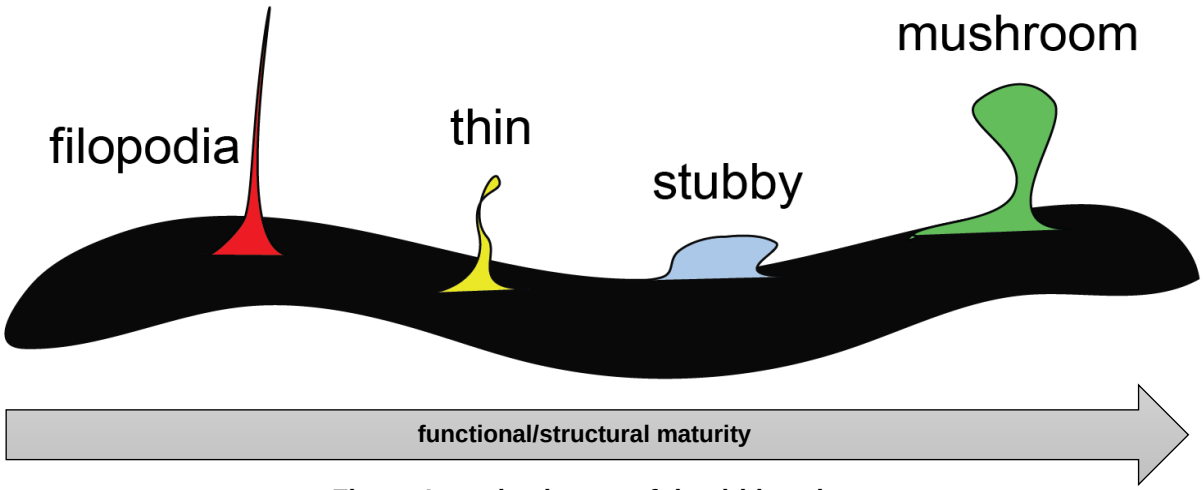

Figure 1 - main classes of dendritic spines

Schematic from D. Stajano, showing different morphological protusion present on a neuronal dendrite (black), such as immature structures like filopodia-like protusions (red), thin (yellow) and stubby (blue) spines or mature mushroom (green) spines.

Chemical synaptic transmission occurs when an increase of the Calcium ion(Ca^{2+}) at the pre-synaptic compartment triggers the exocytosis of synaptic vesicles loaded with chemical messengers, namely neurotransmitters, and the consequent release of these in the synaptic cleft in a high concentration. Eventually, the neurotransmitter ligands contact synaptic receptors at the postsynaptic neurons and can trigger a conformational change in these, activating them. Synaptic receptors can be divided into ionotropic (ligand-gated ion channels) and metabotropic (G protein-coupled or tyrosin kinase) receptors according to their structure and transduction signaling downstream pathway. The synaptic transmission ends with the clearance of the neurotransmitter from the synaptic cleft, undergoing degradation or uptake from the pre-synaptic neuron and/or glial cells surrounding the synapse.

Activation of ionotropic receptors at the post-synapse leads to a change in the influx and/or exit of ions from the cell. The alteration of their local concentration represents a

change in the transmembrane potential. Hence, the difference in voltage takes the name of post-synaptic potential. A current provoking the reduction of the transmembrane potential (depolarization) has an excitatory effect. Conversely, hyperpolarizing currents result in an inhibition of the post-synaptic neuron.

In addition, metabotropic receptor activation by neurotransmitter binding can trigger downstream molecular pathways and indirectly lead to a modulation of ion channel opening. Also, this mechanism can alter the post-synaptic transmembrane potential.

1.5 The excitatory post-synaptic compartment

The most common localization for post-synaptic compartments at excitatory synapses is represented by dendritic spines, i.e., dendritic branched protrusions that provide a highly specialized structure for fine-tuned and localized signaling among neurons. Dendritic spines are characterized by a “neck,” proximal to the dendritic body, and a “head”, in which the post-synaptic compartment resides. Different classes can be distinguished according to the spine head diameter and the spine length (Figure 1) and from their different functions and properties.

Thin spines are characterized by a narrow neck and tiny head. They are associated with the development of new synapses or changes in synaptic strength andthey are considered highly dynamic. Conversely, mushroom spines are shorter and present a wider head. They are more stable and play a role in the preservation of long-term memory. Stubby spines are defined by the absence of a neck and a wide head; their density is relatively low in physiological conditions and are considered to participate in the modulation of synaptic strength. Filopodia are thin and long protrusions without a head, usually involved in the initial steps of synaptogenesis. (Holtmaat & Svoboda, 2009; Risher et al., 2014). Several types of proteins can be found in the post-synaptic compartment in a very complex and dynamic level of organization. Multiple scaffold proteins, such as PSD-95, Shank, and Homer, assemble to structurally support the other components of the post-synapse. The latter includes synaptic receptors (see “Glutamate receptors paragraph”) and signaling molecules, such as protein kinase A (PKA) and C (PKC) and Ca2+/calmodulin-dependent protein kinase II (CamKII), that

modulate the signal transduction, vesicle trafficking, chemotactic activity, and cell polarity. In addition, the main structural components are represented by actin filaments, which can be reorganized in an activity-dependent manner and therefore influence the shape of the dendritic spine (Figure 2) (Eric R. Kandel, 2012; Holtmaat & Svoboda, 2009)

1.6 Synaptic Plasticity

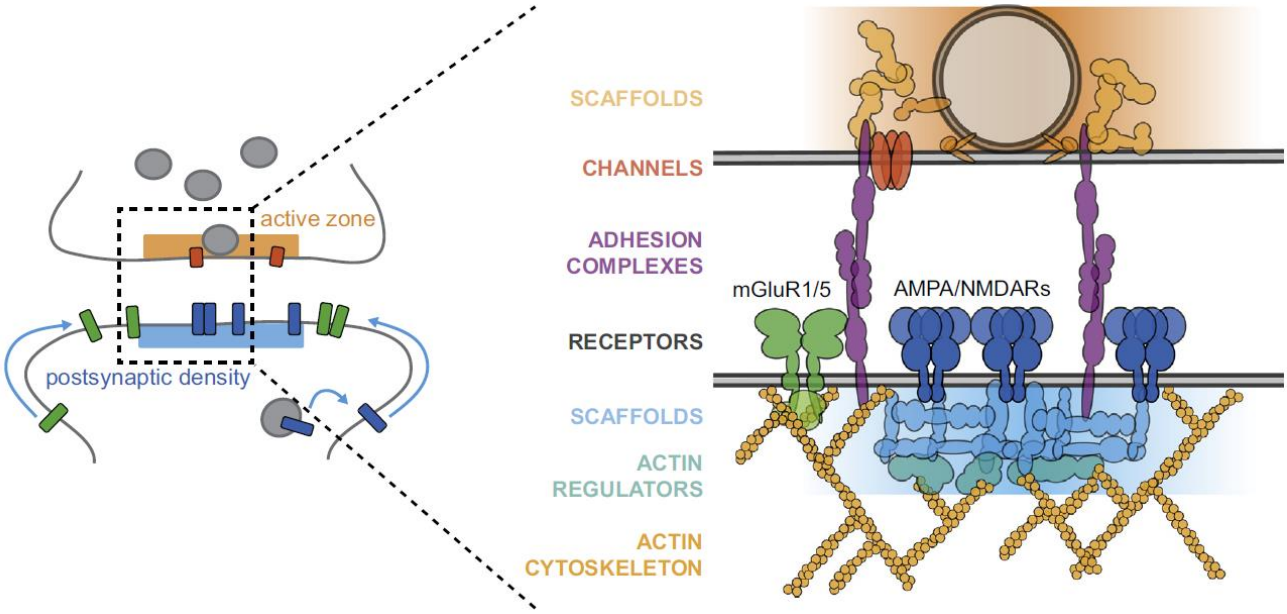

Figure 2 - excitatory chemical synapse

Left: overview of an excitatory chemical synapse with a presynaptic axonal terminal (top) and a postsynaptic dendritic spine head (bottom) divided by the synaptic cleft space. Right: inset from the black dotted box; mGluR: metabotropic Glutamate receptors; AMPA/NMDAR: ionotropic glutamate receptors; Adapted from (Scheefhals & MacGillavry, 2018).

The ability of chemical synaptic connections to modulate their strength represents a mechanism leading to the so-called synaptic plasticity. When these synaptic changes last in the range of hours and days they take the name of long-term plasticity. While the strength of synaptic connection takes the name of Long-Term Potentiation (LTP), the weakening is referred to as Long-Term Depression (LTD).

At the molecular level, neuronal activity can modulate the biochemical status and the interaction among proteins, triggering changes in the cytoskeleton and the synthesis of new proteins. At dendritic spines, the reorganization of the actin cytoskeleton and translational activity leads to the remodeling of the spine structure, with a potential

volume decrease in the LTD and increase in LTP events. Several neurological pathologies, such as Autistic Spectrum Disorder (ASD) or Fragile X Syndrome (FXS), are linked to dysregulations in the synthesis of new protein and in long-term synaptic plasticity and consequently to altered dendritic spine morphology. (Aloisi et al., 2017).

1.7 Glutamate Receptors

The divalent anion of glutamic acid is known as glutamate. In general conditions, this molecule acts as the main excitatory neurotransmitter at the CNS and can bind different types of receptors at the post-synapse. α-Amino-3-hydroxy-α-amino-3-hydroxy-5-methyl-4-isoxazolepropionic acid receptors (AMPA), N-methyl-D-aspartate receptors (NMDAR), and kainic acid receptors (KARs) represent three different classes of ionotropic receptors for the glutamate (iGluRs).

1.8 The mGluR family

The metabotropic receptor for glutamate (mGluR) family is composed of G-protein coupled receptors (GPCRs) subdivided into three groups according to the synaptic localization, second messenger, pharmacological properties, and sequence [Figure 3].

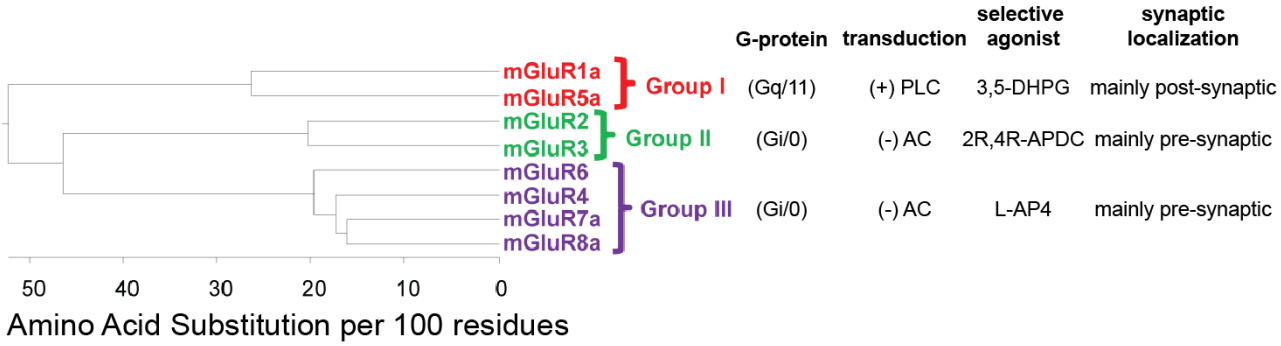

Figure 3 - Human mGluR family

Overview of metabotropic glutamate receptor (mGluR) family. Homology distance was calculated by alignment of amino acid sequences. (+): promotion. (-): inhibition. PLC: Phospholipase C; AC: Adenylate Cyclase; 3,5-DHPG: Dihydroxyphenylglycine; 2R,4R-APDC: 2R,4R-4-Aminopyrrolidine-2,4-dicarboxylate; L-AP4: L-2-amino-4-phosphonobutyric acid. Adapted from (Willard & Koochekpour, 2013) and (Conn & Pin, 1997)

1.9 Glutamatergic receptor post-synaptic localization

Recent studies have investigated the nanoscale localization of glutamatergic receptors at the post-synaptic compartment of excitatory synapses, taking advantage of super-resolution microscopy techniques. At the surface of the dendritic spine head, ionotropic AMPA and NMDA receptors are mainly clustered in the core of the post-synaptic density (PSD), in front of the synaptic active zone. In contrast, post-synaptic mGluRs are predominantly confined at the periphery of the PSD, in the so-called perisynaptic space, assuming a non-clustered distribution (Figure 5) (Goncalves et al., 2020; Scheefhals & MacGillavry, 2018). Depletion of mGluR5 from the perisynaptic space

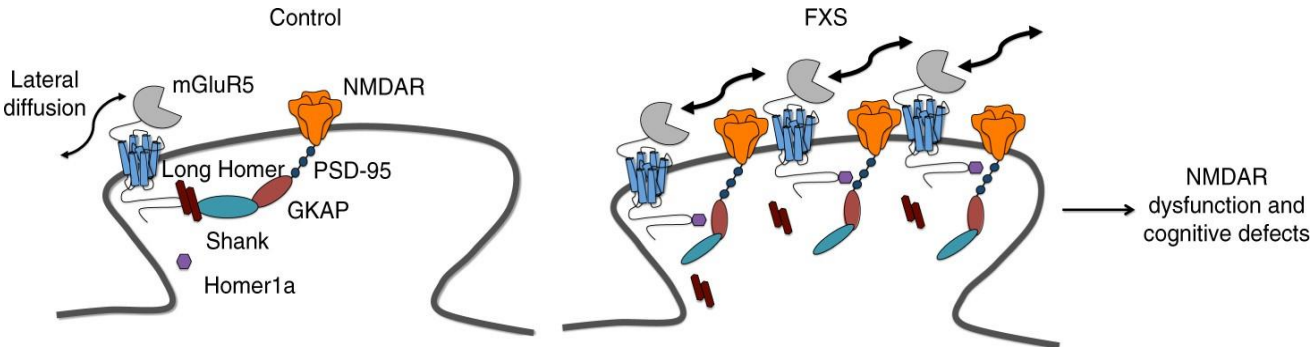

Figure 5 - post-synaptic compartment in control and FXS dendritic spines

In physiological conditions mGluR5 is in direct interaction with Homer, and preferentially with the long isoforms of this scaffold protein. The latter are promoting both the anchoring of mGluR5 at the perisynaptic space and the coupling with post-synaptic density by binding with Shank proteins. In Fragile X Syndrome (FXS) mGluR5 binding with -Long Homer is disrupted and mGluR5 is redirected to the short Homer1a isoform, therefore leading by passive diffusion in the membrane to the invasion of the PSD and abnormal clustering with NMDARs. (Aloisi et al., 2017)

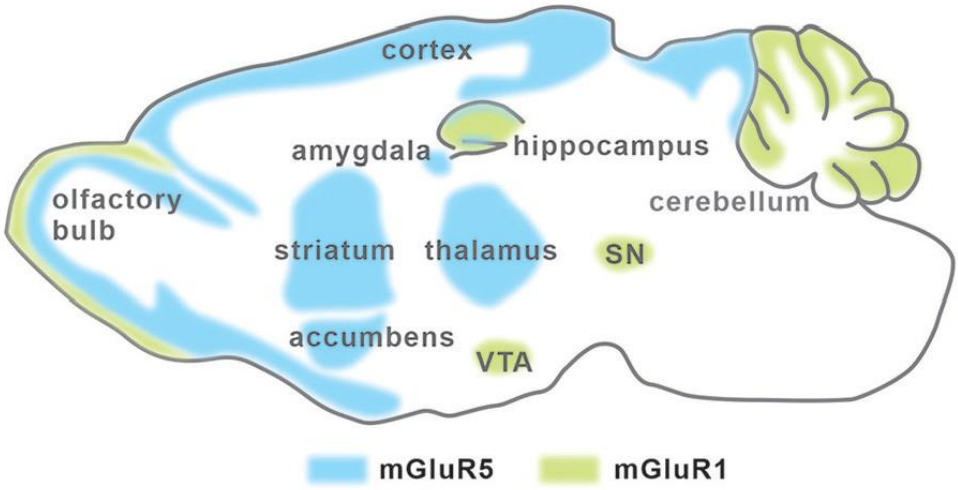

Figure 4 - Group 1 mGluR expression in the brain

Schematic of sagittal section of mouse brain. Blue: mGluR5 Green: mGluR1 VTA: Ventral Tegmented Area; SN: Substantia Nigra.(Su et al., 2022)

and/or invasion of the PSD core region have been observed in neurological disorders, such Rett´s Syndrome (Dani et al., 2005) and Fragile X Syndrome (Aloisi et al., 2017) (Figure 5), which are linked to synaptic plasticity abnormalities.

1.10 Group I mGluR brain expression

Although mGluR1 and mGluR5 are in part co-expressed at the olfactory bulb, in general, they present a complementary pattern of expression in the brain: mGluR1

expression has been observed at the Ventral Tegmented Area (VTA), the substantia nigra and the cerebellum. Conversely, mGluR5 expression can be detected also in the cerebral cortex, amygdala, striatum, nucleus accumbens, and thalamus (Su et al., 2022) (Figure 4). Interestingly, both receptors can be found at the hippocampal formation; However, while mGluR5 is enriched in the CA1 and CA3 region, mGluR1 is highly expressed only in the CA3 (Bordi & Ugolini, 1999).

1.11 Group I mGluR molecular pathway

Group I mGluRs (GluR1 and mGluR5) couples with Gαq protein, which leads to the activation of the Phospholipase C enzyme at the plasma membrane and the following

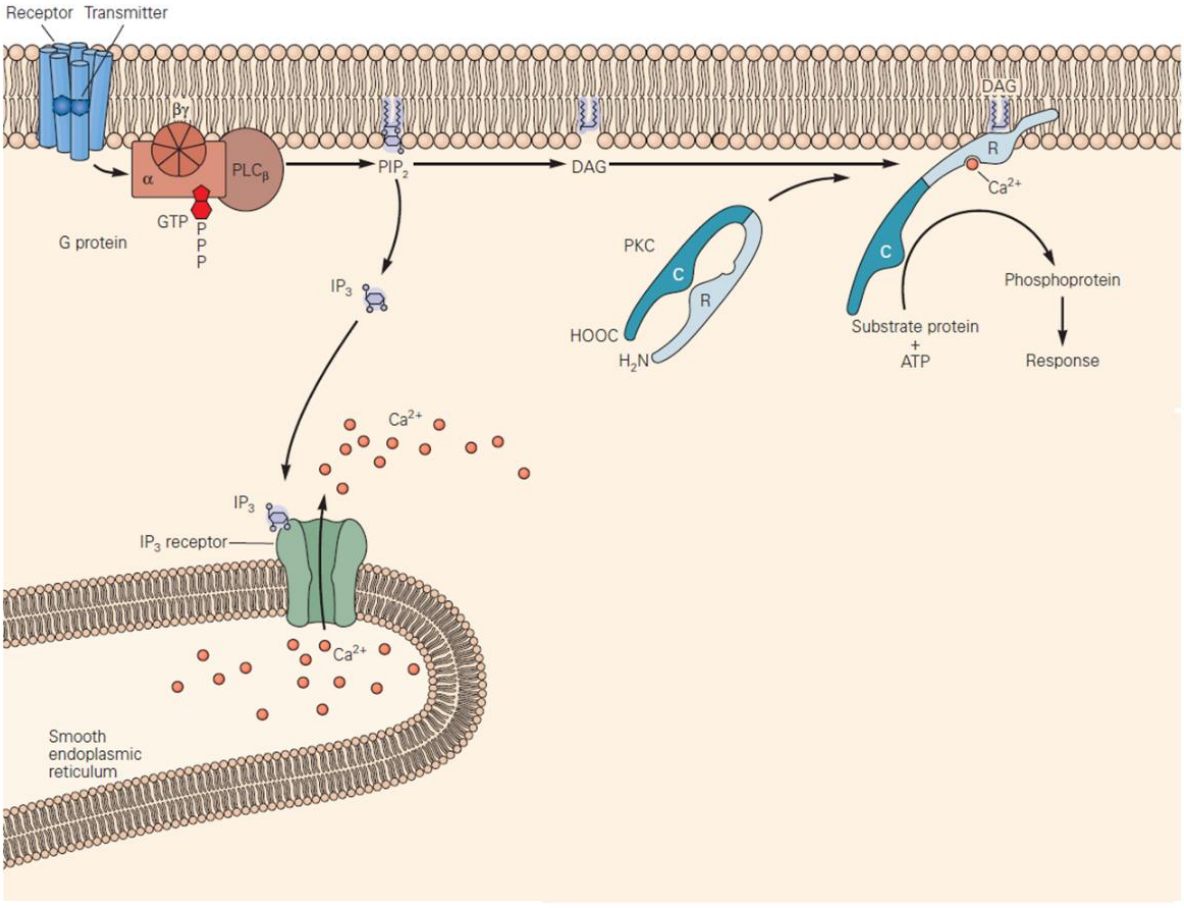

Figure 6 - GPCR activation of PKC

Acrivation of GPCR (G-protein coupled receptor) coupled with Gq/11 protein leads to the PLCß lysis of Phosphatidylinositol 4,5-bisphosphate (PIP_2) in inositol 1,4,5-triphosphate (IP3) and diacylglycerol (DAG).
Consequently, released Ca^{2+} from the endoplasmatic reticulum promotes the activation of protein kinase C, recruited at the plasma membrane by DAG, enventually leading to the downstream transduction of the signal through phosphorylation of secondary messengers. Adapted from (Eric R. Kandel, 2012).

formation of diacylglycerol (DAG) and inositol 1,4,5-triphosphate (IP3) from the lysis of Phosphatidylinositol 4,5-bisphosphate (PIP2). (Conn & Pin, 1997) (Figure 6). IP3 represents a ligand for the IP3 receptor, able to open the Ca^{2+}-permeable ion channels at the Endoplasmatic Reticulum (ER) and trigger an increase in Calcium concentration in the cytosol. Calcium can bind to the regulatory subunit of Protein Kinase C (PKC) and stop the auto-inhibition of the catalytic subunit. Overall, simultaneous Calcium and DAG binding leads to the PKC activation and stabilization at the plasma membrane and the phosphorylation of downstream effectors.

As a long-term effect, this can trigger the activation of transcription factors and the following change in transcriptional activity in the cell. In addition, activation of Group I mGluRs can therefore promote the Ser-880 phosphorylation of GluA2 AMPAR subunit via the PKC pathway and eventually their internalization from the plasma membrane and the accomplishment of the mGluR-dependent LTD. Different other proteins can be activated by the mGluR5 transduction pathway, i.e. p38 mitogen-activated protein kinase (p38 MAPK), extracellular signal-regulated kinases (ERKs), Activity-regulated cytoskeleton-associated protein (Arc), striatal-enriched protein phosphatase (STEP)], phosphoinositide 3-kinase (PI3K), protein tyrosine phosphatases (PTP).

1.12 The endocytic compartment

In every cell type, the trafficking of biological cargi towards and from different types of membranes represents a crucial process for trophic sustainment, intra- and intercellular signaling, cell adhesion, migration, and proliferation. The ensemble of distinct organelles and vesicles which act as temporary sorting and storing stations during the endocytosis of different biological elements can be defined as an endosomal compartment (Figure 7). These distinct stations can be identified by Rab GTPases (hereafter referred to simply as Rabs) and other proteins, and they assume different functions in the orchestration of endocytic trafficking. Once a protein, such as a receptor, is internalized from the plasma membrane into the intracellular environment, it may join the endosomal compartment starting from the early endosomes, small organelles identified by the EEA1 protein biomarker. The cargo is then transferred to sorting endosomes (SE), marked by Rab4, Rab5, and Rab22. From the SE, the internalized protein may undergo two possible destinies: (i) if directed toward degradation, the transfer to late endosomes, identified by Rab7 and Rab9, and from there to lysosomes, marked by Rab7, will expose the internalized cargo to a low-pH environment and the hydrolytic activity of lysosomal enzymes; (ii) on the other hand, internalized proteins can be reinserted in the plasma membrane by joining the fast recycling or slow recycling routes. In the first scenario, the recycling protein is transferred from the SE to fast-recycling vesicles, identified by Rab4 and Rab35, and it travels back to the plasma membrane. In the slow recycling route, the protein is first transferred from the SE to the endocytic recycling compartment (ERC), marked by Rab11. At this station, several cargoes have been suggested to undergo different kinds of modifications, which can modify their activity/conformation and possibly restore their level of functionality. From the ERC, then the recycling cargo moves towards the slow recycling vesicles, identified by the Rab11 and Rab14 GTPase, to later travel back to the plasma membrane. (Allgood & Neunuebel, 2018)

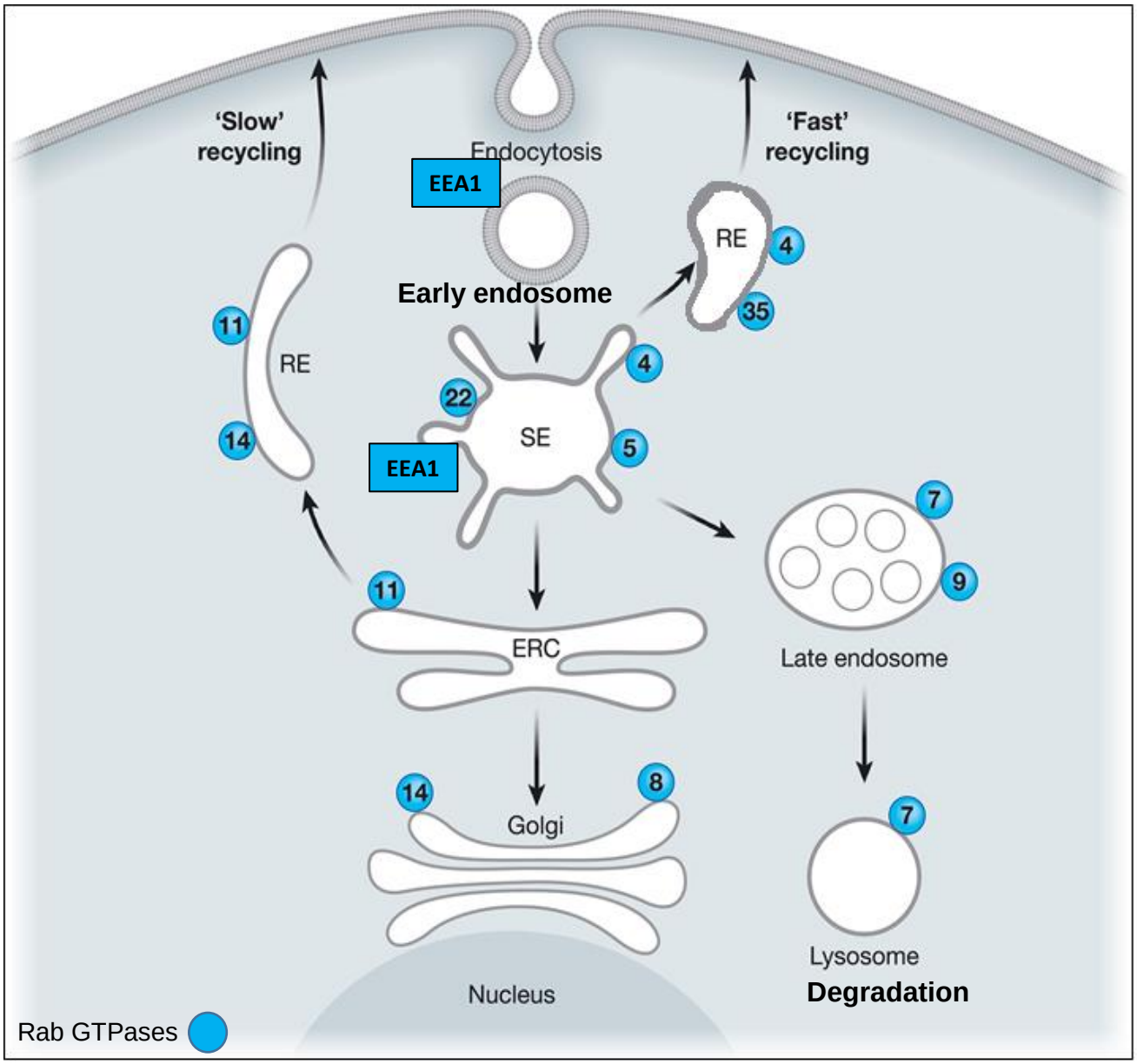

Figure 7 – Simplified schematics of endosomal compartment

The endosomal compartment represents the ensamble of vesicles and organelles working as temporary storing and sorting stations for internalized cargos. Different components serve distinct functions and can be identified by individual members of the Rab GTPase protein family or other biomarkers as the EEA1 protein for the early endosomes. Adapted and Modified from (Allgood & Neunuebel, 2018)

1.13 Receptor trafficking and mGluR5 recycling

Endocytic trafficking of synaptic receptors is crucial for synaptic activity and plasticity (Collingridge et al., 2004). Once internalized from the plasma membrane, synaptic receptors can be directed either to lysosomal degradation or back to the plasmalemma via recycling endosomes (Sheff et al., 1999). In the past, the recycling trafficking of AMPARs has been extensively investigated (Correia et al., 2008; Huganir & Nicoll, 2013; Park et al., 2004; van der Sluijs & Hoogenraad, 2011). AMPAR endosomal recycling mediates synaptic plasticity mechanisms of long-term potentiation (LTP) and long-term depression (LTD) (Granger et al., 2013; Kneussel & Hausrat, 2016; Park et al., 2004; Petrini et al., 2009). In contrast, the endocytic recycling trafficking of other glutamatergic receptors (e.g. mGluRs) and their contribution to synaptic plasticity remains poorly understood (Cheng et al., 2013; Gu & Huganir, 2016; Piguel et al., 2014; Suh et al., 2010). Recent studies suggest that proteins from the Rab GTPase family and downstream effectors are crucial for synaptic receptor internalization and endocytic cycling. As for many other GPCRs, mGluRs are promptly desensitized to avoid overstimulation upon activation. This event consists in the downregulation of the activity of the receptor which is achieved by its phosphorylation exerted by G protein-coupled receptor kinase (GRK) and the recruitment of β-arrestin. Once internalized inearly endosomes, mGluR5 can undergo degradation via ubiquitination-dependent sorting into lysosomes. Alternatively, mGluR5 can reach the endocytic recycling compartment (ERC) to be dephosphorylated by Protein phosphatase (PP2A and PP2B)-mediated dephosphorylation, restoring the basal receptor activity level. The receptor takes the slow recycling route to return to the plasma membrane via Rab11 GTPase-positive vesicles. (Dhami & Ferguson, 2006; Scheefhals et al., 2019)

1.14 Social behavior

Social interaction is crucial for the survival of several animal species. Aggressive behavior represents a shade of socially motivated behaviors and it consists of multiple patterns of behaviors. In general, it has been defined as an adaptive strategy exerted to resolve circumstances in which physical engagements occur. This behavior can be motivated by the social hierarchy establishment, competition for resources, protection of offspring, and defense of territory. Performing aggressive behavior, animals exert a cost/benefit analysis. When the mechanisms underlying this kind of elaboration are altered exaggerated and escalated aggressive behavior may take place. In humans, different psychiatric disorders and comorbid conditions show exaggerated aggressiveness as the main pathological tract (**Table 1 – Human pathological condition characterized by exaggerated aggressive behavior** 1), for example in Fragile X Syndrome(Zoicas & Kornhuber, 2019). The latter is characterized on the molecular level by mislocalization and dysregulation of mGluR5 signaling. In turn, mGluR5 has been extensively shown as a key modulator of social behavior since mGLuR5 antagonist treatments have been linked in several studies with an increase in social investigation and attention to social stimuli (Aguilar-Valles et al., 2015; Chung et al., 2015); (Burket et al., 2011; Oberman, 2012; Spooren et al., 2000). Interestingly, mGluR5 has been shown on the one hand to play a role in human pathological conditions characterized by escalated aggressiveness (Table **1**), and on the other hand to mediate synaptic plasticity concerning aggressive behavior in rodents (Borland et al., 2020) .Therefore, it represents a valuable therapeutical target to study in this context.

Table 1 – Human pathological condition characterized by exaggerated aggressive behavior

Pathology	Reference
Autistic Spectrum Disorder	(Frye, 2018)
Anxiety disorder	(Dryman & Heimberg, 2018)
Depression	(Porcelli et al., 2019)

Schizophrenia	
Alzheimer´s Disease	
Addiction disorders	(Oliveira et al., 2018)
Fragile X Syndrome	(Hagerman et al., 2018)

1.15 Extracellular vesicles

In addition to intracellular trafficking, synaptic receptors, and other biological elements can be secreted in the extracellular space via extracellular vesicles (EVs). The latter are double-membranous structures that can be subdivided into three groups according to their origin and size (Figure 8): (i) exosomes, and luminal vesicles forming from endosomes that represent the smallest EV subtype; (ii) microvesicles, released from the surface of the plasma membrane; (iii) apoptotic bodies, which originate from the plasma membrane in the late steps of apoptosis, the programmed cell death. (Budnik et al., 2016; Gurung et al., 2021; Schnatz et al., 2021; van Niel et al., 2018).

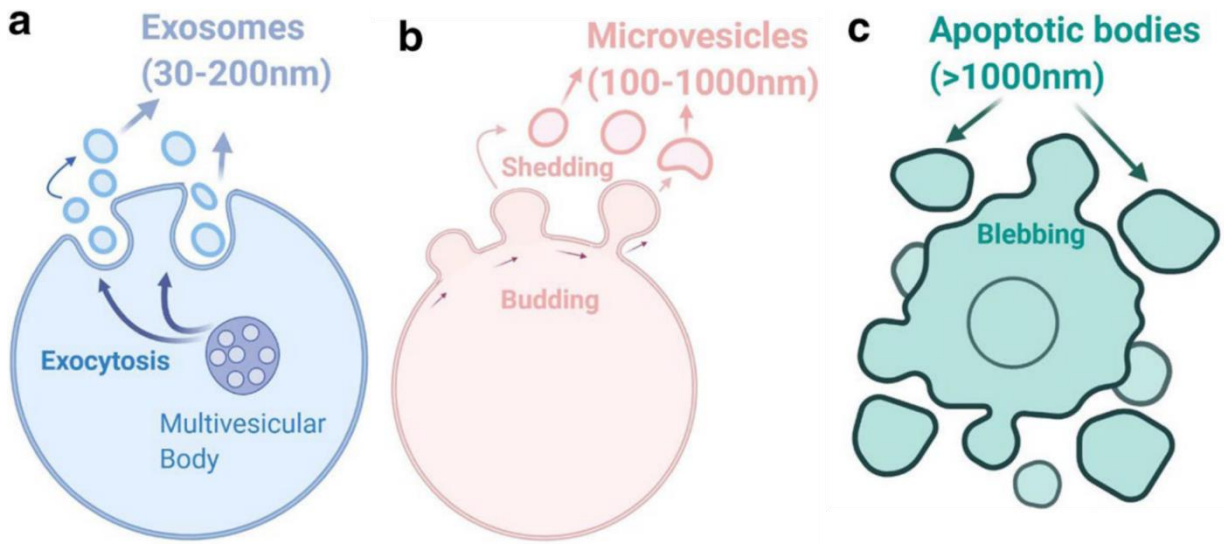

Figure 8 - Extracellular vesicles

Extracellular vesicle groups and relative diameter. (A) Exosomes and (B) Microvesicles are released from healthy cells, while (C) apoptotic bodies originate from cells in programmed cell death. (Gurung et al., 2021)

EVs exert a particular modality of intercellular communication that allow the transfer of biological elements, among different cells and tissues. (van Niel et al., 2018). In general, nucleic acids, metabolites, proteins, and lipids confer the biological composition of extracellular vesicles (EVs) with high heterogeneity. Transmembrane integral and anchored protein can be found at the lipidic double-layered membrane,

acting as ligands, receptors, adhesion molecules (integrins), molecular facilitators (tetraspanins, see “Tetraspanin protein family” paragraph), or self-recognition element (major histocompatibility complex, MHC). The vesicle lumen hosts nucleic acids, such as messenger RNA (mRNA), long non-coding RNA (lncRNA), microRNA (miRNA), DNA; cytoplasmic proteins, such as syntenin, Alix, flotillin, tumor susceptibility gene 101 (TSG101), Ribosomal-binding proteins (RBP), Heat-shock proteins (HSP); Metabolites, such as amino acids. (Figure 9)(Teng & Fussenegger, 2020)

1.16 Role of Extracellular Vesicles in the brain

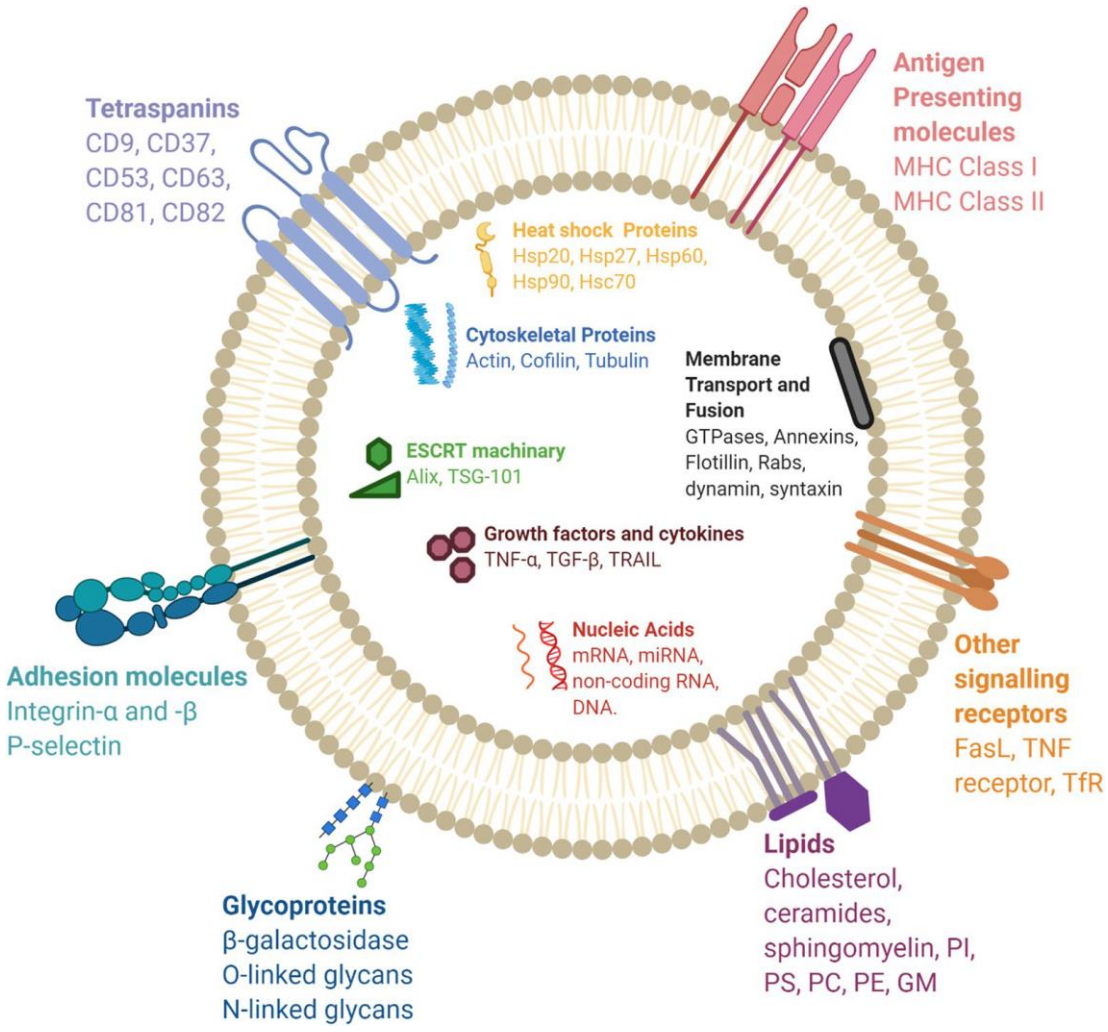

Figure 9 - biological element on EVs

Hsp: heat shock proteins; Hsc: heat shock cognate; ESCRT: endosomal sorting complexes required for transport components; CD: a cluster of different. PI: phosphatidylinositol; PS: phosphatidylserine; PC: phosphatidylcholine; PE: phosphatidylethanolamine; GM: gangliosides; TSG: tumor susceptibility gene; TNF: tumor necrosis factor; TGF: Transforming growth factor; TRAIL: TNF-related apoptosis-inducing ligand; FasL: Fas ligand; TfR = Transferrin receptor. (Gurung et al., 2021)

At the CNS, EVs can be released by both neuronal and glial cells (e.g. astrocytes, oligodendrocytes, microglia) and they are thought to play an important role in synaptogenesis, neuronal signaling, and cell survival. (Budnik et al., 2016; Fröhlich et al., 2014). Chemical synapses represent crucial hubs for the communication between neurons and several studies suggest the importance of EV in their physiology. Interestingly, pre- and post-synaptic proteins, such as synaptobrevin and the GluA2 subunit-positive AMPA receptors have been detected in EVs and their release seems

to be activity-dependent. (Lachenal et al., 2011; Vilcaes et al., 2021) On the other hand, EVs have been identified as potential vehicles for the spreading of neurodegenerative disorders (e.g. Alzheimer's disease, Parkinson's disease, amyotrophic lateral

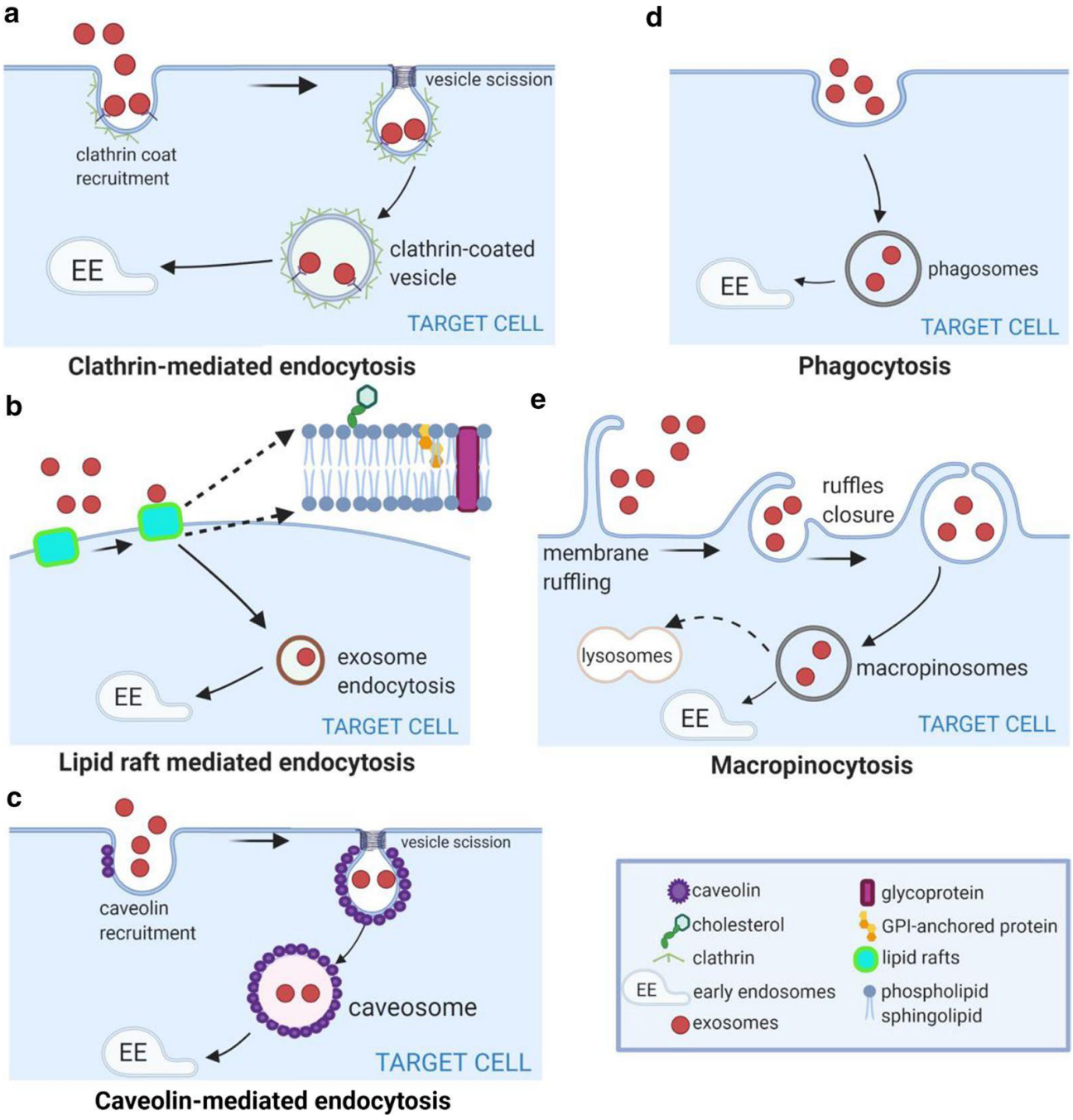

Figure 10 - mechanism of extracellular vesicles internalization

(A) clathrin-mediated endocytosis. (B) Lipid-raft mediated endocytosis. (C) caveolin-mediated endocytosis. (D) phagocytosis. (E) micropinocytosis. (Gurung et al., 2021)

sclerosis, and Huntington's disease) and cancer (Zhang & Wrana, 2014). In addition to the several functions that the EVs perform in donor and recipient cells, EVs contribute to physiological processes in the extracellular environment. For example, it has been suggested that EVs can decrease the extracellular concentration of toxic elements such as extracellular amyloid-beta by microglial uptake and therefore present a neuroprotective role (Malm et al., 2016).

1.17 Mechanism of extracellular vesicles transfer

The modulation of EV docking and uptake at recipient cells is crucial for EV-mediated intercellular communication. Different mechanisms seem to contribute to the transfer of EVs to target cells. Upon contact with the target cell, EVs and cell surface receptors undergo three main mechanisms of uptake: (i) the interaction can trigger the docking of the EV and the transduction of downstream intracellular signaling in the recipient cell, usually via protein-protein interaction; (ii) alternatively, the membrane of the EV can fuse with the plasma membrane with the following release of biological elements in the cytosol of the target cell; (iii) the EV can be internalized inside the recipient cell through different mechanisms such as clathrin-dependent endocytosis, caveolin-mediated uptake, macropinocytosis, phagocytosis, or lipid raft-mediated internalization (Figure 10). The uptake is exerted preferentially via one of the above-mentioned mechanisms according to the composition of the target cell and of the individual EV, often also in a cell- / tissue-specific manner (Mulcahy et al., 2014)

1.18 Tetraspanin protein family

Tetraspanins (Tspans) represent an evolutionarily conserved set of small (200-300 AA) transmembrane proteins. This protein family shows common structural features, such as luminal N- and C-termini, four transmembrane domains, and a small (SEL) and a large (LEL) extracellular loop (Levy & Shoham, 2005). The latter is characterized by the presence of cysteine residues which, based on the cysteine number, defines 4 subfamilies and which lead to the formation of 2 to 4 disulfide bonds inside the most conserved region of this domain. On the other hand, the LEL also presents the region

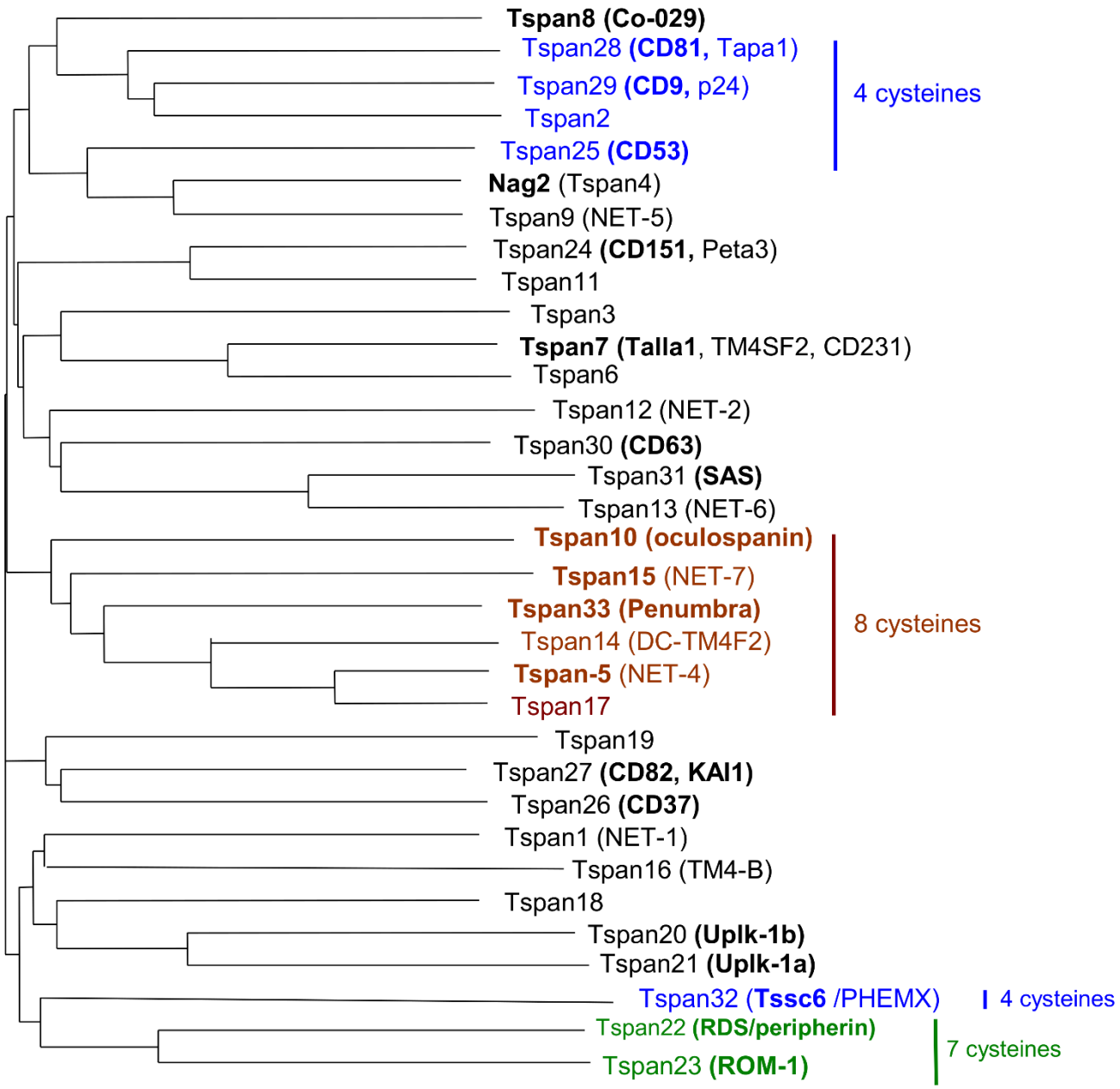

Figure 11 - Homology tree of human tetraspanins

Homology distance was calculated on the base of sequence alignment. Bold: name used commonly. If not specified, tspans present 6 cysteins at the large extracellular loop (LEL). Blue: 4 cysteines LEL subfamily. Red: 8 cysteines LEL subfamily. Green: 7 cysteins LEL subfamily. (Bonnet et al., 2019)

with the highest variability in the protein family, working as a binding domain for non-Tspan transmembrane proteins.(Kitadokoro et al., 2001; Seigneuret et al., 2001; Yauch & Hemler, 2000)

1.19 Tspan post-translational modifications

In addition, the Tspans host post-translational modifications such as N-glycosylation at the LEL and palmitoylation at conserved cysteine residues at the luminal domains.(Boucheix & Rubinstein, 2001). The latter consists of the covalent binding of palmitate to cysteines and is crucial for the binding with other palmitoylated proteins and allowing Tspan-Tspan interactions at biological membranes. (Berditchevski et al., 2002; Charrin et al., 2014; Charrin et al., 2009; Yang et al., 2002)

1.20 Tspan family

A wide range of species express tetraspanins, including vertebrates, insects, plants, fungi, and amoebas (Huang et al., 2005). A total of 33 tetraspanins have been identified in humans. Approximately 30,000 to 100,000 copies of tetraspanins have been found in almost every type of cell and tissue (Hemler, 2005) (Figure 12). Individual tetraspanins, however, exhibit very different expression patterns. Many of these molecules, such as CD81 and CD151, are expressed in almost all tissues, whereas others are expressed only in certain tissues.

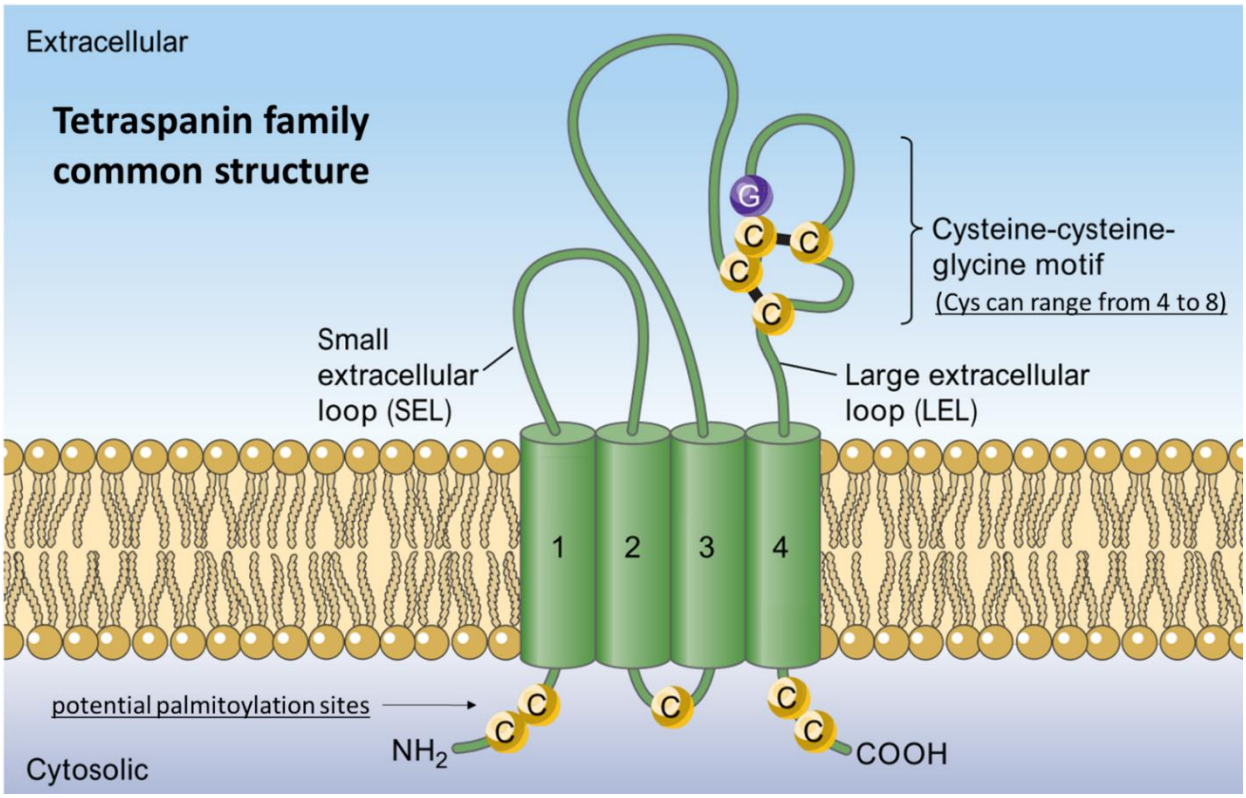

Figure 12 - Structure of Tetraspanins

Tetraspanins (green) presents four transmembrane domains (1 - 4) spanning across different types of biological lipidic bilayers (ocra). The luminal/cytosolic side is characterized by cysteine residues (C, yellow), acting as potential palmitoylation sites. The outer/extracellular side shows a small (SEL) and a large (LEL) extracellular loop. The latter hosts a variable number of cysteines, defining the testraspanin subfamily, and can be potentially glycosylated.Schematics adapted from (Levy & Shoham, 2005).

1.21 Tetraspanins as molecular facilitators

In the cell, tetraspanins are mainly found on endosomal/lysosomal membranes and in the plasma membrane. Moreover, different tetraspanins are abundantly localized on extracellular vesicles, which are released in the extracellular space upon fusion with the plasma membrane (Charrin et al., 2009; van Niel et al., 2006).

At biological membranes tetraspanins assemble among themselves, organizing their interaction partners in functional complexes on platforms called TEMs (Tetraspanin-enriched microdomains). In TEMs, interaction partners of different tetraspanins can be stabilized in close proximity and therefore tetraspanins are also referred to as molecular facilitators contributing to several biological processes (Levy & Shoham,

2005) (Termini & Gillette, 2017) (Figure 13): Tspans are involved in adhesion-mediated signaling interacting with Integrins-Focal adhesion kinase (FAK) and thought to mediate cell migration, lymphangiogenesis, immune signaling, and morphology processes; different tetraspanins have also been linked with receptor-mediated signaling, affecting cell proliferation, the enzymatic activity of sheddases, lamellopodia, fillopodia, and dendritic spine formation, and interestingly also involved in GPCR signaling. Indeed, in *Drosophila* the lysosomal Tspan Sunglasses (Sun) is responsible for the internalization of Gq-stimulated peripheral photoreceptor rhodopsin protein 1 (Rh1) endocytosis in a PLC-independent manner. In addition, Tspans have been also demonstrated to play a role in intracellular signaling, by modulating the transduction

pathways of different molecules, such as PKC-alpha, PI4K, Rho GTPases, and Beta-Catenin (Termini & Gillette, 2017)

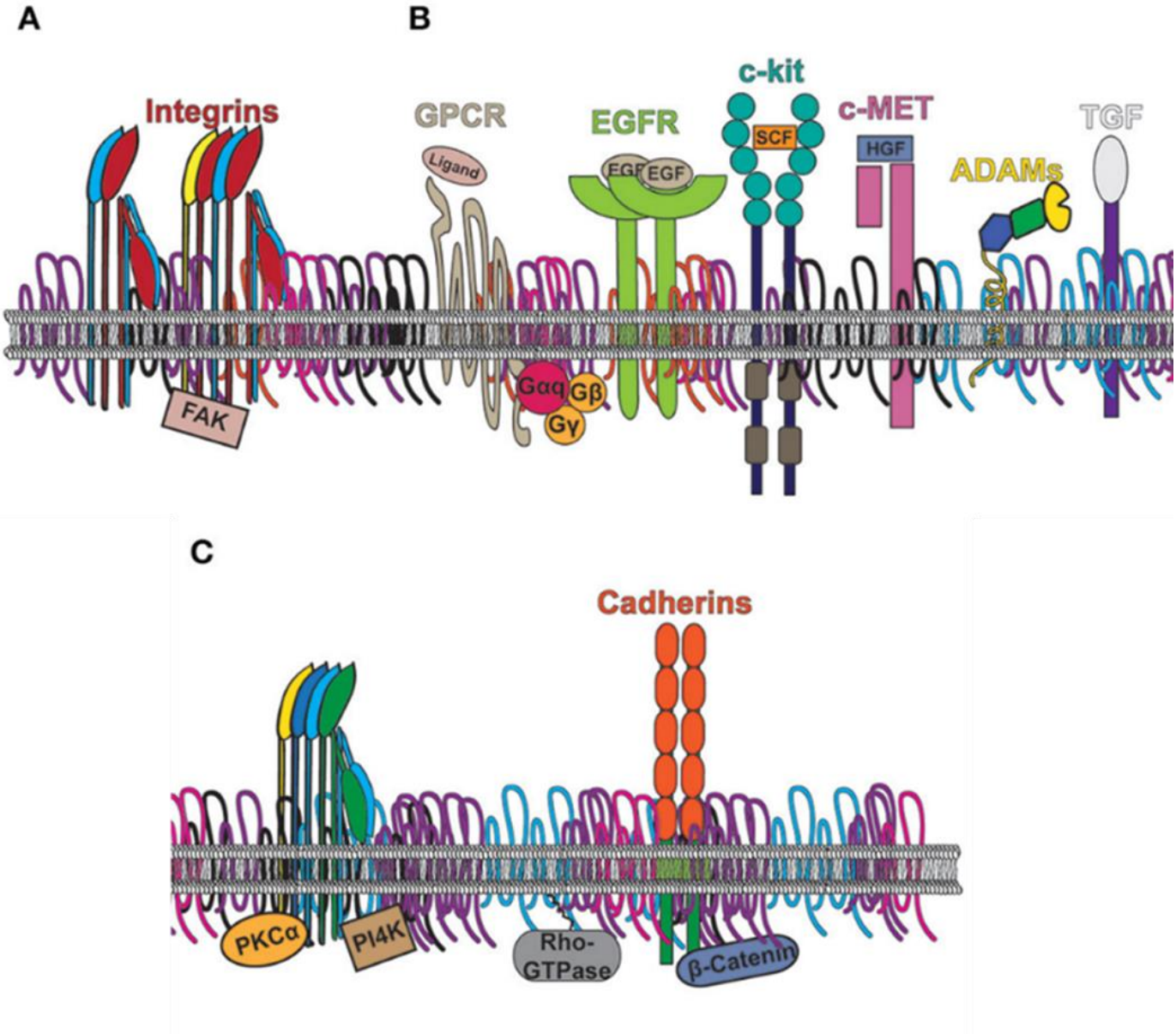

Figure 13 - Tetraspanins act as molecular facilitators.

Tetraspanins act as molecular facilitators in several biological processes at TEM, such as (A) Integrin-mediated signalling; (B) Receptor-mediated signalling; (C) intracellular signalling. Modified from (Termini & Gillette, 2017))

1.22 Tspan localization and function as a regulator of endocytic trafficking

Interestingly, Tetraspanins can modulate endocytic trafficking of their interacting partners (e.g. receptors, enzymes, or membrane integral proteins) by either promoting the insertion and stabilization in biological membranes or by facilitating the internalization from the plasma membrane. (Nishiuchi et al., 2005). In particular, it has been demonstrated that Tspan3 can promote and stabilize the interaction between the ligand Nogo-A and the sphingosine-1-phosphate-receptor-2 (S1RP2), a G-protein coupled receptor (GPCR). (Thiede-Stan et al., 2015)). In addition, Tspan5 and Tspan7 have been linked to the cellular trafficking of α-amino-3-hydroxy-5-methyl-4-isoxazolepropionic acid receptor (AMPA) ionotropic glutamatergic receptors at the plasma membrane and consequent dendritic spine and neuronal signaling abnormalities. Tspan5 can facilitate the exocytosis of AMPARs to the plasma membrane, while not influencing the internalization of the receptor. Mechanistically, Tspan5 interacts simultaneously with AMPARs, the auxiliary AMPAR subunit Stargazin and the adaptor protein complex AP4. The presence of Tspan5 in this tetrameric complex is necessary to promote the trafficking of AMPARs from the endoplasmic reticulum (ER) or ER-Golgi intermediate compartment (ERGIC) vesicles to the post-synaptic density via recycling endosomes (Moretto et al., 2023) Tspan7 genetic mutations have been linked to X-linked intellectual disability phenotypes. In physiological conditions, the protein-interacting-with-C-Kinase-1 (PICK1) can modulate AMPAR endocytosis and recycling trafficking. Tspan7 associates to PICK1-AMPAR complex, possibly regulating the strength of this interaction and therefore AMPARs endocytic trafficking.

1.23 Tspan15

Tetraspanin 15 (Tspan15) is abundantly expressed in the brain, especially in the hippocampal formation and cortical regions (Figure 14).

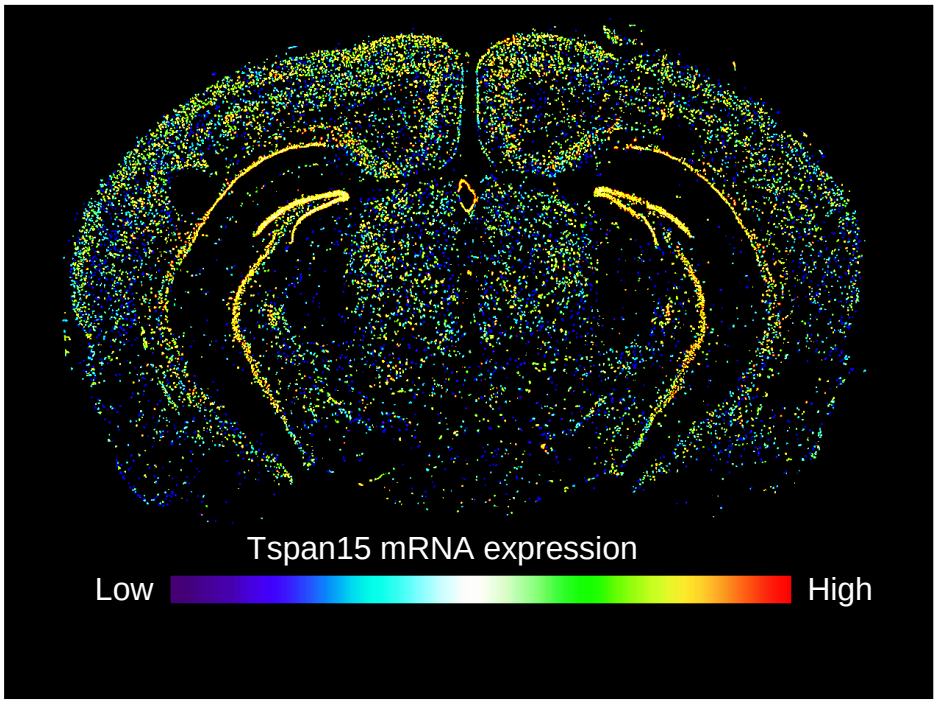

Figure 14 - Tetraspanin15 mRNA expression in the brain

In Situ Hibridization showing Tspan15 mRNA expression levels in a mouse brain coronal section. High expression is detected at the hippocampal formation and in the cortex. (Allen brain mouse expression atlas. *https://mouse.brain-map.org/gene/show/46264*)

1.24 Tspan15 regulation of ADAM10 trafficking and activity

Recent studies have identified Tspan15 as an interactor of enzyme A disintegrin and metalloproteinase (ADAM10). The latter is responsible for the cleavage of the ectodomain of different substrates at the cell and extracellular vesicle surface with physiological and pathological consequences (**Table 2**). For example, it has been demonstrated that the dysregulation of ADAM10-mediated cleavage of the Amyloid Precursor Protein (APP) provokes detrimental synaptic and behavioral alterations in Fragile X Syndrome (Pasciuto et al., 2015).

Table 2 - Effect of Tspan15 on ADAM10 substrates

ADAM10 Substrate	Biological Effect	Cell Line	Reference
Amiloid Precursor protein	Cleavage increase	N2a, HEK293	(Prox et al., 2012)
	Cleavage decrease	PC3, COS7, HEK293	(Noy et al., 2016; Prox et al., 2012)
N-Cadherin	Cleavage increase	PC3, COS7, HEK293	(Jouannet et al., 2016)
Notch receptor	Downregulation of Notch pathway	P3, U2OS-N1	(Jouannet et al., 2016)

1.25 Tetraspanins and Tspan15 in cancer

Several members of the Tspan protein family have been linked to the oncology field and recent studies suggest that they could potentially facilitate tumor growth by affecting infective and immunological processes, coagulation of platelets, and modulating angiogenesis, i.e. the formation of new blood vessels (Hemler, 2005) (Hemler, 2008); (Huang et al., 2022) et al., 2022). In addition to its role in the central nervous system, Tspan15 has also been shown to play a role in cancer. In fact, Tspan15 expression is increased in different types of tumors such as pancreatic, lung, breast, and colorectal cancer. In these types of tumor, the upregulation of Tspan15 correlates with lower survival expectancy and more aggressive cancer development resulting from increased tumor cell migration, invasion, and metastasis formation. It has been suggested that Tspan15 expression promotes these effects because of its ability to interact with other proteins at the cell surface in Tetraspanin-enriched

microdomains, which have been demonstrated to play a role in cell migration, proliferation, and regulation of enzymatic activity.

2 Objective of the thesis

Different members of the tetraspanin family have been shown to participate in synaptic plasticity by modulating synaptic receptor trafficking or acting as biomarkers for extracellular vesicle (EV) communication. To date, despite the high expression of Tetraspanin15 (Tspan15) at the hippocampal formation and its well-known interaction with the EV-resident protein ADAM10, Tspan15 has not yet been linked to the above-mentioned functions. Therefore, during my doctoral path, I have focused my efforts on elucidating the role of in the context of synaptic and extracellular vesicle-mediated intercellular communication within the central nervous system. To achieve these goals, a constitutive knock-out Tspan15 mouse line (Tspan15KO) was used and characterized.

On the one hand, I aimed to study the effects of Tetraspanin15 (Tspan15) depletion concerning metabotropic glutamate receptor 5 (mGluR5) trafficking and signaling. Molecular cloning of a Myc-Tspan15 construct allowed to overcome a lack of specific antibodies working in immunocytochemistry. In addition, *in vivo* mouse experiments were performed to shed light on potential social behavioral alterations in the absence of Tspan15 expression.

In a parallel project, I investigated the contribution of Tspan15 in extracellular vesicle (EV)-mediated interneuronal communication, specifically in the contacting phase between the extracellular vesicle and target neurons in the mouse brain.

3 Material and methods

3.1 Animals

In this scientific investigation, it was made use of mice constitutively depleted for the tetraspanin 15 protein, previously described in (Seipold et al., 2018). The expression of the Tetraspanin 15 protein was achieved by transcription activator-like effector nucleases (TALEN)-mediated genome editing: a 104 bp deletion in the exon2 of the Tspan15 gene, with the formation of a premature stop codon. Mice were kindly provided by our collaborator Prof. Paul Saftig from Christian Albrechts University.

3.2 Biopsies and isolation of genomic DNA

To obtain the genotype of experimental mice, genomic DNA was extracted from ear punches or tail biopsies collected from 3 to 4-week-old animals. For the extraction, DNA was incubated with Quick Extract Buffer (Biozym Scientific GmbH, Hessisch Oldendorf, Germany) for 15 minutes at 65°C. This latter was then heat-inactivated at 95°C for 2 minutes.

3.3 PCR for experimental animal genotyping

A polymerase Chain Reaction was performed to check the presence of mutated and wild-type alleles in experimental animals for the Tspan15 gene. The following reaction mix (Table 4) was applied to obtain amplification of the Tspan15 exon2, using a forward and reverse primer (Table 3) and a template, the genomic DNA isolated from biopsies.

Table 3 - Genotyping PCR primer list

Primer name	Oligonucleotide sequence (5´→3´)
Tspan15 exon2 forward	AAGCTTGGGCTATAGGCATACACC
Tspan15 exon2 reverse	GGATCCCCAGCATCTCTGTGACAGC

Table 4 - Genotyping PCR master mix protocol

Reagent Stocks	Reaction mix (for 25 µl)
10X Loading Buffer	2.5 µl
dNTPs (2.5 mM)	0.5 µl
Primer (10mM)	0.5 µl
Primer Exon2 Reverse (10mM)	0.5 µl
Taq Polymerase (5U/l)	0.15 µl
Template DNA	0.5 µl
ddH_2O	20.35 µl

The PCRs were performed using a PTC-200 thermocycler (MJ Research) with the following touchdown thermal protocol (Table 5):

Table 5 - Genotyping PCR thermal protocol

Step	Temperature	Time	Function
1	95°C	00:30	Initial denaturation
2	95°C	00:10	Denaturation
3	66°C (-0.5°C x cycle)	01:00	Annealing
4	72°C	00:30	Elongation
5	GO TO step 2 x 36 times-		
6	72°C	10:00	Final elongation
7	4°C	∞	Save PCR product

3.4 Molecular Cloning

The Tetraspanin15 gene sequence was subcloned in an Adeno-Associated Viral vector (pAVV) containing Ampicillin-resistance, under the neuron-specific Synapsin promoter and N-term cMyc tag was added to later be targeted in immunostaining experiments. To obtain the Syn.Myc.Tspan15 construct different restriction enzymes were used as reported in the following map (Figure 15).

Figure 15 - AAV.Syn.Myc.Tspan15 construct

BamHI and HindIII restriction enzyme sequences were used to exciss the Tspan15 (black) gene sequence, successively ligate with a EcorI-BamHI-flanked N-terminal cMyc tag (red) and expressed under the neuron-specific Synapsin promoter (blue). Schematic from D. Stajano

3.5 Bacteria transformation

A heat-shock protocol was applied to transform DH5α competent E.Coli cells: In particular, 100uL of bacterial cells were incubated with DNA on ice for 30 minutes. The mix was incubated for 45 seconds at 42 ^{o}C in a water bath and then set on ice for 45 seconds, inducing the heat shock. Bacteria recovery was achieved by the following incubation at 37 ^{o}C with the addition of S.O.C. media. Recovery incubation time ranged according to the antibiotic resistance present on the plasmid: 30 minutes or 45 minutes respectively for ampicillin and kanamycin.

3.6 Midipreps

A culture of LB bacteria was grown overnight with 250 mL of antibiotic-supplemented LB media. The bacteria were then pelleted at 5000 rcf for 10 minutes at 4°C, and the DNA was extracted and purified with a Nucleobond Xtra Midi EF DNA extraction kit (cat.740420.50, Macherey-Nagel, Düren, Germany) following the manufacturer's instructions. 3.5 ml of isopropanol was added to the eluted DNA and the two phases were mixed. The sample was centrifuged at 15000g for 30 minutes at 4°C with a Fixed-Angle JA-25.50 Rotor in an Avanti J-26 XP centrifuge (Beckman Coulter). The resulting pellet was fastly rinsed with 70%EtOH and then dried at room temperature for 15 minutes. Then the DNA pellet was resuspended in endotoxin-free water and eventually, the DNA concentration and purity were assessed via spectrophotometry.

3.7 Biochemical experiments

Ice-cold solutions and the use of protease and phosphatase inhibitors were standard conditions followed in all the biochemical experiments. All centrifugations were carried out at +4°C. All mice were sacrificed with CO2 followed by decapitation. In the case of embryos, brain dissection was performed in ice-cold Glucose-supplied PBS.

3.8 Post-nuclear tissue lysates

Total brain or isolated hippocampi were placed in a potter filled with ice-cold IM-Ac buffer (20mM HEPES / 100mM CH_3CO_2K / 40mM KCl / 5mM EGTA / 5mM $MgCl_2$ / 1mM PMSF / 5mM DTT + prot./phosp. Inhibitors / pH=7.2 adjusted with 0.5M NaOH.). The tissue was mechanically homogenized by 8 strokes at 900 rpm.

Post-nuclear lysates (S1) were achieved by saving the supernatant resulting from the homogenate centrifugation at 1000 xg for 10 minutes at +4°C. Protein concentration was assessed for S1 fractions with the PierceTM BCA Protein Assay Kit (cat. 23227, Thermo Scientific). Samples were diluted with IM-Ac buffer to obtain equal concentrations.

3.9 Cortical neuronal culture cell lysates

Cell lysates from DIV15 cortical neurons were obtained as follows: after the supernatant was aspirated, cells were washed twice with PBS 0.5% Triton-X / EDTA-free cOmplete protease inhibitor was added to the plate and cells were harvested with a cell scraper. Cells were lysated for 30 minutes on a rotating wheel and then centrifuged at 1000 xg. 4x Laemmli-Urea loading buffer was added to the resulting supernatant, representing the total cell lysate. In the end, the sample was heated for 15 minutes at 65°C.

3.10 Differential centrifugation

A differential centrifugation protocol was performed to isolate from the post-nuclear lysate (S1) distinct subcellular fractions: pellet P2 (plasma membrane and large vesicular organelles membranes); supernatant S3 (small vesicles, large protein complexes, and cytosolic proteins); pellet P3 (intracellular vesicular fraction including microsomes, Golgi and transport vesicles). In detail, the post-nuclear S1 fraction was centrifuged at 10.000 xg for 10 minutes and the resulting pellet was saved as a P2 fraction. In turn, the obtained supernatant (S2) was further centrifuged at 100.000 xg for 1 hour, achieving a pellet and supernatant corresponding respectively to the P3 and S3 fractions. All centrifugations were carried out at +4°C. Pellet fractions were reconstituted in IM-Ac.

All subcellular fractions, including the post-nuclear S1, were then supplied with Triton-X until the final concentration of 1%. Subsequent lysis was performed on a rotating wheel for 30 minutes. In the end, 4x Laemmli-Urea loading buffer was added and the samples were heated for 15 minutes at 65°C.

3.11 Preparation of synaptosomal fractions

Mice were sacrificed and hippocampi were isolated as described above and homogenized in 10 volumes of sucrose buffer 1 (320mM sucrose, 1mM NaHCO3, 1mM MgCl2, 0.5mM CaCl2, 1µM PMSF) supplied with protease inhibitor cocktail (Roche). The resulting homogenates were then centrifuged at 1000 ×g for 10 min. Then, while the supernatants (S1-1) were stored on ice, the pellets (P1-1) were homogenized and centrifuged again for 10min at 700 ×g. The supernatants (S1-1 + S1-2) were then joined and centrifuged at 13800 ×g for 10min. The resulting pellets (P2-1) were homogenized in 500 µl sucrose buffer 2 (320mM sucrose). A sucrose gradient was obtained by gently pouring a 1M sucrose /1mM $NaHCO_3$ solution into a 1.4M sucrose /1mM $NaHCO_3$ solution in an ultracentrifuge tube (Ultra-Clear, 14x95 mm 14ml). Pellet P2-1 was loaded on the top of the gradient and centrifuged for 1.5 hours at 82.500 xg.

The synaptosomal layer was collected from the interface between the two sucrose solutions and sucrose buffer 2 was added to dilute them to 1:4. The solution was centrifuged for 20 minutes at 28.000 xg. The pellet corresponding to the synaptosomal fraction was resuspended in 100µl sucrose buffer 2. To obtain the PSD soluble and insoluble fractions, the synaptosome fraction was diluted 1:1 in 2X T-X buffer (1%Triton-X / 12mM Tris/HCl pH=8.0 / 320mM sucrose), placed on a rotating wheel for 15 minutes at +4°C. and then centrifuged for 1h hour at 70.000 xg. The supernatant was saved as PSD detergent-soluble fraction, while the pellet was resuspended with 40mM Tris-HCl pH8.0 and saved as PSD detergent-insoluble fraction.

3.12 SDS-PAGE and Western Blots

To separate proteins by SDS-PAGE, 4-20% gradient SDS-gels were cast as follows: 4% and 20% acrylamide separating gels were gently mixed to create a gradient. The resulting gradient separating gel presented a higher acrylamide percentage at the bottom and a lower percentage at the top. After its polymerization, a stacking 5% acrylamide gel was added on top of the gradient-separating gel. Once polymerized, 4-2% SDS-PAGE gel was mounted in its support chamber, and filled with 1x SDS Running Buffer. Protein ladder marker and samples were loaded into the gel and, in the case of empty wells, 1x Laemmli-Urea loading buffer was used to balance the loading scheme. At the electrophoretic run end, the separated proteins were transferred from the gel to a PVDF membrane via wet blot or semi-dry blot. In both cases, the PDVF was pre-activated with 100% MeOH. After blotting, the membrane was blocked in 5%milk TBS-T for the standard experiments. 5%IgG-free BSA or PVDF Blocking Reagent for Can Get Signal (Cosmo Bio LTD, TYB-NYPBR01) were instead used as blocking solutions for WB involving phosphorylated antigens or following an immunoprecipitation. Afterward, primary and secondary antibodies were diluted in a solution equal to that of the blocking step. After blocking, membranes were incubated with the primary antibodies overnight at +4°C or 1 hour, depending on the antibody. Then membranes were washed three times in TBS-T for 5 minutes each and incubated for 1 hour at room temperature with secondary antibodies conjugated with horseradish

peroxidase (HRP). Membranes were washed three times in TBS-T for 5 minutes each. In the end, ECL solution, containing the HRP substrate, was added to the membranes and these latter were imaged at the Intas ECL Chemostar Imager. To detect an additional protein on the same membrane, it was first incubated with an acid-stripping buffer (25 mM Glycine / 1%SDS / pH=2.0) for 30 minutes at room temperature. The membrane was then washed three times in TBS-T, blocked again, and reprobed as described above.

3.13 Cell line culture

COS7 and N2A were cultured in 10% fetal bovine serum DMEM supplied with 1% penicillin/streptavidin. Once at about 80% of confluence, cells were split incubating 0.05% EDTA-Trypsin for 5 min at 37°C.

3.14 Primary neuronal culture

To obtain cortical or hippocampal primary neuronal cultures, pregnant female mice were sacrificed by CO_2 followed by cervical dislocation. Embryos, ranging from the embryonic stage 15 to 17, were decapitated. The brain was extracted and dissected in ice-cold Glucose-PBS autoclaved buffer to remove the meninges and isolate hippocampi and cortexes. In the case of an unknown genotype of the embryo, a biopsy from the cerebellum was used to later perform a PCR genotyping, keeping the corresponding cortexes and hippocampi in Hibernating medium. To dissociate the cells, the tissues were incubated in 0.05% EDTA-Trypsin for 5 minutes at 37°C. Then Trypsin reaction was blocked by rinsing the dissociated tissues in pre-warmed HBSS supplied with 10% FBS. Eventually, they were placed in pre-warmed HBSS and two fire-polished glass pipettes were used to triturate mechanically the tissues by suction. Cells were seeded in different recipient plates according to their following usage: For immunofluorescence stainings and extracellular vesicles recipient cultures, cells were seeded on autoclaved 12mm glass coverslips in 24x well plates; For time-lapse imaging experiments cells were seeded on autoclaved 25mm glass coverslips; For

extracellular vesicles donor cultures, cells were seeded in 10-cm plates. All coverslips and the 10-cm cell culture plates were previously coated with poly-L-lysine 1:200 in PBS overnight, washed twice with sterile ddH_2O, and prepared for cell seeding adding pre-warmed Lonza Primary Neuron Growth Medium (PNGM) (Thermo Fisher Scientific, Dreieich, Germany) supplied with 1% pen-strep and 1% L-Glutamine.

3.15 Immunocytochemical staining

For standard stainings, DIV15 hippocampal neuronal cultures were washed briefly with PBS and fixed with PBS / 4% PFA / 4% sucrose. Cells were washed two times with PBS and then incubated with PBS / 0.2% Triton-X for permeabilization. Cells were then washed three times with PBS and incubated with a blocking solution made of PBS / 1%BSA. After 1 hour, the blocking was followed by overnight incubation at 4°C on a shaker with primary antibodies (List of antibodies)in PBS / 1%BSA. After three washing in PBS, the cells were incubated for 1 hour at room temperature with fluorescent secondary antibodies and/or fluorescent dyes (e.g. Phalloidin, DAPI) in PBS / 1%BSA. In the end, cells were washed three times in PBS and the coverslips were mounted on glass with Aqua-Poly-Mount, letting them dry before imaging.

3.16 DHPG treatment and mGLuR5 Surface immunocytochemical staining

In the case of immunostaining direct against the cell surface population of the metabotropic glutamate receptor 5 (mGLuR5), the standard immunocytochemical staining was modified as follows: In detail, DIV15 neurons were incubated with ACSFs (145mMNaCl / 10mM HEPES / C6H12O6 / 2.5mM KCl / 1mM MgCl2 / CaCl2 / pH=7.4 adjusted with 0.5M NaOH.) and treated for 5 min with [100µm] DHPG (R&D systems) followed by 15 minutes of washout period. Cells were then washed with PBS and then fixed in ice-cold PBS / 4% PFA / 4% sucrose for 8 minutes on ice. Cells were then washed three times with PBS and were directly incubated with the blocking solution (PBS / 1%BSA) for 1 hour, skipping the permeabilization step. Then cells were incubated overnight at +4°C in PBS / 1%BSA with a primary antibody targeting

specifically the extracellular N-terminus of mGLuR5 (#AGC-007, Alomone Labs) After three washing in PBS, the cells were incubated with fluorescent secondary antibody for 1 hour at room temperature in PBS / 1%BSA. To additionally stain other target proteins, the cells underwent an additional staining procedure, following the standard staining protocol from the permeabilization step.

3.17 Histological experiments

Mice were sacrificed with CO_2 and transcardially perfused with first saline solution and then with ice-cold 4% PFA and 0.1% Glutaraldehyde in PBS. Brains were extracted and hippocampi were isolated. 300µm thick hippocampal sagittal sections were obtained by cutting with a tissue chopper. Slices were then maintained in PBS / 4% PFA and 0.1% Glutaraldehyde.

3.18 Diolistic dye labeling for hippocampal slices

Diolistic (DiI) dye staining of mouse hippocampal sections was performed as follows: 1.6 µM DiI-coated gold bullets were shot with a Helios Gene Gun system (Biorad) at around 120 psi helium gas pressure through a 3µm grid against the hippocampal slices. DiI-coated gold bullets were prepared as described by (Muhia et al., 2016). Shot slices were placed back in PBS / 4% PFA and 0.1% Glutaraldehyde at room temperature overnight in the dark.

3.19 Image acquisition and processing for dendritic arbor and Sholl analysis

DiI-labeled slices were imaged using a 20x air objective with a Nikon Spinning Disc Confocal microscope equipped with a Visitron system. Z-stacks were acquired from non-overlapping pyramidal CA1 neurons (z: 1µm). The dendritic arbor was then three-dimensionally reconstructed and analyzed using the Neurite Tracer from the FIJI software. Cumulative length for branch order, total dendrites length, number of branch

order, number of branching points, and bifurcation ratio per branch order were elaborated. For the Sholl analysis, 10µm-spaced concentric circles were drawn starting from the soma center and reaching 310µm maximum radius. The number of interactions between dendrites and each concentric circle was plotted against the distance from the soma.

3.20 Image acquisition and processing for dendritic spine analysis

DiI-labeled secondary apical dendrites from pyramidal CA1 neurons were imaged using a 100x oil objective with a Nikon Spinning Disc Confocal microscope equipped with a Visitron system. Z-stacks were acquired with a 1µm step size and the image was deconvolved with the AutoQuant software. Imaris software was then used to select sections of interest. Spines were counted and classified with the FIJI software according to the following parameters: Fillopodia (length >2µm); Thin: (length <2µm, presence of head); Stubby (length: wide ratio<1); Mushroom (width >0.6µm c.a.) (Risher et al., 2014).

3.21 Time-lapse Imaging

N2A, COS7, and DIV10 Primary cell cultures were transfected as previously described. 24-48 hours later, after checking transfection efficiency under a normal epifluorescence microscope, the cells were moved into a Time-lapse imaging ring filled with Time-lapse Imaging Hepes Buffer (10mM HEPES / pH=7.4 / 135mM NaCl / 5mM KCl / 2mM CaCl2 / 2mM MgCl2 / 15mM Glucose). The cells were imaged at 5%CO2 and 37°C with a spinning disc confocal microscope (Nikon Eclipse Ti) equipped with a CCD camera (Digital Camera C9100, EM-CCD, Hamamatsu) and a Visitron system. A 100x oil objective was used for the cell recording.

3.22 Conditioned media N2A assay

N2a were grown in 10-cm plates until 60% of confluence. Cells were then transfected with CD63-mCherry and Tspan15-EGFP or EGFP-N2 using Lipofectamine 2000 as

previously described. After 24 hours, the expression of the constructs was assessed under an epifluorescent microscope. Cells were then washed with pre-warmed PBS and detached by pipetting up and down in 6ml of Opti-MEM™ (reduced serum medium). N2a was split 1:2 by adding 3ml to a new plate. After 48 hours of enriching, the raw EV-enriched conditioned media (CM) was processed to remove cell debris: In detail, the CM was centrifuged at 300 xg and moved to a new tube three times. In addition, centrifugation was performed at 3000 xg. The CM was then filtered with a 0.22 µm filter and warmed up at 37°C in a water bath. 1ml of EV-enriched processed CM was added to the culture for 48-72 hours recipient (untransfected) N2A, previously seeded at low density on 12mm glass coverslips in a 24x well plate. In the end, recipient cells were fixed for 7 minutes in ice-cold PBS / 4%PFA on ice in the dark. After fixation cells were washed three times with PBS, the EGFP signal was occasionally boosted with immunofluorescence using an anti-GFP antibody (Rb, A11122; Abcam), later recognized by an anti-Rb 488. Cells were mounted with Aqua-Poly-Mount and imaged at the confocal microscope Olympus Fluoview FV1000.

3.23 Cell density quantification

Neuronal cortical cultures were obtained from wildtype or Tspan 15 knockout mice. At DIV14 neurons were fixed with 4% PFA in PBS and stained with 4',6-diamidin-2-fenilindolo (DAPI) for 10 minutes. Cells were washed with PBS 3 times and then mounted with Aqua Polymount on glass coverslips. Imaging of the samples was performed using an Olympus Fluoview FV1000 confocal microscope. Nucleai were quantified and used to estimate the cell density.

3.24 Extracellular vesicles internalization assay

Tspan15-EGFP or control GFP were expressed in N2a cells and extracellular vesicles were isolated in 100,000 x g fraction. DIV15 neurons or N2a cells were incubated for 45 minutes at 37°C or at C (internalization negative control) with N2a-derived EVs or 100,000 x g supernatant (EV-depleted negative control). Cells were fixed as previously reported. Samples were permeabilized with 0.1% Triton-X PBS for 10 minutes. After PBS washing, cells were blocked in 1% BSA/PBS, and primary antibodies anti-GFP

and anti-EEA1 were incubated at 4°C overnight. After rinsing the samples with PBS, secondary antibodies donkey anti-guinea pig Cy5 and donkey anti-rabbit were incubated for 1 hour. 1% BSA/PBS was used as a general antibody incubation buffer. Samples were acquired as reported above in confocal imaging. The EEA1 colocalization with Tspan 15-GFP was analyzed making use of the JAKOP ImageJ plugin, estimating the relative Mander´s overlap coefficient.

3.25 Extracellular vesicle isolation

At DIV15, cortical neuronal media was harvested and supplied with EDTA-free cOmplete protease inhibitor (Roche). Media was centrifuged at 4°C for 10 minutes at 2000 xg. The resulting supernatant was further centrifuged at 4°C for 30 minutes at 20000 xg in an Ultra-Clear (14x95 mm) centrifuge tube using a swinging-bucket SW40Ti rotor in an OPTIMA L-80 XP Ultracentrifuge (Beckman Coulter). The supernatant was then filtered with a 0.22 µm filter and centrifuged with the above-mentioned setup for 90 minutes at 100000 x g. The resulting EVs-enriched pellet was reconstituted with PBS / protease inhibitors, previously filtered with a 0.22 µm.

3.26 DiI-labeling of extracellular vesicles

NTA/WB-validated EV extracts from cortical neurons or N2A or 0.5% BSA were stained with DiI (0.25 µg/µl) for 1 hour at 37°C in the dark. Samples were moved into Microfuge Tube Polyallomer (9.5x38mm), filled with filtered (0.22µm) VT1 water until 1ml. Samples were then centrifuged at 100000 xg with a TLA110 rotor (10E30108) at 4°C with an Optima MAX-XP Ultracentrifuge. The resulting supernatants were discarded, while the pellets were reconstituted in filtered (0.22µm) PBS.

3.27 EVs interaction assay upon Tspan15 KO in acceptor cells

Cortical neurons on 12mm glass coverslips were transfected at DIV13 as previously described with a GFP-C1 vector. After 24 hours wild-type and Tspan15KO cells were incubated with wt DIV15 DiI-labeled EVs or DiI-labeled 0.5% BSA. At different time points (45 minutes and 24 hours) neurons were rinsed with PBS and fixed for 5 minutes with ice-cold PBS / 4% PFA. Coverslips were mounted on glasses with Poly Aqua

Mount and let dry at 4°C. Cells were imaged with a Nikon spinning disk confocal microscope equipped with a Visitron system. Z-stacks were acquired for each GFP-transfected neuron with a z: 1µm, using a 100x oil objective.

3.28 EVs interaction assay upon Tspan15 KO in donor cells

Wt cortical neurons on 12mm glass coverslips were transfected at DIV13 as previously described with a GFP-C1 vector. After 24 hours, wt cells were incubated with DIV15 DiI-labeled EVs from wt or KO donor cortical neuronal culture or DiI-labeled 0.5% BSA. After 45 minutes cells were fixed for 5 minutes with ice-cold PBS / 4% PFA. Samples were further processed and imaged as described for the previous EV interaction assay.

3.29 EVs interaction quantification analysis

To quantify the EV uptake levels in the two above-mentioned functional experiments, the number of EVs in contact with the neuron was normalized on the GFP+ volume of neuronal cells. In detail, the GFP+ volume was estimated by the use of the Volumest (Volume estimator) plugin from the ImageJ software. The number of DiI-labeled EVs was manually quantified with the use of the Cell Counter tool from ImageJ.

$$EVs\ uptaken = \frac{number\ of\ EVs\ \ in\ contact}{GFP\ volume\ (\mu m^3)}$$

3.30 Transfection with Lipofectamine2000

N2A, COS7, and primary neuronal culture were transfected with the use of Lipofectamine™ 2000 Transfection Reagent. In the case of cell lines, transfection was performed when cells were at 60% of confluence. DNA mix or Lipofectamine2000 was incubated for 5 minutes in two different OPTIMEM solutions (dilution media). The solution containing the DNA was then added to the one containing Lipofectamine. The mix was vortexed, incubated at room temperature for 20 minutes, and then added to the cells. Volumes and DNA amount range (

Table 6) were set according to the manufacturer protocol (Invitrogen). For primary neuronal cultures, transfections were performed ranging from DIV10 to DIV13. A DNA / Lipofectamine mix was prepared as previously described. Part of the neuronal media was saved at 37°C and the transfection mix was added to the well. Neurons were then incubated at 37°C for 1 to 2 hours. After rinsing the cells with pre-warmed Hepes buffer (10mM HEPES / pH=7.4 / 135mM NaCl / 5mM KCl / 2mM CaCl2 / 2mM MgCl2 / 15mM Glucose), the conditioned media previously saved were added to the neurons. For primary neurons, volumes and DNA amount range were set as described in (Table 7).- Transfection reagents for primary neurons

Table 6 - Transfection reagents for cell lines

Culture plate	Surface area/well	Vol. of plating media	Vol. of dilution medium	DNA	Lipofectamine 2000
24-well	2 cm 2	500 µl	2 x 50 µl	0.8-3 µg	2.0 µl
6-well	10 cm 2	2 ml	2 x 250 µl	4.0 µg	10 µl
10-cm	60 cm 2	15 ml	2 x 1.5 ml	24 µg	60 µl

Table 7 - Transfection reagents for primary neurons

Culture plate	Surface area/well	Vol. of incubation media	Vol. of dilution medium	DNA	Lipofectamine2000
24-well	2 cm 2	100 µl	2 x 50 µl	4 µg	6 µl
6-well	10 cm 2	2 ml	2 x 250 µl	4.0 µg	10 µl

3.31 Electron Microscopy

The media from cortical cell cultures was processed as previously described to obtain a 100,000 x g of extracellular vesicles. This fraction was resuspended in 2% paraformaldehyde (PFA) Phosphate Buffer. The same solution was adsorbed to

electrically charge for 20 minutes carbon-coated Formvar grids (EMS, Germany). Samples were washed with PBS and post-fixed with 1% glutaraldehyde (GA) in PBS. Then, ice-cold methylcellulose-uranyl acetate solution was added for 30 minutes. Grids dried and were checked by electron microscopy.

Immunogold labeling was performed as reported in (Théry et al., 2006) EVs were added to the grids and washed in PBS, incubated in 20 mM lycine in PBS, and eventually blocked in 1% BSA for 10 minutes. Then the samples were incubated for 2 hours with the primary antibody rabbit anti-CD81 (1:200, #10037, Cell Signaling Technology). CD81 was targeted by Protein A coupled to 10nm colloidal gold particles (G. Posthuma, University Medical Center Utrecht) (1:50).

In order o perform DAB staining of Tspan-EGFP, primary neurons were cultured on Aclar foil (Ted Pella) until DIV10. Cells were transfected with Lipofectamine2000 to express Tspan 15-EGFP. Neurons then were fixed with 4% PFA and 0,1% GA in PB. Permeabilization was carried out with ascending ethyl alcohol concentration steps (10 minutes each) as follows: 10% EtOH – 20% EtOH – 40% EtOH – 20% EtOH – 10% EtOH. The coverslips were washed with PBS and incubated for 15 minutes with 10% horse serum (HS) supplied with 0,3% bovine serum albumin (BSA) in PB. Then they were incubated overnight in PBS containing 1% PS and 0.2% BSA with goat anti-GFP-biotin (1:200).

The coverslips were rinsed in PBS, then incubated with secondary antibody rabbit anti-biotin (1:1000) in the antibody incubation buffer for 1,5 hours. After washing, the cells were incubated with ABC (Vector Labs 1:1,000) in PBS for the same time. Additional PBS washing step later, the coverslips were treated with 50 mM TRIS and reacted in diaminobenzidine (DAB)-H202 solution (Sigma) for c.a. 10 min. The samples were washed in 0.1 M sodium cacodylate buffer (pH 7.2-7.4) (Sigma-Aldrich) and fixed on ice by supplying 1 % osmium tetroxide (Science Services) for 10 minutes. The samples were dehydrated as mentioned before with a gradient of EtOH solutions and finally, they were rinsed in 100% Ethanol embedded in Epon and polymerized at 60°C for 48 hours. Sample acquisitions were achieved using 400 200kV on a JEM- 2100Plus Transmission Electron Microscope (Jeol, Germany).

3.32 Nanoparticle tracking analysis

Nanoparticle tracking analysis (NTA) was performed using a NanoSight LM14C (Malvern) to measure the concentration and size of isolated extracellular vesicle samples. Three aliquots for each sample were diluted 1:1000 in filtered (0.22µm) PBS to a final volume of 1 ml. A blank level was set by measuring the filtered (0.22µm) PBS. For each aliquot, 10 recordings were acquired to elaborate on the concentration and the size mode. For each sample, the number and size of extracellular vesicles were estimated by calculating the averages of the three aliquot mean values. The following parameters were used for the measurement (

Table 6) and the analysis (NanoSight NTA software).

Table 8 - NTA setting for extracellular vesicles detection

Camera Type:	**sCMOS**
Laser Type:	Green
Camera Level:	12
Slider Shutter:	1200
Slider Gain:	146
FPS:	25.0
Number of Frames:	249
Temperature:	23.5°C
Viscosity:	(Water) 0.920 - 0.921 cP
Detect Threshold:	7
Max Jump Distance:	(auto) 9.3 - 10.8 pix

3.33 Immunoprecipitation

Immunoprecipitation assays were performed at 4°C. 30 µl “Dynabeads Protein G” (Life Technologies, Darmstadt, Germany) were rinsed with PBS and supplied with 2-5 µg of antibody targeting the focal protein or rabbit IgG (control) for 20 min. The antibody-

coupled beads were washed with PBS and IM-Ac-buffer (20 mM HEPES, 100 mM K-Acetate, 40 mM KCl, 5 mM EGTA, 5 mM MgCl2, 1% Triton-X-100, 1x Complete Protease Inhibitor Cocktail (Roche, Mannheim, Germany), 1mM PMSF, 5 mM DTT; pH 7.2). Then they were incubated for 2h with N2A post-nuclear supernatant (S1, 1000 x g supernatant) or mouse brain endosomal vesicle enriched subcellular (P3, 100,000 x g pellet). Before the incubation, biological samples were pre-cleared with uncoupled G Dynabeads. Beads were washed with IM-Ac-buffer, and Laemmle-Urea Sample Buffer was added (10 min at +65°C). The samples were then analyzed by SDS-PAGE followed by Western Blot.

3.34 Immunofluo mGluR5 for STORM imaging

For the dual Stochastic Optical Reconstruction Microscopy (dSTORM) imaging WT and Tspan15 KO DIV15 neurons were stained as reported by (Goncalves et al., 2020) and (Haas et al., 2018). In brief, mouse anti-PSD95 (1:300) and rabbit anti-mGluR5 (1:100, extracellular epitope) was used to label the neurons. To stain the surface mGluR5, the antibody targeting the extracellular domain of the receptor was incubated on live cells at 37°C for 5 min, following fixation. Cells were fixed in 4% PFA and stained as previously described. Primary antibodies were detected with goat anti-mouse Alexa 532 (A21242, Thermo Fisher Scientific) and goat anti-rabbit Alexa 647 (A21244, Thermo Fisher Scientific). Multiple color fluorescent microspheres (TetraSpeck, Invitrogen) were used as reference markers to perform long-term acquisition (c.a. 20 min for each channel) and correct the lateral translation of the acquired field. PSD95 and mGluR5 puncta localization was obtained using WaveTracer software working as a plugin of MetaMorph software (Levet et al., 2019) The homemade PALMTracer (Metamorph Plugin) was used to reconstruct the super-resolution images with a 40 nm pixel size for lateral drift. Double-channel images (532 and 647 nm) were acquired using the identical dichroic mirror. For each color, clusters were segmented using an intensity–based threshold. Only mGluR5-positive dendritic spines were included in the mGluR5 density analysis, identified with the PSD95 marker. At the level of the postsynaptic compartment, the post-synaptic density (PSD) was identified as PSD95-

positive, while the perisynaptic space was defined as the immediately surrounding area. All analyses were performed in blind.

3.35 Primary neuron viral infection

An Adeno-associated virus (AAV) serotype PhP.eB carrying the Syn.Myc.Tspan15 construct was provided by Dr. Ingke Braren (Vector Facility Institute of Experimental Pharmacology and Toxicology University Medical Center Hamburg-Eppendorf). Primary neurons from WT hippocampal culture were then infected at DIV10.

3.36 Electrophysiology

Electrophysiological recordings were performed by Jan Schröder, blind to the genetic backgrorund. Male and female age-matched WT and Tspan15 mice were anesthetized with 80% CO2 / 20% O2 and sacrificed by decapitation. Brains were collected and incubated in ice-cold slicing solution (110 mM choline chloride, 25 mM NaHCO3, 25 mM D-glucose, 11.6 mM sodium L-ascorbate, 7 mM MgSO4, 1.25 mM NaH2PO4, 2.5 mM KCl, 0.5 mM CaCl2, pH 7.4, 305-315 mOsm/kg, saturated with 95% O2 / 5% CO2). The Brain hemispheres were divided and glued with cyanoacrylate to a Compresstome (VF-200-0Z Microtome, Precisionary Instruments). 1.2% agarose was used to sustain the tissue, and 350 µm-thick slices were harvested. Sections were incubated with artificial cerebrospinal fluid (ACSF) (124 mM NaCl, 26 mM NaHCO3, 10 mM D-glucose, 1 mM MgSO4, 1 mM NaH2PO4, 4 mM KCl, 2.4 mM CaCl2, pH 7.4, 302-305 mOsm/kg, saturated with 95% O2 / 5% CO2) for 15 minutes at 33 oC. Then, they were recovered at 30 °C for additional 45 minutes before placing them into the recording chambers (4 chamber Synchroslice, Lohmann Research Equipment), perfused with ACSF supplied with the mGluR1 inhibitor YM298198 (2 µM) (30 °C, flow rate 2.5 ml per minute). In CA1 stratum radiatum, two stimulation electrodes were located and a

recording electrode was applied in proximity to the stratum pyramidale. Stimulations (200 µs) were provided to arise field excitatory postsynaptic potentials (fEPSPs) of about 2 mV for 50 minutes every 30 s for each electrode. Input-output curves were evoked and the stimuli intensity was tuned to arise a half-maximum amplitude fEPSP. Then, the baseline was recorded for 45 min and only the last 35 minutes were analyzed. The mGluR5 agoinst DHPG was applied for 10 min at 45 min after the start of the experimentat with a working concentration of 100µM. Later the slices were incubated only in ACSF. Recordings were excluded if fEPSPs changed by more than 10% during the 35 min baseline (4 of 32 slices). For each response, the fEPSP slope was measured (30-70%). The baseline fEPSP slope is the mean from the 35 minutes immediately preceding the drug application. Slopes were normalized by dividing by the average baseline value. Plotted are the mean ± S.E.M. of the individually normalized recordings. Statistics were performed with GraphPad Prism (non-parametric). Unblinding occurred only after inclusion or exclusion of recordings from the analysis.
Statistics were performed with GraphPad Prism (non-parametric). Unblinding occurred only after inclusion or exclusion of recordings from the analysis.

3.37 Behavioral test

The Tspan15 KO line was backcrossed and kept in a C57BL/6 genetic background. Animals destined to mouse behavior investigations were generated from heterozygous mating trio schemes (two heterozygous females with one heterozygous male) Littermate mice of the same sex (e.g. brothers or sisters) were housed in couples of opposite homozygous genotype (one WT and one Tspan15 KO). Mice were hosted with a stable temperature (22 ± 1°C) and humidity (50 ± 5%) in a vivarium with an inverted 12h:12h light-dark cycle. On the homepage, the animals were maintained with

ad libitum access to water and food. Mice were 16-18 weeks old at the beginning of the behavioral investigation. All behavioral tests were conducted during the dark phase of the light cycle. All animal studies fulfilled the European Communities Council Directive (2010/63/EU) on the protection of experimental animals and guiding principles expressed by the German Animal Welfare Act.

The tests were carried out after the approval of the ethics committee of the City of Hamburg (Behörde für Gesundheit und Verbraucherschutz, Fachbereich Veterinärwesen; No. 100/2021). Experiments were conducted on male and female animals. Table 9 indicates the number of mice used per genotype.

Table 9 - Summary of animals involved in behavioral experiments

	WT	Tspan15 KO
Male (M)	10	10
Female (F)	14	14

Focal mice destined for behavioral experiments were previously observed in the home cage environment as described in (Freitag et al., 2003) For this porpoise, a tail mark was applied to the WT and Tspan15 KO cagemates with non-toxic dye on the precedent day. In brief, their behavior in the home cage was annotated for 1 hour to evaluate the spontaneous home cage activity. These observations were also conducted following the cage change to assess the social behavior between cage mates, with a main focus on the dominant-submissive dynamics.

After the spontaneous observations, the mice accomplished the behavioral test reported in Table 10:

Table 10 - Overview of behavioral experiments

Test name	Sex	Test focus	Stress	Reference
Open field	M,F	Locomotor skills, anxiety, exploratory behavior	Low	(Schob et al., 2019)
Elevated plus maze	M,F	anxiety	Low	(Freitag et al., 2003)
Social recognition test	M,F	Social skills	Mild	(Muhia et al.,

				2022)
Urine marking test	M	Social skills, dominant behavior	Mild	(Fellini & Morellini, 2013)
Urine detection test	F	Social skills, social differentiation	Mild	-
Marble burying test	M,F	Obsessive-compulsive behavior	Mild	(Deacon, 2006b)
Focal mice single-caging				
Nesting test	M,F	Nesting behavior	High	(Deacon, 2006a)
Resident-Intruder test	M	Aggressive and dominant behavior	Severe	(Schob et al., 2019)

3.38 Open Field

The Open Field test was carried out as reported by (Schob et al., 2019). Focal animals were accommodated in the arena (50 x 50 x 50 cm) free to explore. The movement was tracked for 30 min and subdivided for the analysis into time bins of 5 minutes. The distance moved, mean minimal distance to the wall, and time spent in the central zone (a 25×25 cm square located in the center of the arena) were analyzed using the EthoVision software.

3.39 Elevated plus maze

The elevated plus maze test has been performed as reported in precedence (Freitag et al., 2003) The elevated plus maze presents, four arms, two open and two closed, joined as a cross, with a central square. In brief, the animals were moved to the central square and placed toward an open arm. Mice were free to explore the maze for 5 min. the Ethovision tracking software was used for the tracking and analysis of behavior.

3.40 Social novelty preference test

The social novelty preference test was performed to investigate the social abilities of Tspan15 KO mice. As described in (Muhia et al., 2022), initially the focal animal was moved to the empty arena (50 x 50 x 50 cm) and habituated to the arena environment

for 5 minutes (habituation phase). Then, two cage-chamber were added to the arena and placed at opposite corners. A first cage was used to allocate the first sex-matched age-matched partner mouse, while the second cage chamber remained empty. At this point, the focal mouse was left free to explore the chambers and familiarize itself with the partner mouse for 10 minutes (familiarization phase). In the end, the cage chambers were moved to the other two opposite corners and also the second partner mouse was placed into the empty cage chamber. The focal mouse location and movement were tracked for 10 minutes (testing phase). Later, the discrimination index was calculated (formula 2) to assess the social preference of the focal mouse toward the familiar and the unfamiliar partner mice.

$$Discrimination\ index = \frac{Unfamiliar\ partner\ time - familiar\ partner\ time}{Unfamiliar\ partner\ time + familiar\ partner\ time}$$

The discrimination index can range from −1 to +1, suggesting respectively a preference for the familiar mouse or the unfamiliar partner mouse.

3.41 Urine marking test

The social dominance and territoriality of male mice were assessed through the urine marking test. As reported by (Fellini & Morellini, 2013), the arena (50 x 50 x 50 cm) was prepared by placing a 50 x 50 cm Whatman filter paper (grade 4) on the ground surface. Then three WT female mice were allocated behind a fenestrated plexiglass separè at one corner of the arena (50 x 50 x 50 cm). The focal male mouse was introduced in the arena and left free to explore and interact with the females through the separé fenestrations for 30 minutes. In the end, Whatman filter paper was collected and placed under UV light to count the biological stains. These latter were subdivided by shape and size. In the first category, the urine marks can be recognized as a tiny couple of puncta (1mm) or parallel thin lines, which are left by the mouse as traces rich in pheromones. A second category is represented by urine spots and larger and circular urine stains. Urine marks and spots were counted either for the total surface or per quadrant.

3.42 Urine detection test

Whatman paper with urine marks and spots from three WT male mice was placed in a fenestrated plastic dish (diameter 4 cm). The plate was allocated in a corner of the arena (50x50 cm). Female mice were introduced into the arena and left free to explore for trials of 5 minutes. At the end of each trial, the Whatman paper was substituted with a new one bringing urine marks and spots belonging to the same set of male mice. For the last trial, the urine marks and spots were selected from a different of set WT males.

3.43 Marble Burying test

The marble burying test was performed as previously reported by (Deacon, 2006b). In brief, the mice were placed in a fresh cage under 10 lux light conditions. The cage was previously provided with bedding pellets (5 cm in height) and 20 beads of black color were placed on the pellet surface. The beads were collocated on five rows and four columns at equal distances. The number of buried beads was annotated during the 30 minutes of the test. Only beads that were buried for more than half were counted.

3.44 Nest building test

A week before the test a new nesting material made of cotton was introduced to the mice. This allowed the mice to familiarize themselves with the nesting test material before the test. At the beginning of the active phase (1 hour before the light switch off), then the mice were single-caged in a fresh cage presenting 3.0 grams of nest-building material. After 12 hours, the nesting activity was evaluated by the percentage of the quantity of material used.

3.45 Resident Intruder

The resident intruder test was carried out as reported by (Schob et al., 2019)). Male focal mice were socially isolated for 72 hours. The cage top was replaced with a fenestrated Plexiglas panel and the nest was removed. The focal mouse was left to habituate for 5 min and then a WT C57Bl/6J age- and body-weight-matched unfamiliar male, i.e. the intruder, was introduced into the cage of the focal animal, i.e. the resident.

The mice's behavior was video recorded for 10 min. The social interaction analysis was performed with "The Observer" software after the experimenter trained himself until reaching 80% of consistency in the Reliability Test.

3.46 Statistical analysis

Graph generation and statistical analysis were performed with the Prism software (GraphPad, version 9.0.1). If outliers were detected, the related GraphPad algorithm was applied to the entire dataset. Data are shown as mean ± S.E.M. unless differently specified.

3.47 List of solutions

List 1 - Solutions

Solution	Chemical composition
2XHBS	280mM NaCl / 10mM KCl / 1.5mM Na_2HPO_4 / ddH_2O / 12mM dextrose / 50mM HEPES /pH=7.5 adjusted with 0.5M NaOH.
10X PBS	1.37M NaCl / 27mM KCl / 100mM Na_2HPO_4 / 18mM KH_2PO_4
10X SDS-Running Buffer	250mM Tris / 2.5M Glycine / 15% SDS / fill up to 1L with ddH_2O / pH=8.3
10X TBS-T	200mM Tris-Base / 1.5M NaCl / 1% Tween
50X TAE	For 1L 242g Tris-Base / 57.1ml glacial Ac. Acid / 0.5M EDTA pH=8
4X Laemmli Loading Buffer	250mM Tris pH=8.8 / 8%SDS / 20%Glycerol / DTT400mM / 0.2%Bromophenol Blue / 48%Urea
$CaCl_2$	1M $CaCl_2$
Time-lapse Imaging HEPES Buffer	10mM HEPES / pH=7.4 / 135mM NaCl / 5mM KCl / 2mM $CaCl_2$ / 2mM $MgCl_2$ / 15mM Glucose

IF Antibody incubation buffer	PBS / 1% BSA
IF Blocking Buffer	PBS / 1% BSA
IF Fixation Buffer	PBS / 4% Formaldehyde / 4% sucrose
IF Permeabilization Buffer	PBS / 0.2% Triton X-100
PBS/Triton Lysis Buffer	PBS / Triton X-100 1% + prot./phosp. inhibitors
PBS-Glucose Buffer	PBS /
Perfusion buffer	PBS / 4% PFA / 0.1 Glutaraldehyde
Saline	ddH_2O / 0.09% NaCl
SDS-Transfer Buffer	25mM Tris / 192mM Glycine / 20% MeOH
Sucrose Buffer 1	320mM Sucrose / 1mM $NaHCO_3$ / 1mM $MgCl_2$ / 500mM $CaCl_2$ / 1mM PMSF
DHPG incubation buffer	145mMNaCl / 10mM HEPES / C6H12O6 / 2.5mM KCl / 1mM MgCl2 / CaCl2 / pH=7.4 adjusted with 0.5M NaOH.
IM-Ac buffer	20mM HEPES / 100mM CH_3CO_2K / 40mM KCl / 5mM EGTA / 5mM $MgCl_2$ / 1mM PMSF / 5mM DTT + prot./phosp. Inhibitors / pH=7.2 adjusted with 0.5M NaOH.
Blotting Buffer (Semidry)	25mM Tris / 150mM Glycin / 20%MetOH
Blotting Buffer (Wet)	48mM Tris / 39mM Glycin / 0.037%SDS % / 20%MetOH
Sucrose Buffer 2	320mM Sucrose / 1mM $NaHCO_3$
Sucrose gradient	1M sucrose / 1mM $NaHCO_3$ + 1.4 M sucrose /1mM $NaHCO_3$

PSD insoluble fraction resuspension buffer	40mM Tris-HCl pH=8.0
2xTX buffer	1%Triton-X / 12mM Tris/HCl pH=8.0 / 320mM sucrose
Stripping Buffer	25mM Glycine / 1%SDS / pH=2.0

3.48 List reagents

List 2 - Additional reagents

Reagent	Catalog #.	Company
(RS)-3,5-DHPG	0342	R&D Systems
Aqua Poly Mount 1	18606-20	Polysciences, Eppelheim
Acrylamide/Bis- acrylamide	A2917	Sigma-Aldrich
Ampicillin sodium salt	K029.1	Carl Roth GmbH and Co. KG,
Ammonium persulfate (APS)	9592.1	Carl Roth GmbH and Co. KG,
BSA	A3156	Sigma-Aldrich
DH5-alpha	C2989K	New BioLabs, England
DiI	C7000	Thermo Fisher
3,3′-Diaminobenzidine tetrahydrochloride hydrate	D5637	Sigma-Aldrich
1,4-Dithiothreit (DTT)	6908.2	Carl Roth GmbH and Co. KG,
DMEM	61965026	Thermo Fisher
DNA ladder	15615-016	Invitrogen
dNTPs	U1240	Promega
Ethanol	9065.4	Carl Roth GmbH and Co. KG,
Ethanol, denatured	2211-	Chemsolute
Paraformaldehyde (PFA)	335.3	Carl Roth GmbH and Co. KG,
HBSS	14170-088	Invitrogen
Glutaraldehyde (GA)	G5882	Sigma-Aldrich
Hibernating medium-E	A12476-01	Thermo Fisher
Phenylmethylsulfonyl fluoride (PMSF)	6367.1	Carl Roth GmbH and Co. KG,

Isopropanol	6752.2	Carl Roth GmbH and Co. KG,
Kanamycin A	T832.3	Carl Roth GmbH and Co. KG,
Phosphatase inhibitors set	04906845001	Sigma-Aldrich
Pierce ECL Western Blotting Substrate	32106 / 32109 / 32209	Thermo Scientific
Sodium dodecyl sulfate	L4509	Sigma-Aldrich
PNGM	cc-4462	Lonza
Poly-D-Lysine	P7886	Sigma-Aldrich
Protease complete inhibitors mini	04693132001	Sigma-Aldrich
Protease inhibitors set	1206893	Roche
TEMED	T9821	Sigma-Aldrich
Triton X-100	3051.2	Carl Roth GmbH and Co. KG
Protein ladder	MWP04/03	NIPPON Genetics
PVDF Blocking Reagent for Can Get Signal	TYB-NYPBR01	Cosmo Bio LTD
Rhodamine Phalloidin	PHDR1	Cytoskeleton
Trypsin/EDTA	25300054	Invitrogen

3.49 List of antibodies

List 3 - Antibodies

Antibody	Catalog #.	Company	Application
donkey anti-rabbit Alexa Fluor® 488	#711-545-152	Dianova	ICC 1:1,000
Goat anti-GFP biotin-tagged	#600-106-215	Rockland™	DAB 1:100

donkey HRP-conjugated anti-mouse IgG	#715-036-15	Dianova	WB 1:15,000
donkey HRP-conjugated anti-rabbit IgG	#711-036-152	Dianova	WB 1:15,000
rabbit anti-biotin	#100-4198	Thermo Fisher	DAB 1:1,000
Mouse anti-GAPDH (6C5)	#GTX28245	GeneTex	WB 1:1,000
mouse anti-GM130	#610823	Biosciences	WB 1:500
mouse anti-TSG101 (4A10)	#GTX70255	GeneTex	WB 1:1,000
rabbit anti-CD81	#10037	Cell Signaling Technology	WB, 1:1,000 Nanogold EM 1:200
rabbit anti-GFP	#A-11122	Thermo Fisher	WB/ICC 1:1,000
Tspan15 (t2ct)	Provided by Prof. Saftig	Custom produce by Pineda	WB 1:500
Guinea Pig anti-EEA1	#237-105	Synaptic System	ICC 1:300-500
Donkey anti-guinea pig Cy5	706-175-148	Jackson Immunoresearch lab.	ICC 1:1000
Mouse cMyc 9E10	MA1-980	Thermo Fisher	ICC 1:100-1:500
Rabbit Anti-Myc	C3956	Sigma-Aldrich	ICC 1:300 -1000
Mouse Anti-Shank1	162 121	Synaptic System	ICC 1:200 -1:500
Mouse anti-PSD95	MA1-046	Thermofisher	ICC 1:300 WB 1:300-1:1000

Guinea Pig Anti-Synaptophysin1	101 004	Synaptic System	WB 1:1000
Mouse Anti-GluA2 (64C)	#MAB397	Millipore	WB 1:500-1:1000
Rabbit anti-Actin	A2066	Sigma-Aldrich	WB 1:500-5000
Rabbit Anti-mGluR5 (D6E7B)	#55920	Cell Signaling Technology	WB 1:500-1:1000
Rabbit anti-mGluR5	AGC-007	Alomone Labs	ICC 1:300-1:500 Live ICC1:50-1:100
Mouse anti-Gamma-Adaptin	610386	BD Transduction Lab	WB 1:2000
Mouse Rab11 GTPase	#2414	Cell Signaling Technology	WB 1:1000
Rabbit anti-ERK1/2	#bs-0022R	Bioss	WB 1:500-1:1000
Rabbit anti-pERK1/2	#44-680G	Thermo Fisher	WB 1:500-1:1000
Alexa Fluor Goat Anti-mouse 532	#A11002	ThermoFisher	ICC 1:1000
donkey HRP-conjugated anti-Guinea Pig IgG	706-035-148	Dianova	WB 1:1000

3.50 List of Plasmids

List 4 - Plasmids

Construct	Catalog #.	Provider	Reference
pEGFP-N2	#6081-1	Clontech	-
CD63-mCherry	-	Prof. Dr. Nicole Meisner-Kober	Corso et al., 2019
CD63-EGFP	62964	Addgene	-

Tspan15-EGFP	-	Prof. Dr. Eric Rubinstein	Dornier et al., 2012
Syn.Myc.Tspan15		*subcloned*	
mCherry-mGluR5	-	Prof. Dr. Brismar	Westin et al., 2014
CFP-Rab11	-	Dr. Kira Gromova Brune	-
Ruby3	-	Prof. Dr. Mikhaylova	-

Table 11 – List of Fluorescent Dyes

Construct	Catalog #.	Provider
DAPI	D9542	Sigma-Aldrich
DiI	C7000	Thermo Fisher
Phalloydin	PHDN1	Cytoskeleton

4 Results

4.1 Tspan15 localizes in the plasma and intracellular membranes at the dendrites

It has been extensively established that tetraspanins are present on several types of membranes and work as molecular facilitators for a broad range of biological processes (Levy & Shoham, 2005). To elucidate the role of Tspan15 in hippocampal neurons, the subcellular localization, and enrichment of Tspan15 were investigated with biochemical, live-imaging, and immunocytochemical assays. At first, a differential centrifugation protocol was performed on hippocampal homogenate to isolate a total lysate (S1), a plasma membrane-enriched fraction (P2), and an intracellular membrane-enriched fraction (P3). Western blot analysis on different fractions showed enrichment of Tspan15 protein in the endosomal compartment (Figure 16A).

In addition, due to the lack of a specific antibody working in immunocytochemistry, hippocampal neurons were infected with an AAV.Syn.Myc.Tspan15 viral construct.

In accordance with the previous biochemical data, it was observed a vesicular-like pattern in the dendrites (Figure 16B). This pattern was further confirmed by live-cell imaging of neurons transfected with Tspan15-EGFP, and the volume marker Ruby3. Interestingly, Tspan15-EGFP+ vesicle-like particles were observed moving along the dendrite passing by the spines neck (Figure 16C).

Altogether, this data suggest that in neurons Tspan15 localizes at the plasma membrane and potentially at the vesicular compartments in the dendrites.

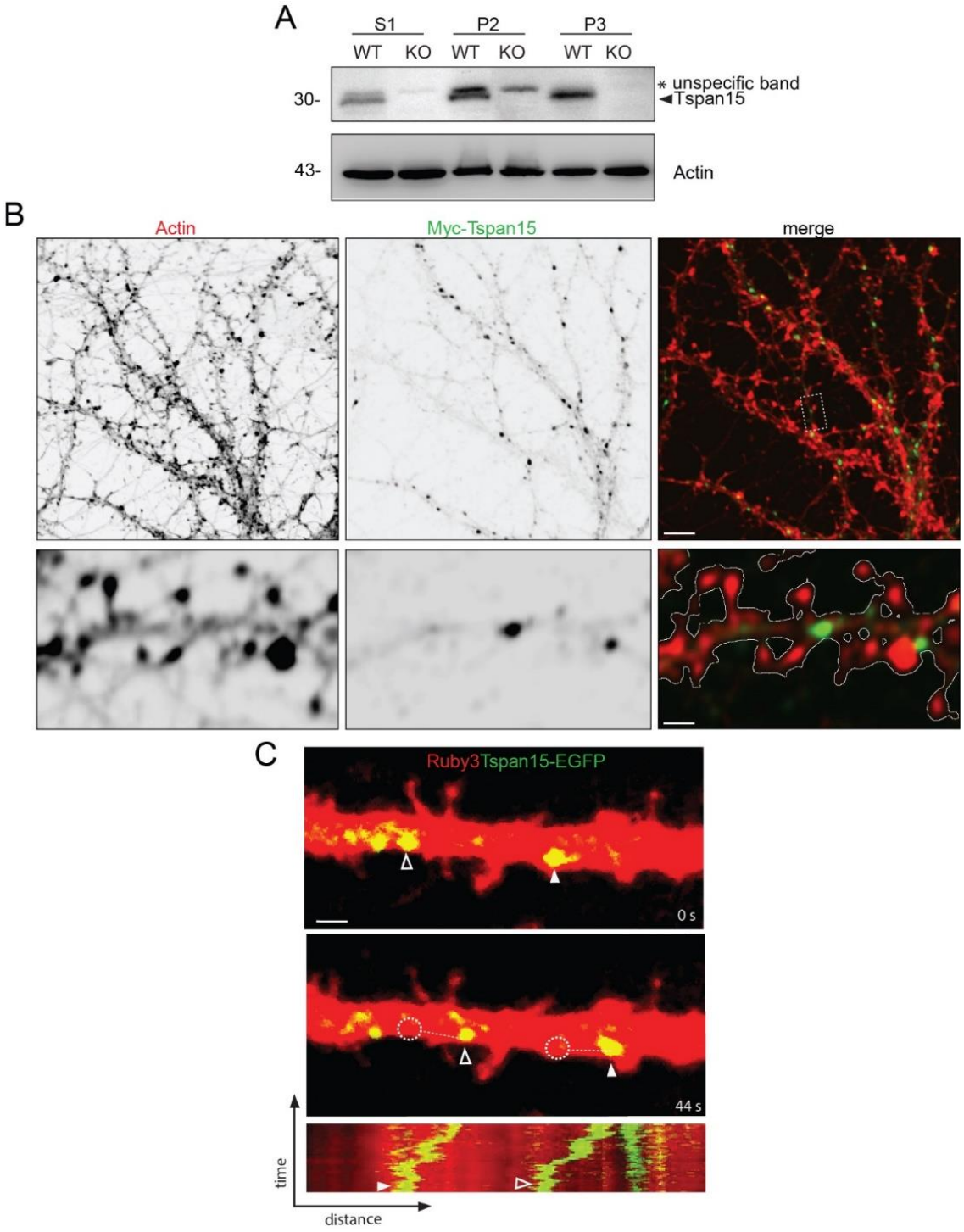

Figure 16 - Tspan15 localizes in the plasma and intracellular membranes at the dendrites

(**A**) A differential centrifugation protocol was applied on hippocampal homogenates to isolate from the total lysate (S1) , a plasma membrane-enriched fraction (P2) and an intracellular membranes-enriched fraction (P3). Western blot showed enrichment of endogenous Tspan15 protein in the P2 and P3 fractions. *: unspecific band. (**B**) Hippocampal neurons infected with the AAV.Syn.Myc.Tspan15 construct showing immunostaining of F-actin (red) and the Myc tag (green). In accordance with the previous biochemical data, Myc.Tspan15 displays a vesicular-like pattern in the dendrites. Scale: 10µm . Inset from dashed white box. Scale: 1µm (**C**) Cell-live imaging of neurons transfected with Tspan15-EGFP (green), and the volume marker Ruby3 (red). Scale: 2µm. At the bottom, kymograph showing the movement from time:0 to time:44 seconds of two different Tspan15-EGFP+ vesicle-like particles (full and empty arrows).

4.2 Tspan15 is present in the postsynaptic compartment but absent from the PSD core zone in neurons

Furthermore, immunostaining of Myc-Tspan15 revealed the presence of this protein in the dendritic spine head and colocalization with the post-synaptic scaffold protein Shank1 (Figure 17A). Synaptosomal fractions from mouse hippocampus demonstrated that Tspan15 is absent from the synaptosomal detergent-insoluble fraction, partially representing the PSD zone, but it is expressed in soluble l fraction (Figure 17B). Taken together, these data suggest that although Tspan15 is not expressed in the PSD, but can potentially localize in the post-synapse of dendritic spines.

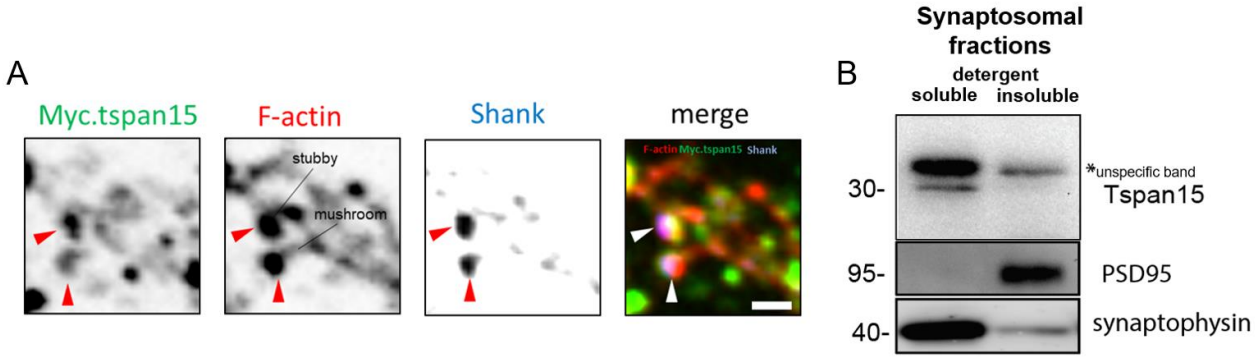

Figure 17 – Myc.Tspan15 localizes at the postsynapse, but is absent from the PSD core

(**A**) Labeling of F-Actin (red), Shank (blue), and Myc.Tspan15 (green) in dendritic spines of DIV15 hippocampal neurons. (**B**) Tspan15 expression in synaptosomal detergent-soluble and –insoluble fractions, validated respectively with PSD95 and synaptophysin enrichment. n: 3 hippocampal WT lysates. N: 3 inpendent biochemical preparations.

4.3 Tspan15 KO CA1 pyramidal neurons present morphological abnormalities at the apical dendritic tree

Since Tspan15 resulted in highly expressed in the vesicles-like particles and the postsynaptic compartment of neuronal dendrites (Figure16, Figure17), the morphology of CA1 hippocampal pyramidal Tspan15KO neurons was investigated to find if ablation

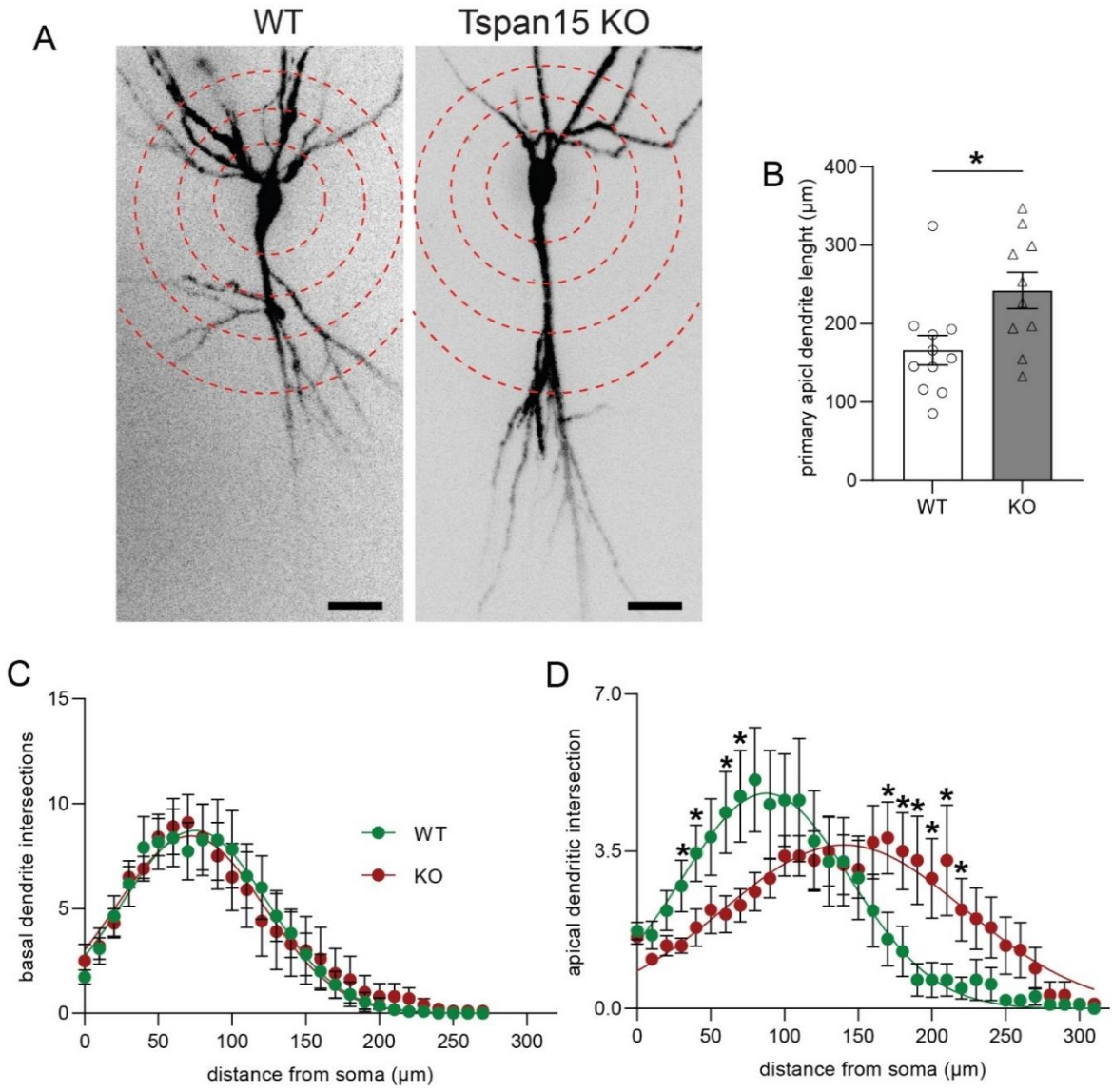

Figure 18 - Tspan15 KO CA1 pyramidal neurons present morphological abnormalities at the apical dendritic tree

(A) DiI stained CA1 pyramidal WT and Tspan15KO neurons. (B) Quantification of primary apical dendritic length. (C, D) Sholl analysis of reconstructed neurons revealed an altered apical, but not basal dendritic tree for Tspan15 KO neurons. Statistical significant was assessed with a t-Student test. p: <0.05 (*). n = 11 neurons (WT), n = 11 neurons (Tspan15KO). N: 3 mice per genetype.

of Tspan15 can affect the structure of the dendritic arbor and spines. To achieve this goal, Hippocampal slices from WT and Tspan15KO mice were labeled with (DiI), a lipophilic dye able to emit fluorescence light and diffuse in biological membranes (Figure 18A). Sholl analysis of the apical dendrites (Figure 18D), but not the basal (Figure 18C) dendritic tree from the reconstructed neurons indicated abnormalities for the Tspan15 KO genetic background. Tspan15KO pyramidal neurons present a longer primary apical process (Figure 18B) which originates a shift for the entire apical dendritic arbor to a more distal position.

4.4 Tspan15 KO CA1 pyramidal neurons show altered spine density

With an analogous approach as above, the morphology of dendritic spines in WT and Tspan15KO neurons was investigated (Figure 19A), specifically focusing on non-primary apical dendrites. Tspan15 KO neurons presented higher total spine density, originating from the thin and stubby classes (Figure 19B). In conclusion, this data potentially indicate Tspan15 ablation provokes morphological alterations in CA1 pyramidal neurons in the apical dendrites.

4.5 mGluR5 subcellular distribution is altered upon Tspan15 depletion

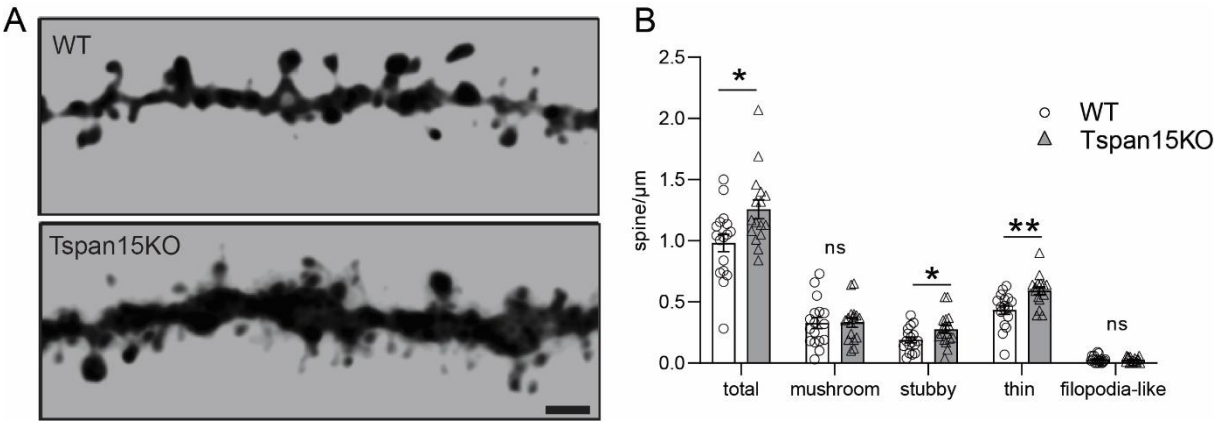

Figure 19 - Tspan15 ablation correlates with dendritic spines abnormalities

(A) Non-primary dendritic branches from DiI-stained CA1 pyramidal WT and Tspan15KO neurons.Scale: 2µm (B) Quantification of dendritic spine density from experiment A. Statistical significant was assessed with a t-Student test. p: <0.05 (*). p: <0.01 (**). n = 17 dendrites (WT), n = 16 dendrites (Tspan15KO) N: 3 mice per genotype. Outliers were identified and removed with GraphPad algorithm.

Given the above-reported subcellular localization of Tspan15 and the dendritic spines' morphological abnormalities in Tspan15KO neurons, one could hypothesize that this phenotype can potentially correlate with an altered expression and/or subcellular distribution of synaptic receptors. GluA2 and mGluR5 represent two synaptic receptors and well-known synaptic plasticity players. Therefore their total expression and subcellular distribution were biochemically quantified in WT and Tspan15 KO genetic backgrounds. For both receptors, the total expression in brain lysate (S1 fraction) was unaltered upon Tspan15 depletion (Figure 20A-D). However, while GluA2 subcellular distribution showed no difference (Figure 20E, F), mGluR5 distribution into the intracellular membrane-enriched (P3) fraction resulted in a decrease in Tspan15 KO mice (Figure 20G, H).

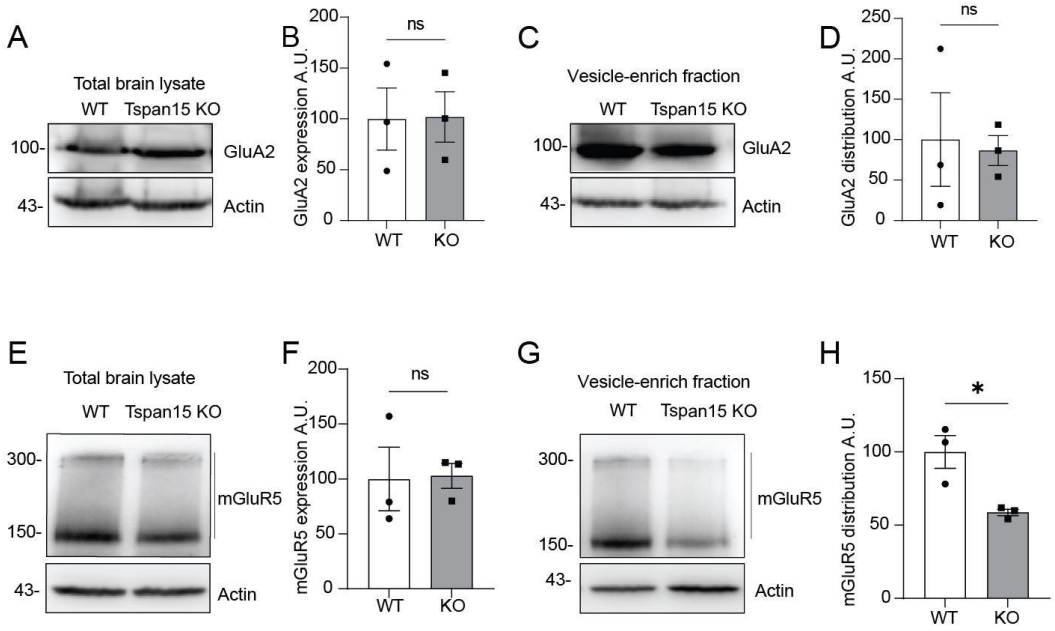

Figure 20 - mGluR5 subcellular distribution is altered in Tspan15 KO mice

Western Blot membranes showing total expression in brain lysate for (A) GluA2 and (E) mGluR5 in WT and Tspan15 KO samples. (B, F) Quantification from experiments A and E. No difference was observed in both receptors for the total expression. (C, G) GluA2 (C) and mGluR5 (G) distribution in the intracellular membranes-enriched fraction (P3). (D, H) Quantification for C and G. Statistical significant was assessed with a t-Student test. p: <0.05 (*). n = 3 WT and Tspan15KO mouse brains. N = 3 independent preparations.

4.6 Tspan15 interacts and co-transported with mGluR5

Since the differential centrifugation demonstrated an altered subcellular distribution of mGluR in absence of Tspa15 (Figure 20), it was then tested whether Tspan15 represents a novel binding partner of mGluR5. To answer this question at first hippocampal neurons were infected with the Syn.Myc.Tspan15 construct and immunostained for c-Myc, F-Actin, and mGluR5. Interestingly, Tspan15 and mGluR5 showed colocalization as suggested by the fluorescence intensity line plot and Pearson´s correlation coefficient (R:0.53) (Figure 21A). Furthermore, mCherry-mGluR5 and Tspan15-EGFP were expressed and imaged in live hippocampal neurons. The two tagged proteins were observed in co-transport along the dendrite as shown by the kymograph (Figure 21B).

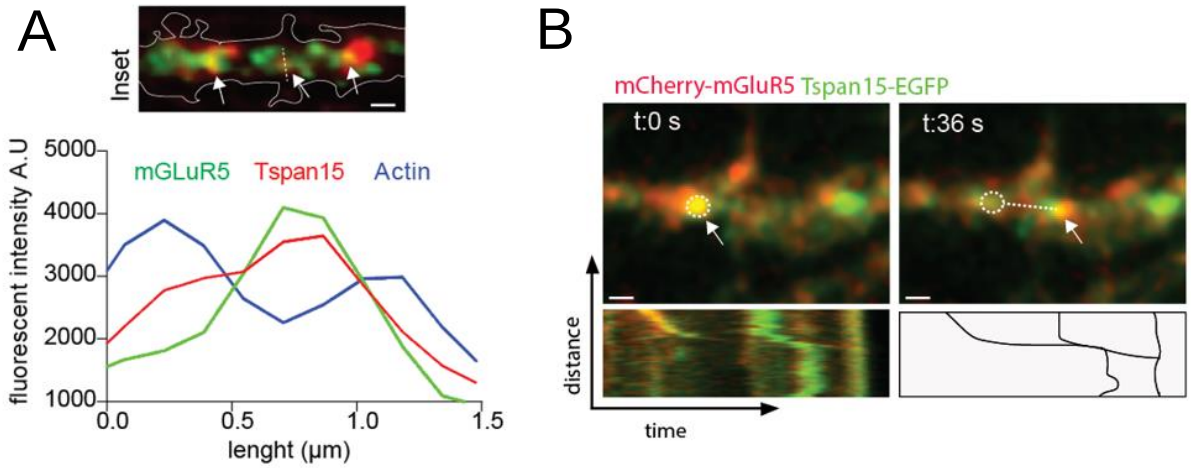

Figure 21 - Tspan15 colocalizes with mGluR5

(A) Labeling of Myc.Tspan15 (red) and endogenous mGluR5 (green) show positive degree of colocalization (Person´s coefficient: 0.53) in DIV15 neuronal dendrites. White arrows point cololization clusters. Line-scan show fluorescent intensity for the different channels along the dashed white line N: 3 independent experiments. (B) mCherry-mGluR5 and Tspan15-EGFP cotrasport in neuronal dendrites.

4.7 Tspan15 and mGluR5 are co-trasported on Rab11-positive endosomal vesicles

Endocytosis and recycling to the plasma membrane are crucial for activity recovery upon desensitization of GCPRs.To properly replace the pool of receptors previously activated, mGluR5 is known to recycle through Rab11-positive vesicles. The occurrence of Tspan15 interaction with mGluR5 in Rab11-positive endosomes was assessed by expressing mCherry or mCherry-mGluR5 and GFP or Tspan15-EGFP in N2A cells. GFP immunoprecipitation not only confirmed Tspan15 binding with mGluR5 but interestingly showed co-immunoprecipitation of endogenous Rab11. (Figure 22A)

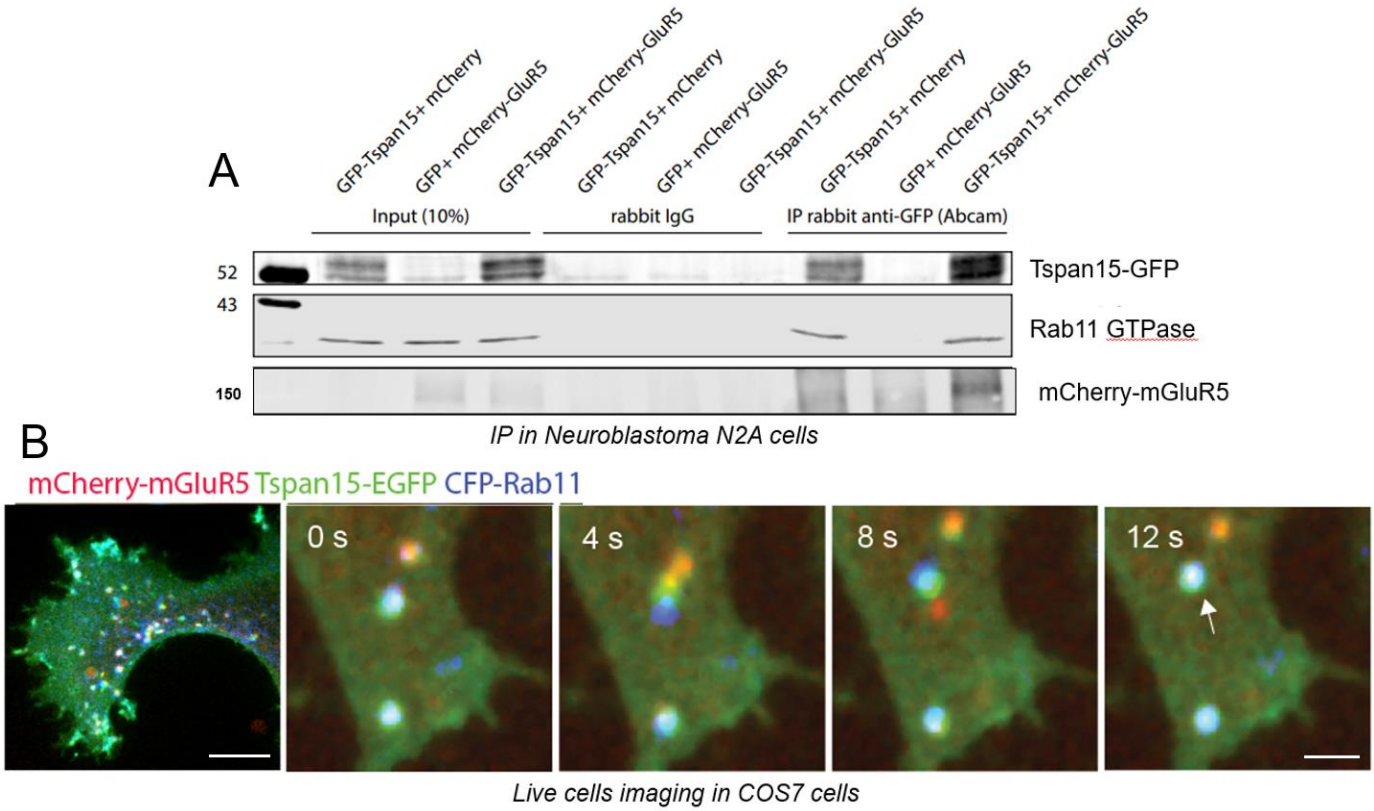

Figure 22 - Tspan15 interacts with Rab11 GTPase and mGLuR5

(A) GFP immunoprecipitation assay from N2A cotransfected with Tspan15-GFP/GFP control and mCherry-GluR5/mCherry control. (B) Cell-live imaging of COS7 cotransfected with mCherry-mGluR5, CFP-Rab11 and Tspan15-GFP. Left panel: overview. Scale: 10µm. Inset panels, scale: 5µm. White arrow indicates triple-colocalization.

Experiment performed in collaboration with Mr. Christoph Janiesch (Kneussel Lab, ZMNH). In addition, also an expression of Tspan15-EGFP, mCherry-mGluR5, and Rab11-CFP in COS7 cells revealed triple-colocalization and co-transport (Figure 22B), confirming the occurrence of this protein complex.

4.8 mGluR5 redistributes from the perisynaptic space to the post-synaptic density in Tspan15 mice

Localization of mGluR5 at the periphery of the PSD zone is crucial for their correct recycling trafficking and functional activity (Figure 2Figure 5). Therefore, detergent-soluble and -insoluble fractions from WT and Tspan15 KO hippocampal synaptosomes were isolated. Validation of the biochemical preparation was performed by observing respectively an absence and an enrichment for PSD95 (Figure 23A). Then the expression of mGluR5 was detected in the synaptosomal insoluble fraction, representing the post-synaptic density zone. Interestingly, it was found 2.5–be fold more enriched upon Tspan15 depletion (Figure 23B, C), suggesting receptor redistribution. In addition, double immunolabeling of endogenous PSD95 and surface mGluR5 combined with dual-color Stochastic Optical Reconstruction Microscopy (dSTORM) imaging was performed in collaboration with the research group of Prof. Dr. Daniele Choquet, Dr. Eric Hosy and Dr. Hanna Ziegert (Figure 23D). Compared to WT, in Tspan15 KO neurons the surface mGluR5 density is not only strongly increased at the PSD synaptic zone, represented by the PSD95 cluster area (Figure 23E, H), but also depleted at the perisynaptic zone (Figure 23E, G) and overall at the post synapses (Figure 23E, F). Altogether, this data suggest that in the absence of Tspan15, the surface mGluR5 density is diminished at dendritic spines and that it mislocalizes at the synaptic zone (Figure 23I).

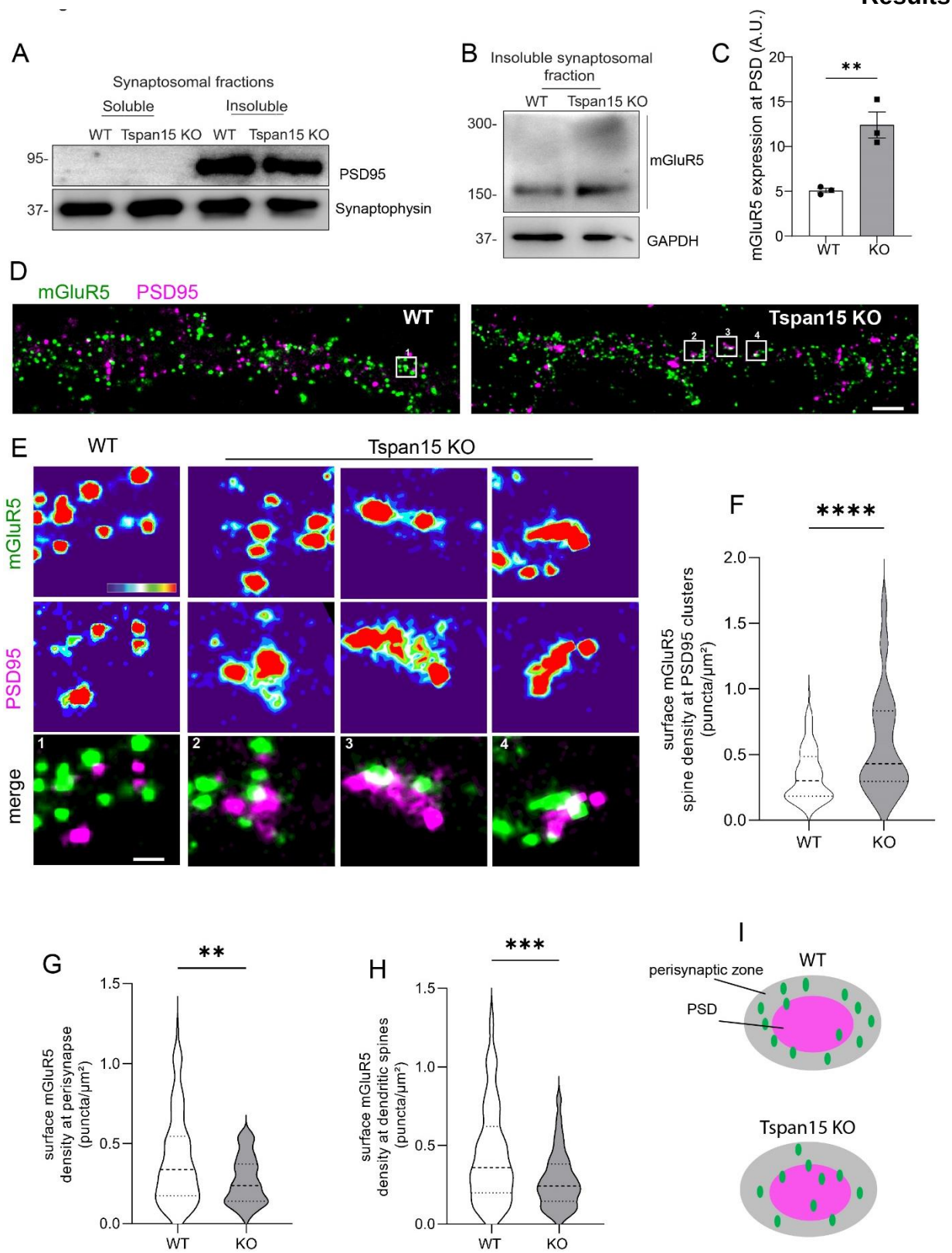

Figure 23 - mGluR5 redistributes from perysnapse to post-synaptic density in Tspan15KO mice

(A) Biochemical validation of synaptosomal detergent-soluble and –insoluble fractions. (B) Western Blot membrane of synaptosomal detergent-insoluble fractions probed for mGluR5 and GAPDH. (C) Quantification from B. Statistical significant was assessed with a t-Student test. p: <0.01 (**). n = 3 WT and Tspan15KO hippocampi N: independent synaptosomal preparations. (D) Labeling of endogenous surface mGluR (green) and total PSD95 (magenta) in dSTORM imaging. (15 µm). (E) Inset from WT (#1) and Tspan15 (#2-5) from experiment D. Single channels in thermal color LUT. Scale: 1µm. (F-H) Quantification from experiment D for

mGluR5 density. (F) in dendritic spines n = 110 spines (WT), n = 71 spines (Tspan15KO); (G) in the perisynaptic space n = 125 spines (WT), n = 58 (Tspan15KO); (H) in the postsynaptic density n = (WT). (I) Schematic of the mGluR5 distrubution at the WT and Tspan15KO postsynapse n = 110 spines (WT), n = 65 spines (Tspan15KO). Statistical significant was assessed with a Welchs´s t-test after identification and removal of outliers with the GraphPad integrated algorithm. p: <0.01 (**). p: <0.001 (***). p: <0.0001 (****). All experiment and analysis were performed by Daniele Stajano. dSTORM imaging was carried out at the Bordeux Neurocampus imaging facility. Technical support was provided from Dr. Hanna Ziegart. Dr. Eric Hosy performed super-resolution reconstruction. (Prof. Choquet Research Group).

4.9 Tspan15 expression facilitates the activation-dependent endocytosis of mGluR5

Our previous data suggest that the co-transport of mGluR5 and Tspan15 is relevant for the subcellular distribution of the receptor between the post-density and the recycling compartment. Hence, potential alterations of mGluR5 signaling were assessed at the functional level in Tspan15 KO mice. At first, surface mGluR5 was immunostained and the fluorescence intensity was compared in WT and Tspan15 KO hippocampal neurons upon the saline solution (control) or DHPG agonist treatment (Figure 24A).Although at control conditions no abnormalities were observed for Tspan15 KO neurons, while WT neurons exhibited a significant decrease in surface mGLuR5 fluorescence intensity, in Tspan15 neurons the surface receptor pool resulted unaffected following the DHPG stimulation (Figure 24B).

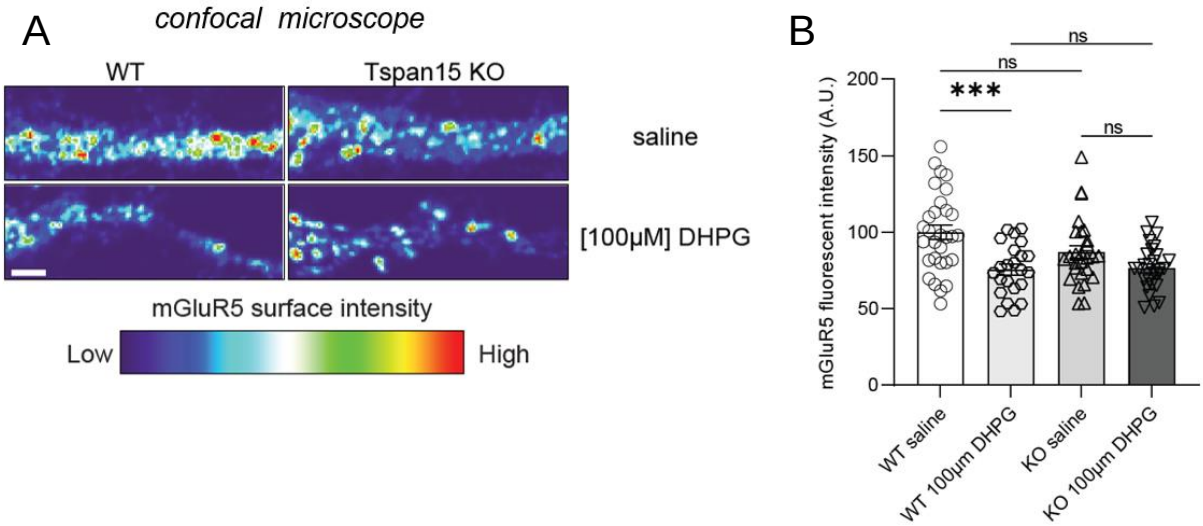

Figure 24 - Tspan15 expression facilitates the activation-dependent endocytosis of mGluR5

(A) Hippocampal WT and Tspan15KO mouse apical main dendrites labeled for the endogenous surface mGluR5 treated with saline control solution (top panels) or with [100µM] mGluR1/5-specific agonist DHPG (bottom panels). (B) Quantification from A. Outliers were identified and removed using the GraphPad integrated algorithm. Welch´s ANOVA test and post-hoc Dunnet Test were used to assess statistical significance. p:< 0.001 (***). n = 30 dendrites (WT saline), 23 dendrites (WT DHPG), 26 dendrites (Tspan15KO saline), 27 dendrites (Tspan15KO DHPG). N: 3 independent experiments.

4.10 mGLuR5-dependent LTD is altered by the lack of expression of Tspan15

Next, an electrophysiological approach was performed in collaboration with Dr. Christine Gee and Mr. Jan Schröder (Oertner Lab, ZMNH) to understand whether the mGLuR-mediated long-term depression is influenced by the expression of Tspan15. Acute hippocampal slices from WT and Tspan15 KO mice were investigated under the administration of YM298198, a specific inhibitor of mGluR1. This treatment permitted the isolation of the contribution of mGluR5 to the mGluR-dependent LTD upon DHPG stimulation. In the hippocampal formation, the Schaffer collaterals activity from the CA3-CA1 circuit was recorded (Figure 25A). Initial registration at the basal condition of the Input-Out curve shows that current stimulations of similar intensity evoke an equal fEPSP in the Tspan15KO and WT slices. In addition, although upon DHPG treatment an initial depolarization has been observed for both genetic backgrounds, Tspan15 KO

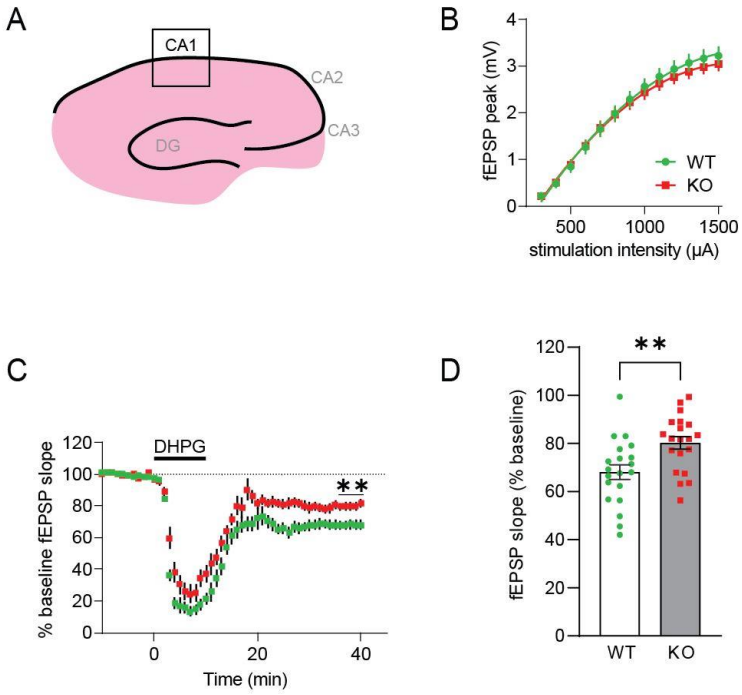

Figure 25 - The mGLuR5-dependent LTD is altered by the lack of expression of Tspan15

(A) Schematics representation of electrophysiology experimental setup in mouse hippocampal acute slices. Stimulating electrode was located in the middle of CA1 *stratum radiatum* and the recording electrodes were placed in the *stratum radiatum* above the cell body layer. Generated by Daniele Stajano. (B) Input-Output curve from WT and Tspan15KO mice. n = 28 fEPSPs/14 slices/5 mice per genotype. (C) fEPSP recording upon treatment of WT and Tspan15KO slices with mGluR1/5-selective agonist DHPG and the mGLuR1 antagonist LY367385. (D) Quantification of fEPSP slope from last 5 minutes of the experiment in C. Student t-test was used to assess statistical significance. p:<0.01 (**). n = 20 fEPSPs/11 slices/5 mice per genotype. All Experiments were performed by Mr. Jan Schröder and analyzed by Jan Schröder and Dr. Christine Gee (Oertner Lab, ZMNH).

mice failed to sustain the LTD in the last 5 minutes of registration (Figure 25C, D). In conclusion, these data strongly present Tspan15 as a modulator of mGluR5 surface expression and that ablation of Tspan15 leads to electrophysiological deficits related to the mGluR5-mediated synaptic plasticity.

4.11 Abnormal phosphorylation level for the mGluR5 downstream effectors ERK1/2 in Tspan15 KO mice.

Given the deficiency in mGluR5-mediated synaptic plasticity, mirrored by the morphological abnormalities at the dendritic arbor and spine apparatus in Tspan15 KO mice, alterations relative to the mGluR5 downstream transduction pathway were investigated. The phosphorylation level of ERK1/2 was tested biochemically in brain lysates (Figure 26A). Interestingly, western blot quantification shows a statistically significant reduction of the pERK/ERK ratio in the absence of Tspan15 expression (Figure 26B).

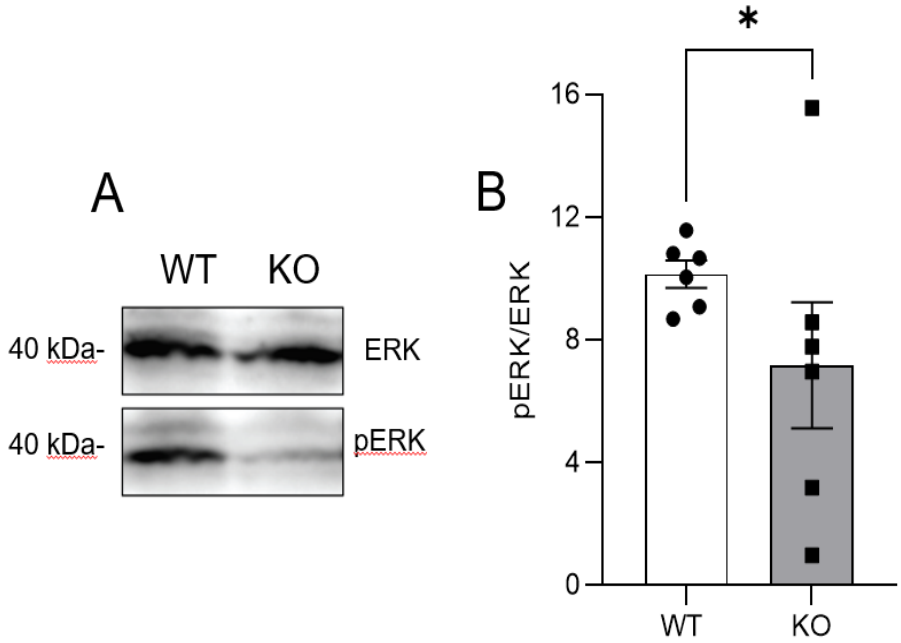

Figure 26 - Abnormal phosphorylation for the mGluR5 effector ERK1/2 in Tspan15 KO mice.

(**A**) Biochemical analysis of ERK1/2 and phospho-ERK1/2 in total brain lysate. (**B**) Quantification of phosphor-ERK/ERK ratio from A. Kolmogorov-Smirnov test was used to assess statistical significance. p: < 0.05 (*). n = 6 WT and Tspan15KO brain lysates. N: 6 independent sample preparations.

4.12 Ablation of Tspan15 expression leads to social behavioral alterations

mGluR5 has been established as a molecular key player in the modulation of social behavior, especially in the regulation of aggressive and dominant behavior in rodents (Been et al., 2016). On the other hand, also the hippocampus, where both mGluR5 and Tspan15 are highly expressed, has been linked to the disinhibition of motivated behaviors as social aggression. Therefore, Male WT and Tspan15 KO littermates were housed together as single couples, and their behavior was investigated with different paradigms (Table 10).

In the Open Field and Elevated Plus Maze, Tspan15 KO mice did not show any abnormal locomotor activity, exploratory behavior, and anxiety level (data not shown). Regarding their social behavior, while in the social recognition test (Figure 28A), Tspan15 KO mice did not present an altered preference index toward the familiar or the unfamiliar mouse (Figure 28B), they showed an increased amount of time spent in close proximity with a stranger mouse (social time) (Figure 28C).

In addition, mice dominance was assessed with the urine marking test (Figure 27A). Although no difference was observed in the number of marks left in the whole arena (Figure 27B), Tspan15 KO mice showed increased marking specifically for the area quadrant in which the three females were hosted (Figure 27C).

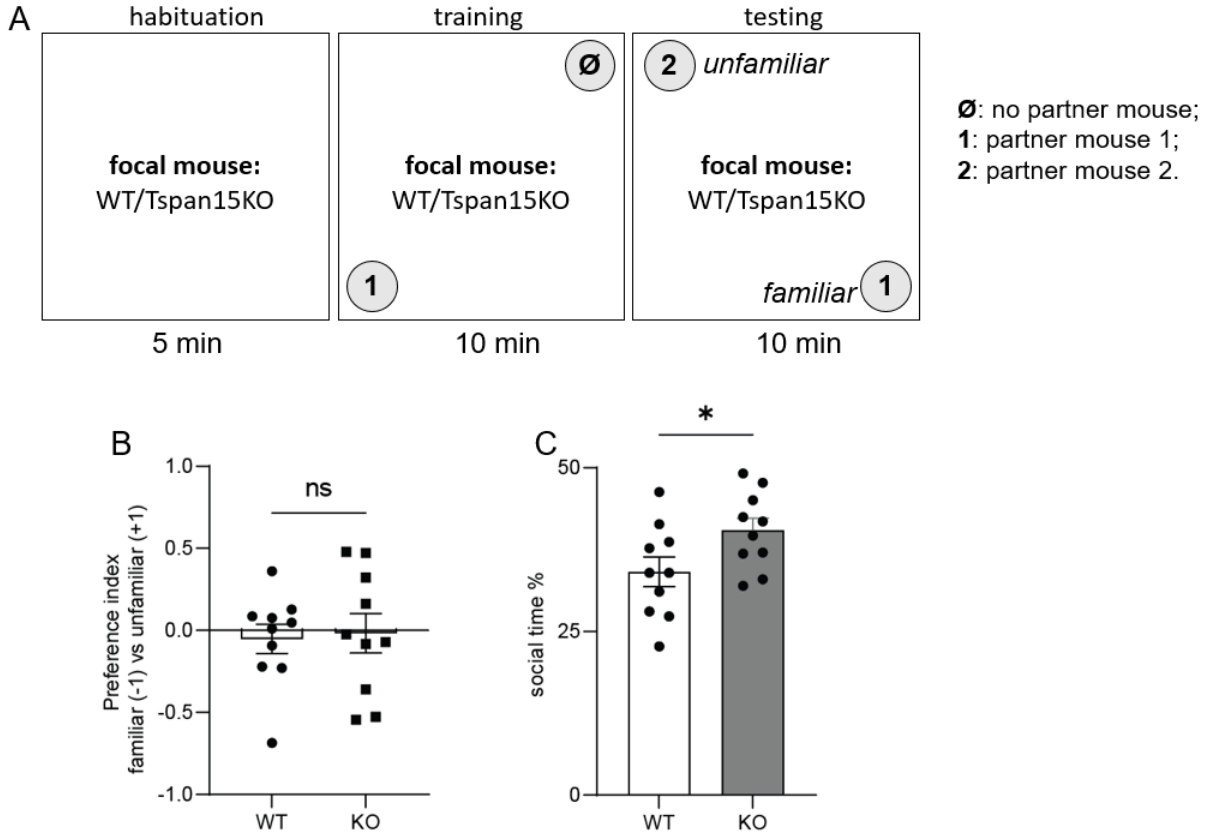

Figure 28 - Tspan15KO mice show increased social investingation time.

(A) Schematics of Social Recognition test. (B) Social preference quantification from the testing phase of experiment A. (B) Duration of total time spent in proximity with a mouse (social time). t-student test was used to assess statistical significance. p: <0.05 (*). n: 10 male mice per genotype; N: 4 cohorts.

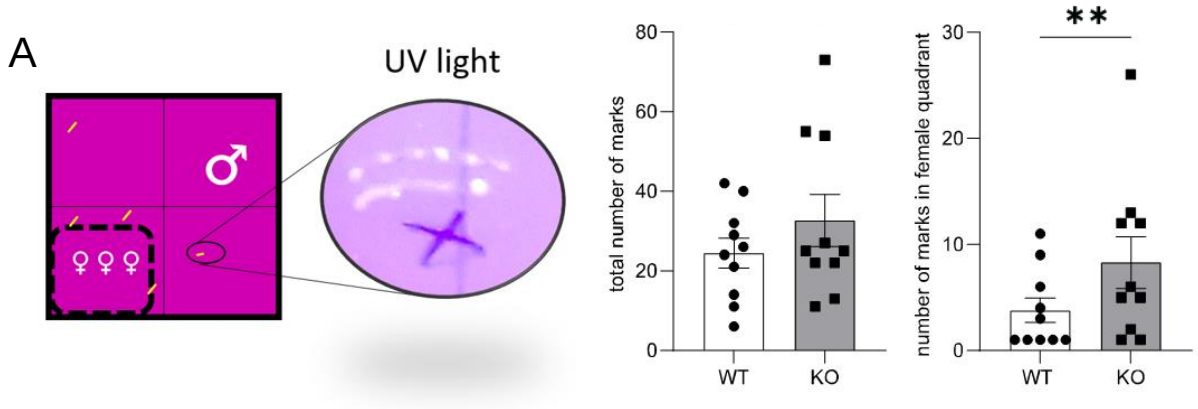

Figure 27 - Tspan15KO male mice show increased dominant behavior

(A) Schematic of Urine Markin test. Three WT female mice (♀♀♀) sit behind a fenestrated plexigas wall. The focal WT or Tspan15KO male mouse (♂) is free to explore the arena and release pheromones marks, later detected under the UV light (zoom in). (B-C) Quantification of pheromones marks within the whole arena (B) and in the female-hosting quadrant (C). t-Student test was used to assess statistical significance. p: <0.01 (**). n = 10 male mice per genotype; N = 4 cohorts.

The ritualistic aggressive behavior between cagemates was assessed in the instantaneous sampling following the cage change, with Tspan15 KO mice presenting a higher number of aggressions versus their cagemate (Figure 29B). This phenotype was further investigated and confirmed in the Resident-Intruder test (Figure 29A). Lack of expression of Tspan15 correlates with an increased tendency to socially investigate (Figure 29D), perform allogrooming (Figure 29F), and attack (Figure 29C) the intruder, while no difference with WT mice was observed for the time spent in self-grooming (Figure 29E).

Altogether these data show that in mice is present an inverse correlation between the expression of Tspan15 and aggressive behavior, suggesting a potential role for Tspan15 as a molecular modulator of social behavior.

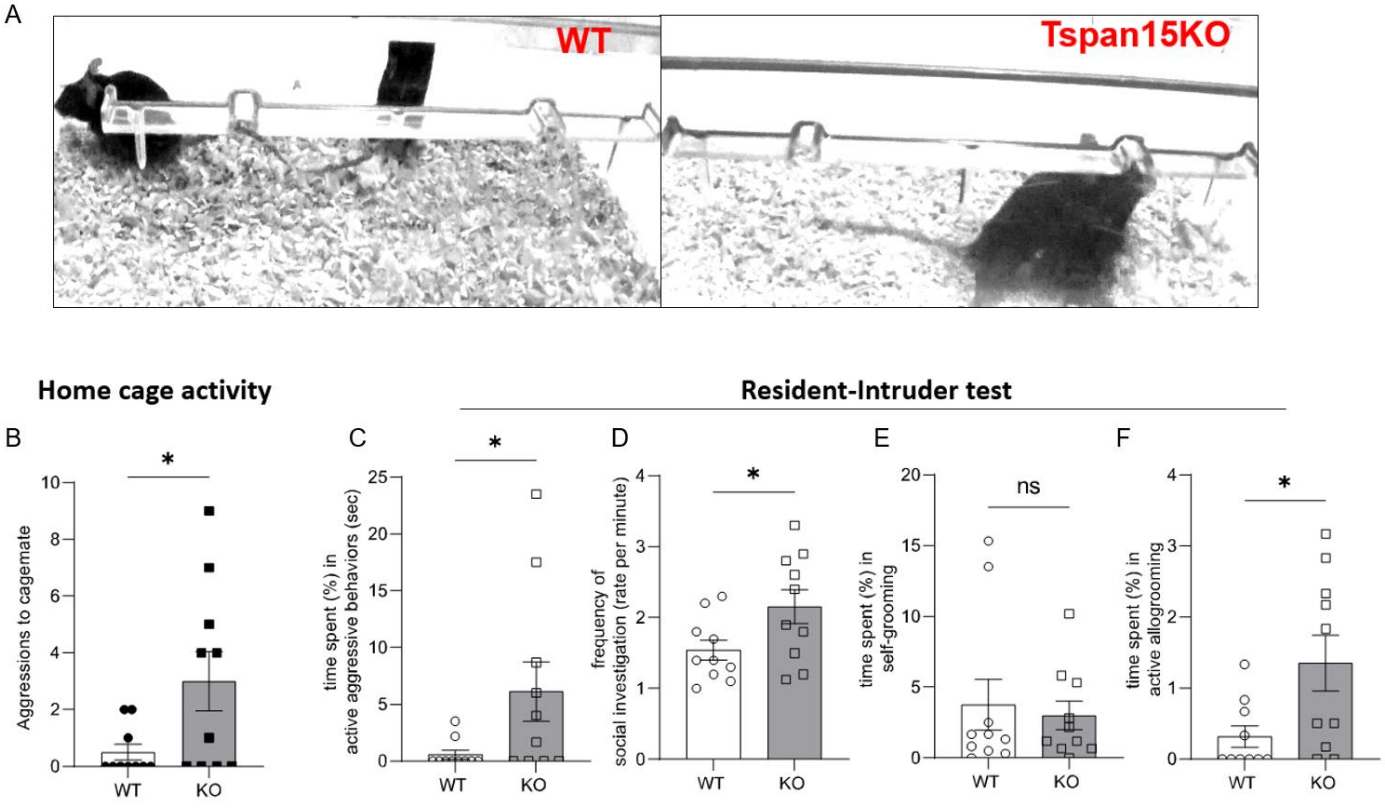

Figure 29 Tspan15KO male mice show increased dominant and aggressive behavior

(A) Frames from WT (left) and Tspan15KO (right) during the Resident-Intruder test video recording. (B) Quantification of aggressions against the cagemate brother during the spontaneous observations upon change of the cage bedding. (C-D) Quantifications from Resident- Intruder experiment performed by the focal resident mouse; (C) duration of active aggressive episode. (D) frequency of social investigation. (E) Duration of self-grooming. (F) Duration of active allogroming. t-Student test was used to assess statistical significance. p: <0.05 (*). n = 10 male mice per genotype; N = 4 cohorts.

4.13 Tspan15 is potentially the resident protein of cortical extracellular vesicles

Tspan15 has been revealed as a key component of endosomal vesicles and represents a novel modulator of mGluR5 trafficking. However, little is known about the role of Tspan15 in the context of extracellular vesicles (EVs). Different members of the tetraspanin (Tspan) family represent biological markers for EVs, such as Tspan8, CD63, CD9, and CD82 (Niel et al., 2018). Since Tspan15 has previously been found to be enriched in the vesicle-enriched fraction of brain lysates, it was assessed whether it is also present in neuronal-derived extracellular vesicles. For this purpose, a differential centrifugation protocol was applied to obtain fractions from embryonic brain cortical cultures media. Combining this procedure with filtering steps, it was possible to isolate a cell media 100,000 x g fraction enriched for extracellular vesicles (hereafter, EV-enriched fraction). The validation of the EV extract was assessed via Western Blot analysis, which showed the presence of canonical EV markers as CD81 and TSG101, and the absence of Golgi apparatus-related proteins as GM130 (Figure 30A). In addition, the EV extracts were analyzed by nanoparticle tracking analysis (NTA) with a Nanosight device. As expected, the EV extract was enriched for particles with diameters ranging from 100 to 300 nanometers (nm) (Figure 30B), typical for the different extracellular vesicles subpopulations of exosomes and microvesicles (Kim et al, 2022; Stahl et al, 2019; van Niel et al., 2018). This size range was further confirmed by the electron microscopy approach, performed in collaboration with Dr. Michaela Schwaizer (Electron Microscopy Facility from ZMNH, Hamburg). Interestingly, immunogold labeling of CD81 showed the presence of this tetraspanin on the membrane of the extracellular vesicles (Figure 30C, D). In the end, Tspan15 expression was detected via Western Blot analysis from validated EVs extracts (Figure 30E). These data suggest that, like other tetraspanins, Tspan15 is a component of extracellular vesicles derived from neurons.

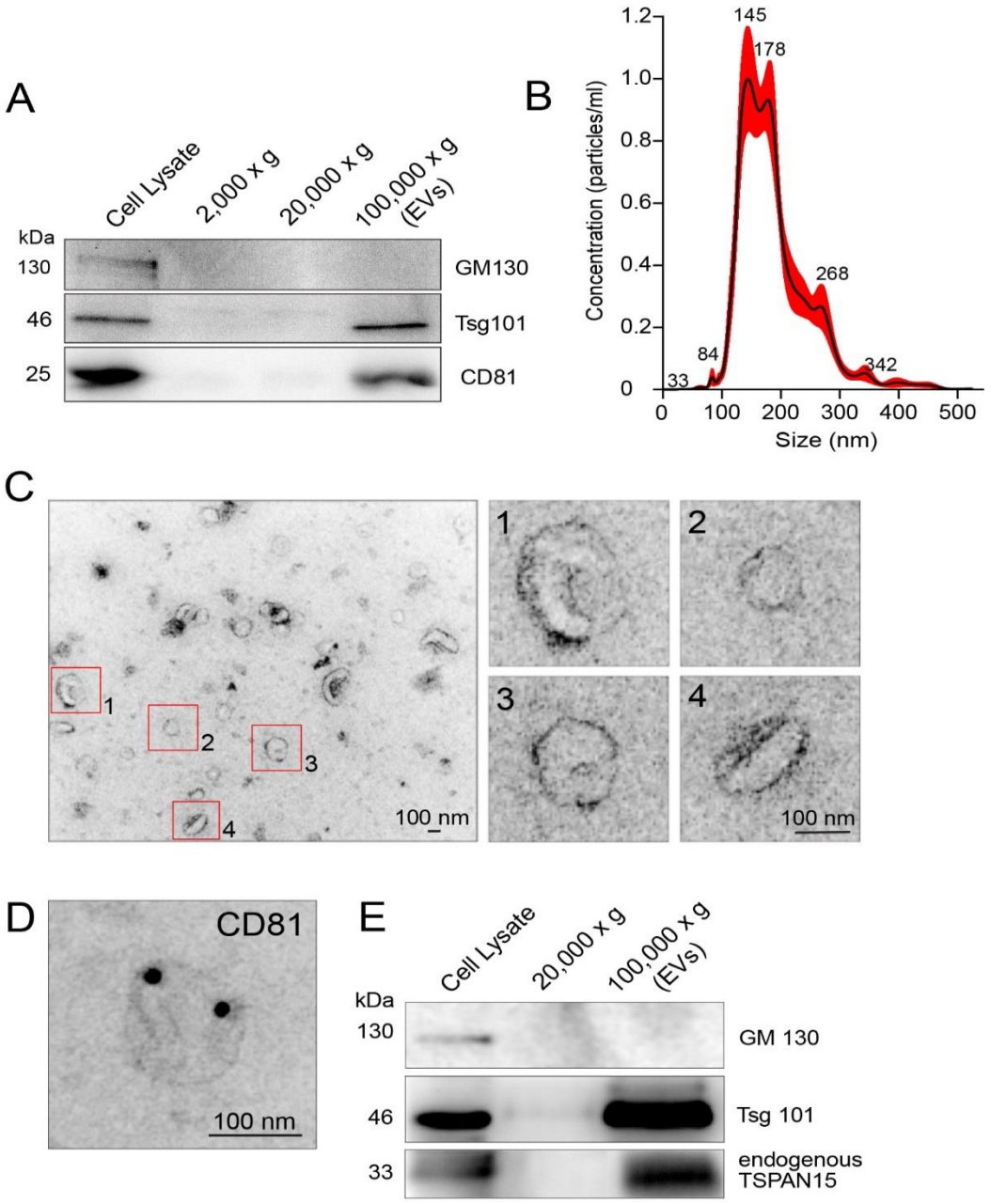

Figure 30 - Endogenous Tspan15 is a potential resident protein of extracellular vesicles

Validation of extracellular vesicle isolation from cortical neuronal cultures obtained with a differential centrifugation protocol. (**A**) Biochemical analysis of the cell lysate, cell media intermediate fractions (2,000 x g and 20,000 x g) and a cell media EV-enriched fraction (100,000 x g). Isolation of EV was validated by the expression of EV resident proteins CD81 and Tsg101 and the absence of Golgi-resident protein GM130. (**B**) Nano Tracking Assay (NTA) quantification of EV diameter from the 100,000 x g fraction in A. (**C**) Electron microscopy imaging of isolated EV ultrastructure. Numbered red regions are zoomed in the right panel (scale bars: 100 nm). (**D**) Nanogold staining and immunoelectron microscopy confirm the exoression of the EV-resident tetraspanin CD81 on EVs hown in C (scale bars: 100 nm). (**E**) Biochemical preparation from cultured cortical neurons. The EV-resident protein Tsg101 and endogenous tetraspanin Tspan15 are expressed in both the post-nuclear cell lysate and in the EV-enriched fraction (100,000 x g). Probing of the Golgi-resident protein GM130 was used as negative control. Experiment C and D were performed in collaboration with Dr. Michaela Sweizer Schwaizer (Electron Microscopy Facility from ZMNH, Hamburg).

4.14 Tspan15-GFP locates in multivesicular bodies and extracellular vesicles

To further confirm the presence of Tspan15 in EVs and to investigate if it can localize in organelles involved in the biosynthesis of EVs, such as Multivesicular Bodies, it was made advantage of a fluorescently tagged version of the Tspan15 protein. A plasmid carrying a Tspan15-GFP construct was kindly provided by Prof. Dr. Eric Rubinstein (Université Paris-Sud, Institut André Lwoff, Villejuif, France). The Tspan15-GFP or GFP (control) plasmids were transfected in N2A cells. Cell lysates and the 100,000 x g EV-enriched fraction were analyzed via Western Blot and compared. (Figure 31A). As expected, the presence of Tspan15-GFP was observed in the EV extract (60kDa band), as well as GFP. In addition, Tspan15-GFP, but not GFP was detected in the EV-enriched fraction.

Moreover, live-cell imaging of N2A cells expressing Tspan15-EGFP and CD63-mCherry, a classical EV marker (Yoshimura et al, 2016), showed abundant colocalization (white signal) of the two proteins (Figure 31B). Remarkably, Tspan15-EGFP expression was also observed in multivesicular bodies (MVBs) from cortical neurons (Figure 31C) in electron microscopy via diaminobenzidine (DAB) immuno-labeling of EGFP (performed in collaboration with Dr. Michaela Schwaizer, Electron Microscopy Facility from ZMNH, Hamburg). In sum, these data confirm that Tspan15 is a component of cortical EVs.

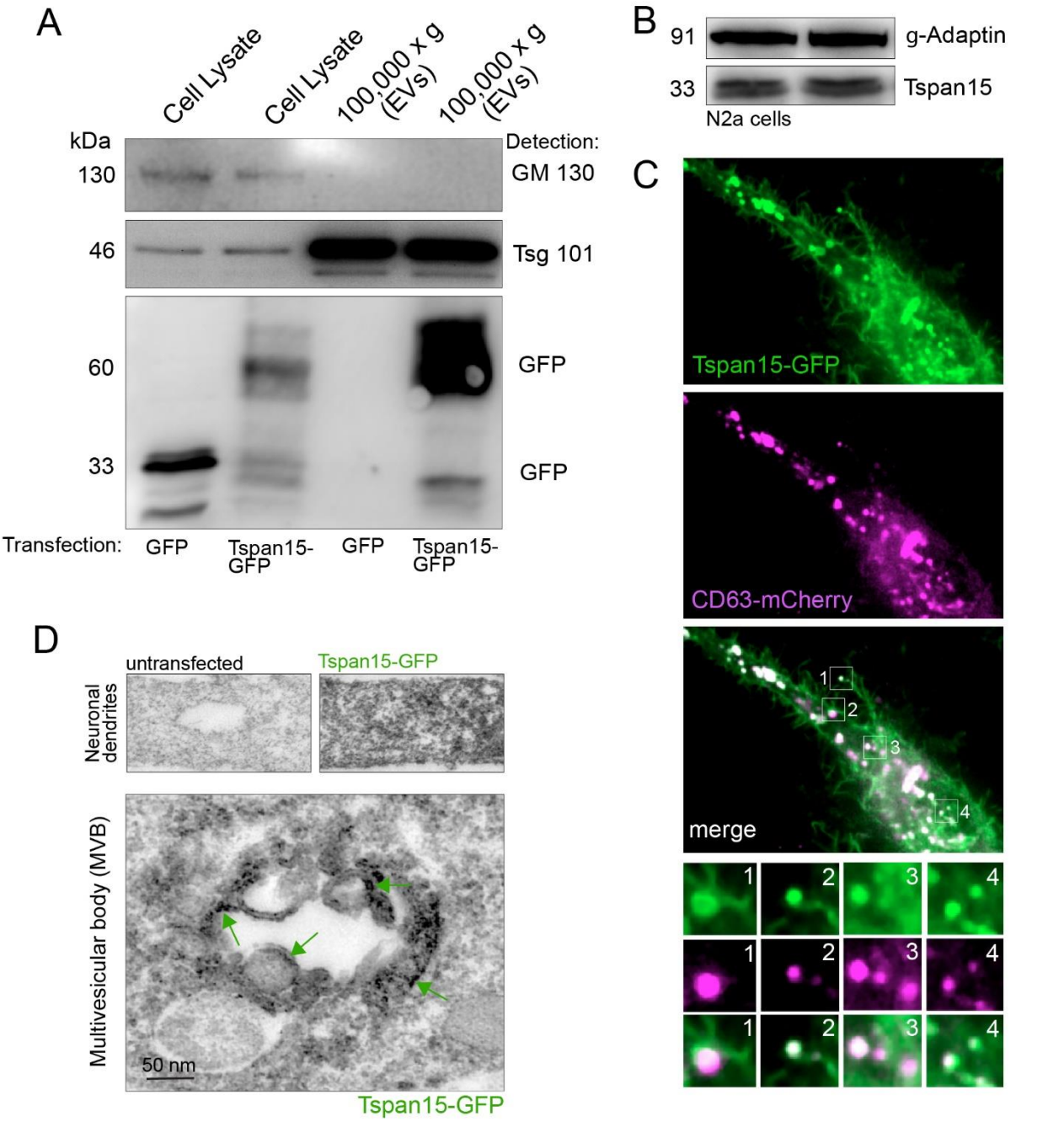

Figure 31 - Tspan15-GFP locates in multivesicular bodies and extracellular vesicles

(A) Analysis of post-nuclear celly lysate and 100,000 x g EV-enriched fractions derived from N2a cells expressing either GFP control or Tspan15-GFP. The EV-resident protein Tsg101 and Tspan15-GFP are expressed in both the post-nuclear cell lysate and in the EV-enriched fraction (100,000 x g). The Golgi-resident protein GM130 was used as negative control. **(B)** Biochemical probing of endogenous expression of Tspan15 in N2a cell lysates. γ-adaptin was used as loading control. **(C)** Cell-live imaging of Tspan15-EGFP (green) and the EV-resident protein CD63-mCherry (magenta) in N2a cells. White signals indicate colocalizations. White boxed-areas 1-4 are magnified at the bottom. **(D)** Immunoelectron microscopy combined with diaminobenzidine (DAB) staining from neurons previously transfected with Tspan15-GFP. Top left panel: dendrite from an untransfected control neuron shows the background signal. Top right panel: dendrite from a neuron expressing Tspan15-GFP. Bottom panel: ultrastructure of a multivesicular body (MVB), involved in EV biosynthesis. Green arrows indicate the expressionn of Tspan15-GFP at intraluminal vesicle membranes. Experiment D was performed in collaboration with Dr. Michaela Sweizer Schwaizer (Electron Microscopy Facility from ZMNH, Hamburg).

4.15 The EV-resident protein Tspan15 can interact with target cells

Since Tspan15 has been identified as an EV component, live cell imaging on N2A cells expressing Tspan15-EGFP was performed. In a time-lapse recording green fluorescence particles from the extracellular environment were observed contacting a recipient N2A cell and the consequent interaction with the plasma membrane (Figure 32A). In addition, Tspan15-EGFP or EGFP were co-expressed with CD63-mCherry in N2A donor cells and the media was consequentially purified to obtain an EV-enriched conditioned media. Application of this latter to recipient untransfected N2A cells led to a significantly increased level of interaction for Tspan15-GFP to target cell when compared to the GFP control condition (Figure 32B, C). Conversely, in both conditions the level of CD63-mCherry transferred was similar, suggesting a similar number of EVs were produced and incubated (Figure 32B, D).

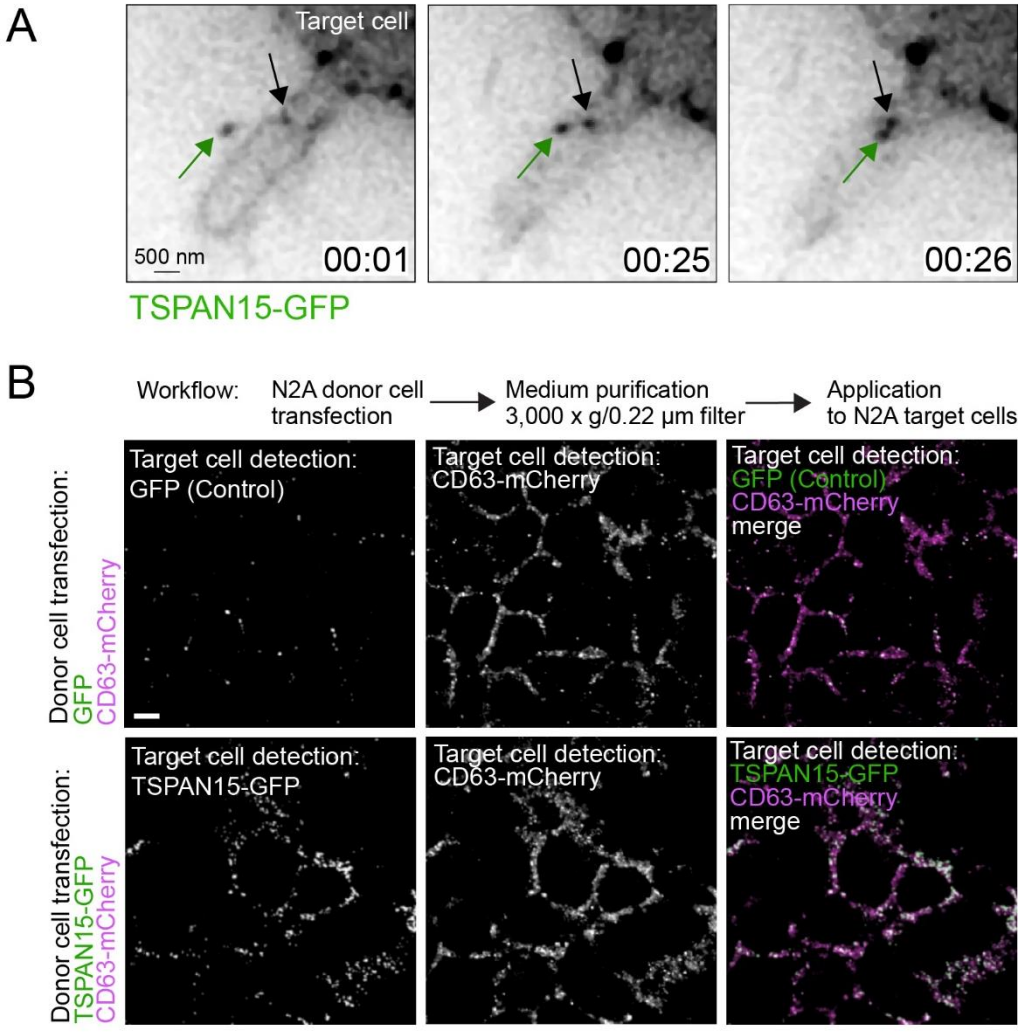

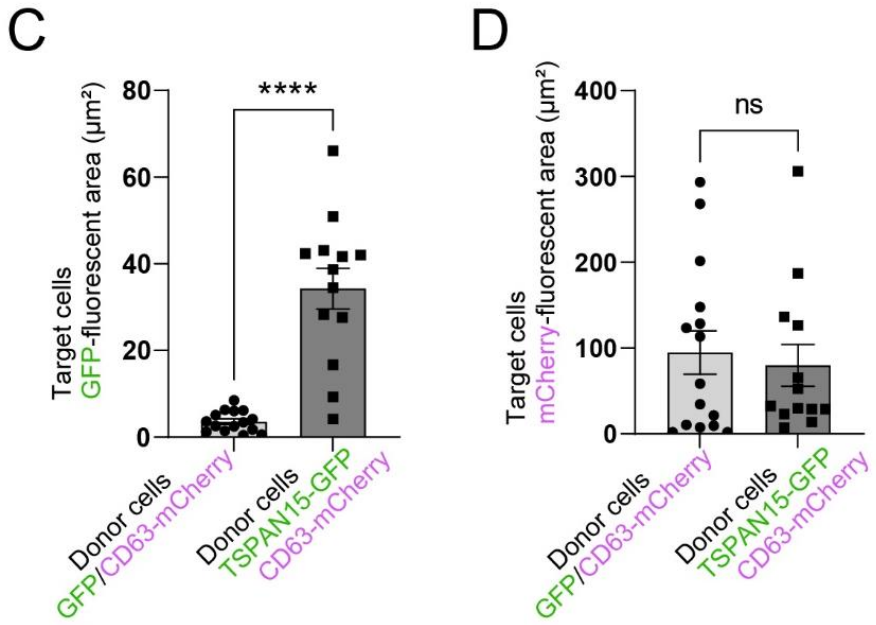

Figure 32 - The EV-resident protein Tspan15 is able to interact with target cells

(A) Time-lapse imaging of Tspan15-EGFP-positive vesicles (arrows) derived from transfected N2a cells. An extracellular vesicle positive for Tspan15-GFP (green arrow; left panel) interacts with the target cell membrane (green arrow, middle panel) and is then observed in contact with the target cell (green arrow, right panel), taking as static reference point the vesicle pointed by the black arrow. Scale bar: 2µm. (B) Fluorescence confocal microscopy of untransfected N2a target cells incubated with EV-enriched media derived from N2a donor cells, co-expressing either GFP negative control (top panels) or Tspan15-GFP (bottom panels) with the EV-resident protein CD63-mCherry (magenta). Tspan15-GFP expressed in donor cells is contacting the target cells. (C) Quantification of GFP+/mCherry+ fluorescent area (µm2) at target cells from (B). (D) Quantification of mCherry+ fluorescent area (µm2) at target cells from (B). Data are represented± SEM. (n = 13 regions of interest, N = 3 independent experiments) Student t-test, P value: * p<0.05.

4.16 Tspan15-positive EVs can potentially be internalized in recipient neurons

To elucidate if Tspan15-positive EVs can be potentially internalized inside the target cells, Tspan15-GFP-positive EVs were applied to untransfected recipient neuronal cells, and potential colocalization with the early endosome antigen 1 (EEA1), an intracellular protein marking the early endosome, was checked. Tspan15-GFP internalization was assessed also in neurons. Incubation of target cells with EVs at +4°C was used as an additional negative control condition since it has been extensively established that mechanisms of endocytosis are inhibited at this temperature (Figure 33A). Remarkably, at +37°C it was observed a significantly higher level of colocalization between Tspan15-GFP and EEA1 at the neuronal processes, compared to the +4°C condition, and no Tspan15-GFP signal was detected in the EV-depleted media condition (Figure 33B-D). This data potentially indicate that, although most of the transferred Tspan15-GFP is localizing at the plasma membrane of the target cell, to a partial extent Tspan15-positive EVs can be internalized by recipient primary neuronal cells. However, such internalization mechanism is likely to be independent from the Testraspanin 15 expression.

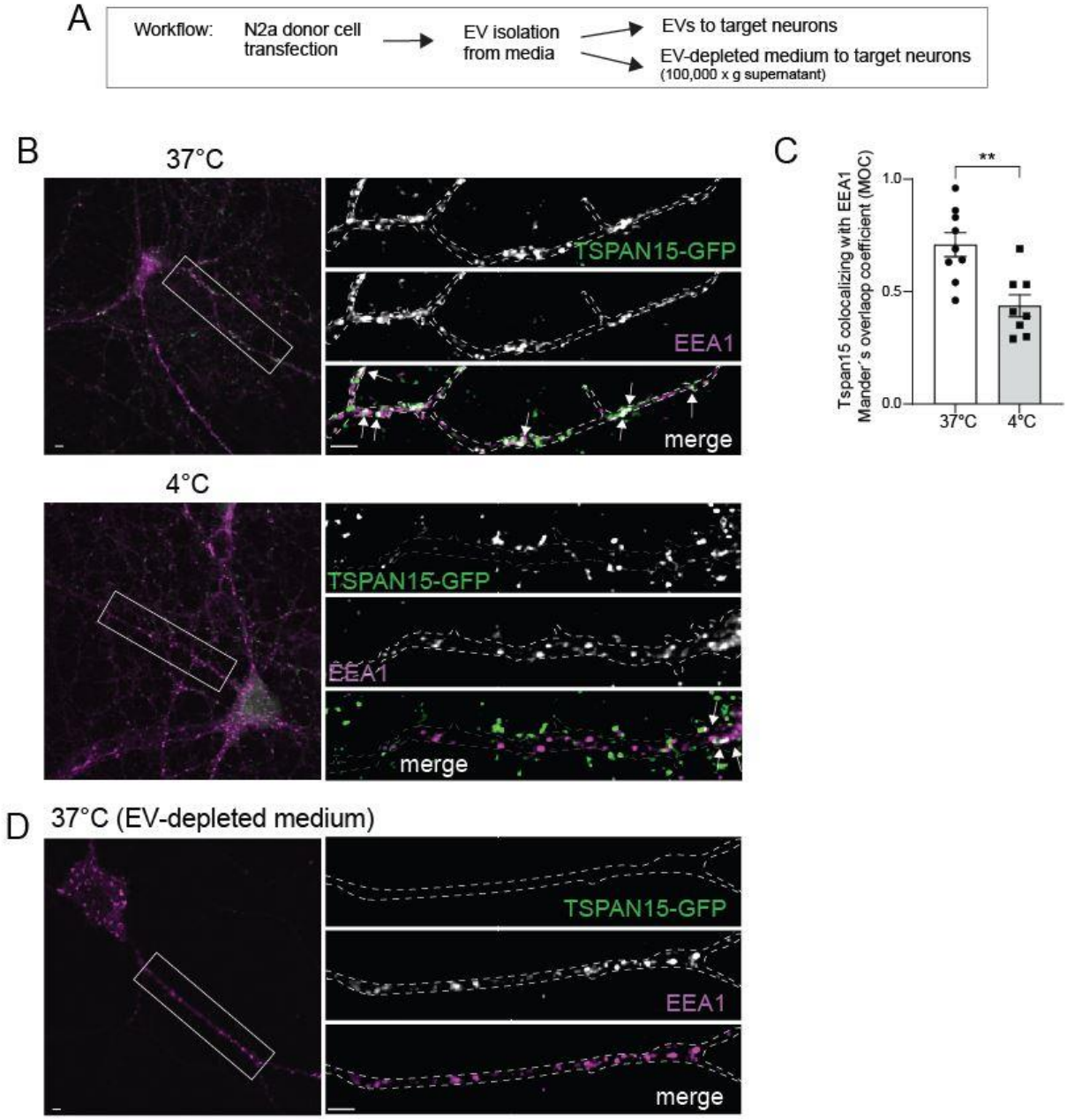

Figure 33 – Tspan15-GFP EVs can be potentially internalized in target cells

(A) Schematic representation of the experimental design. (B) N2a-derived Tspan15-GFP (green) EVs were provied to untransfected target neurons at 37°C (top panel) or 4°C control condition (bottom panel) Scale bar: 5µm. (C) EV-depleted medium at 37°C was used as negative control condition. Scale bar: 5µm. (B,C) Magnification from white boxes show neuronal dendrites. White arrows show Tspan15-GFP colocalization with EEA1, which marks the early endosome. Scale bar: 5µm. (D) Quantification of between Tspan15-GFP signal with EEA1 signal espressed as analyzing the Mander´s coefficient. (B-D) N = 3 independent experiments, n = 12 neurons (37°C); n = 8 neurons (4°C control condition). Student t-test, P value: 0.0018.

4.17 Tspan15 expression in recipient neurons is not necessary for EV contact

To uncover the role of Tspan15 in EV interaction with target cells, it was assessed whether deletion of Tspan15 in recipient neurons can affect contact with EVs (Figure 34A). First, WT cortical-derived EVs were labeled with the fluorescent lipophilic dye DiI. Validation of the labeling was confirmed by NTA imaging, where only EV-like particles (100-300 nm) resulted in fluorescently labeled (red) (Figure 34B). The absence of unspecific labeling was further verified by staining a non-lipidic substance, such as bovine serum albumin (No-EV-control) (Figure 34D), and observing no DiI signal (red). In addition, the ability of DiI to label EVs was confirmed by staining with the dye EVs derived from N2a cells expressing Tspan15-GFP. Double-labeled EVs were provided to neurons. Tspan15-positive DiI-labeled EVs were detected in contact with target neurons in confocal fluorescent microscopy (Figure 34C). In addition, it was assessed that recipient cortical cultures presented equal cell density for both genotypes by DAPI staining of cell nuclei. (Figure 34E, F). The same number of DiI-labeled WT-EVs was provided to WT and Tspan15 KO neurons expressing GFP. (Figure 34G) The orthogonal projection of the z-stack from confocal microscopy was used to discriminate whether the fluorescent EVs were contacting GFP-positive neurons or not Data analysis shows that depletion of Tspan15 expression in recipient neurons does not affect the EV contact when compared with WT control (Figure 34I, J). Altogether, these data suggest that Tspan15 expression in recipient neurons is not altering the EV-target cell contact levels.

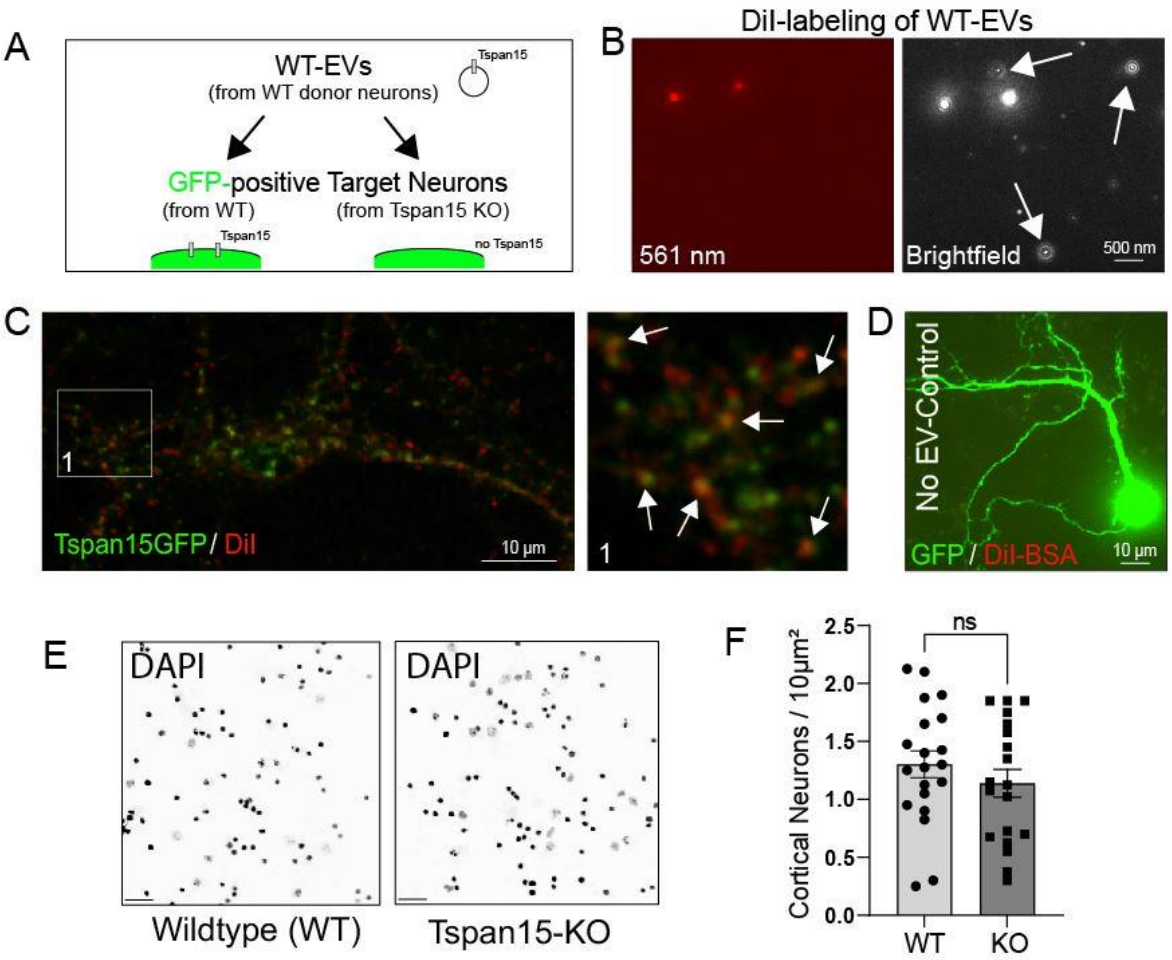
A
WT-EVs
(from WT donor neurons)
Tspan15
GFP-positive Target Neurons
(from WT)
(from Tspan15 KO)
Tspan15
no Tspan15
B
DiI-labeling of WT-EVs
561 nm
Brightfield
500 nm
C
1
Tspan15GFP / DiI
10 µm
1
D
No EV-Control
GFP / DiI-BSA
10 µm
E
DAPI
DAPI
Wildtype (WT)
Tspan15-KO
F
ns
Cortical Neurons / 10µm²
2.5
2.0
1.5
1.0
0.5
0.0
WT
KO

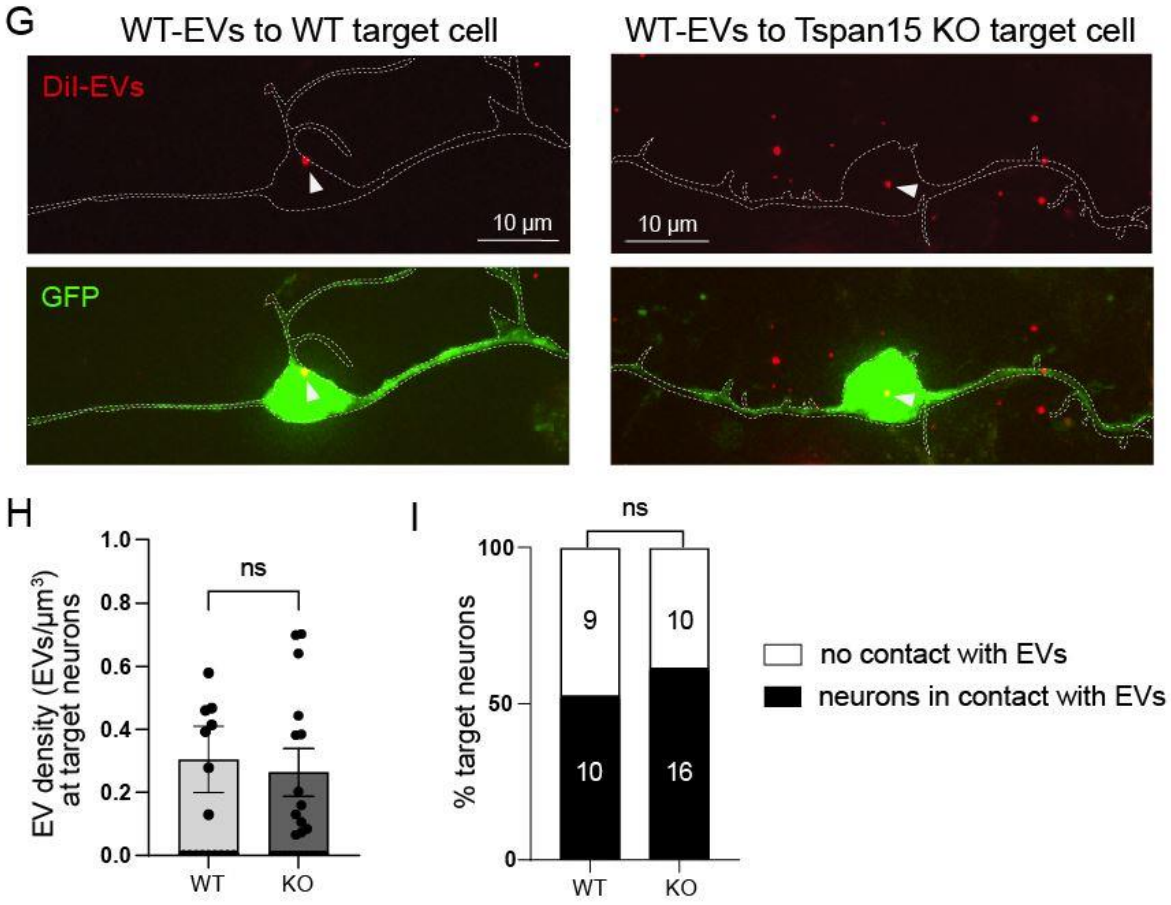

Figure 34 - Tspan15 expression in recipient neurons is not necessary for EV contact

(A) Experimental design: Equal number of EVs, labeled with DiI and derived from wildtype (WT) donor cortical cultures, were incubated to the culture medium of target GFP-transfected cortical neurons (green) from either wildtype (WT) or Tspan15 knockout (KO) mice. **(B)** Nano Tracking Analysis (NTA) imaging of EVs labeled with DiI derived from wildtype (WT) neurons. Left panel: imaging of fluorescent DiI-labeled EVs at 561 nm. Right: imaging of total vesicle-like particles with brightfield illumination. (**C**) Tspan15-GFP-positive DiI-labeled EV in contact with a neuron. Scale: 10µm. (**D**) Z-stack projection of a target cortical neuron expressing GFP upon transfection and DiI-treated BSA 0.5% (control) incubation, indicating specificity of EV staining by DiI (Scale bar: 10µm). (**E**) Wildtype (WT, left panel) and Tspan15 knockout (KO, right panel) cultured cortical neurons stained with DAPI to label the nuclei. n = 19 (WT); n = 20 (Tspan15KO) regions of interest; N = 3 independent experiments. Scale bar 25 µm. (**F**) Quantification of cell density from experiment E. n.s.: not significant. (**G**) Target neurons transfected and expressing GFP volume marker (green) derived from wildtype either wildtype (WT, left panel) or Tspan15KO (KO, right panel), were incubated with EVs derived from wildtype donor cortical cultures (WT-EVs). Scale bar: 10 µm. Arrows show DiI-stained EVs in contact with GFP-positive target neuron. (**H**) Quantification of EV density (number of EVs per GFP-positive volume in μm^3) in interaction with target cortical neurons from experiment H. (**I**) Quantification of the percentage of target cortical neurons undergoing contact with DiI-labeled EVs from experiment H. (**H,I**) Data are represented as means ± SEM. (**H**) The Mann–Whitney U test was applied to evaluate statistical significance. (**I**) The Fisher´s exact test was applied to evaluate statistical significance. n = 19 neurons (WT);: n = 26 neurons (Tspan15KO) . N = 3 independent experiments. ns: not significant. Outliers were identified and removed by the Graphpad software-integrated ROUT algorithm.

4.18 Tspan15 expression in EVs facilitates EV interaction with target cortical neurons

With a similar, but specular experimental design, the effect of Tspan15 depletion from donor cortical cultures was tested and WT-EVs or Tspan15 KO-EVs were incubated in WT recipient neurons (Figure 34A). At first, EV extracts from WT and Tspan15 KO cortical cultures were validated as previously performed (Figure 34B). NTA analysis revealed that the lack of expression of Tspan15 is not affecting the diameter nor the number of EVs produced when compared with WT control (Figure 34C, D). Equal amounts of WT-EVs and Tspan15 KO-EVs were labeled with DiI and incubated in GFP-transfected cortical neuronal cultures (Figure 34E. Remarkably, Tspan15 KO-EVs performed fewer contacts to recipient neurons compared to WT EVs (Figure 34E, F). Accordingly, WT neurons showed higher contacting EV density when compared with Tspan15 KO cells (Figure 34G). In sum, this data suggest that Tspan15 expression on EVs can potentially facilitate the EVs contact with the plasma membrane of cortical neurons.

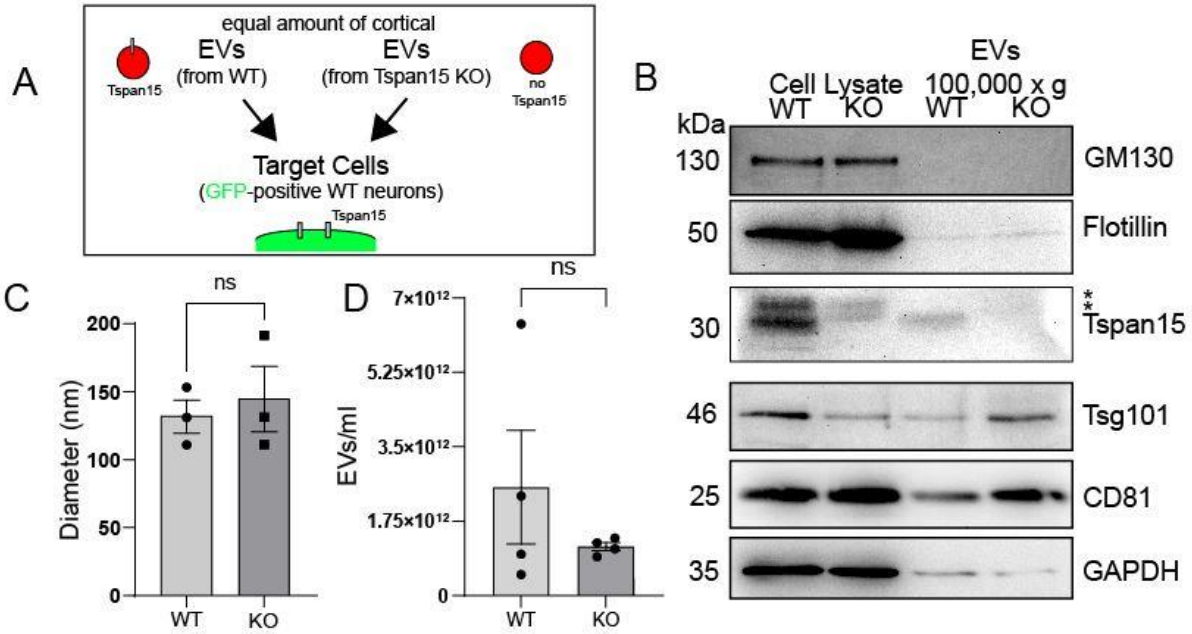

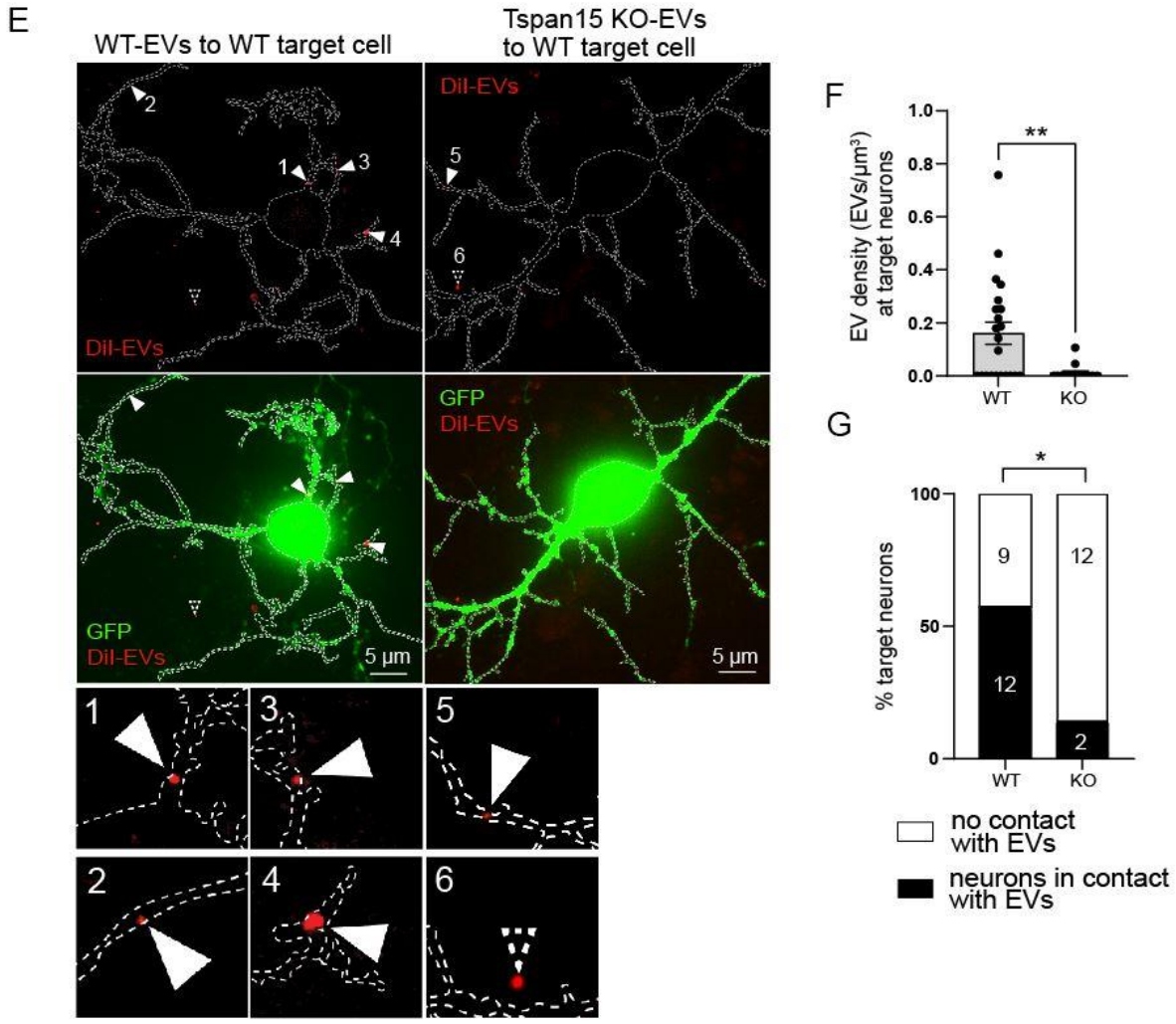

Figure 35 - Tspan15 expression on EVs can potentially facilitate the EVs contacts to the plasma membrane of cortical neurons.

(A) Experimental design: Equal amounts of EVs (red) labeled with DiI from either wildtype donor neurons or Tspan15 knockout donor neurons, were provided to the culture medium of GFP-positive cortical wildtype target neurons (green). (**B**) Wildtype (WT) and Tspan15 knockout (KO) total cell lysates and cell media 100,000 x g EV-enriched fractions. The Golgi-resident protein GM130 served as negative control for EVs; EV-resident proteins flotillin, Tsg101, CD81 were used as positive control, GAPDH served as loading control. Asterisks: unspecific bands. N = 3 independent experiments. (**C**) NTA analysis of EV size and (**D**) number. Data are represented as means ± SEM. The Mann-Whitney test was applied to provide statistical significance. (C) N = 3 independent experiments. (D) N = 4 independent experiments. n.s.: not significant. (**E-H**) GFP-positive target neurons (green) from cortical neuron cultures incubated with DiI-labeled EVs. (**E**) Left panel: wildtype target neuron incubated with control wildtype EVs (WT-EVs) derived from wildtype donor cortical cultures. Scale bar: 5 µm. Right panels: wildtype target neuron incubated with Tspan15-KO EVs (KO-EVs) derived from Tspan15KO donor cortical cultures. Scale bar: 5 µm. Bottom: enlargements from EVs pointed by numbered arrows in the top panels. Orthogonals projections and z-stacks (not shown) served to evaluate if the DiI-labeled EVs (red) were eventually in contact with the target cells. (**F**) Analysis of EV density (number of EVs per GFP-positive volume in μm^3) in contact with target GFP-positive neurons. (**G**) Analysis of the percentage of target GFP-positive neurons showing contact with DiI-labeled EV incubation from E. (**F-G**) Data are represented as means ± SEM. (**F**) The Mann–Whitney U test was applied to determine statistical significance. (**G**) The Fisher´s extact test was applied to evaluate statistical significance. N = 3 independent experiments. Wildtype neurons: n = 21; Tspan15 knockout neurons: n = 14. P-value: *p < 0.05. Outliers were identified and removed by the Graphpad software-integrated ROUT algorithm.

5 Discussion

5.1 General technical limitations

The lack of specific antibodies for Tspan15 immunostaining in mouse tissue has to be acknowledged as a technical limitation of such type of investigation, which in this study was partially overcome by generating a Myc-Tspan15 construct expressed under the neuron-specific promoter of the *synapsin* gene carried on a viral vector (Figure 15). In addition, a constitutive Tspan15KO mouse model was used and characterized to shed light on the contribution of Tspan15 to synaptic plasticity. Although this mouse line represents a precious research tool, it has to be mentioned that a conditional Tspan15 knockout model, ideally neuron-specific, might have led to more unambiguous interpretations.

5.2 Role of Tspan15 in synaptic plasticity

Tetraspanins are transmembrane proteins that promote several biological processes at the surface of biological membranes (Budnik et al., 2016) (van Niel et al., 2018). These proteins arrange in tetraspanin-enriched microdomains (TEMs) at the surface of the plasma membrane and on vesicles (Boucheix & Rubinstein, 2001), assuming cell-specific functions in some cases (Figure 13). For example, in neurons, different tetraspanins, including Tspan5, Tspan6, and Tspan7 have been identified as critical players in synaptic receptor trafficking, participating in the molecular mechanisms underlyingsynaptic plasticity in the glutamatergic system (Moretto et al., 2023). To date, the role of Tspan15 in the context of synaptic plasticity has not been elucidated, despite its high expression in the brain and its ability to promote the endocytic trafficking of partner proteins, such as the sheddase enzyme ADAM10.

5.3 Tspan15 subcellularly localizes at dendrites bodies and in postsynaptic compartments, but not in the PSD core

The data presented indicate that Tspan15 is highly enriched in the endosomal compartment in the mouse brain (Figure 16A) and, although absent from the detergent-

soluble synaptosomal fraction, partially represented by the post-synaptic density (PSD), it is expressed both in the dendritic body and spines (Figure 17), as immunostaining and live cell imaging show expression in dendritic vesicles (Figure 16B, C).

5.4 Depletion of Tspan15 correlates with the altered subcellular localization of mGluR5

It is known that different tetraspanins act as partner proteins of glutamatergic receptors (Becic et al., 2021). Remarkably, quantification of the total expression and subcellular distribution of glutamatergic receptors showed that Tspan15 KO mice present a specific alteration for mGluR5, with a shift from the endosomal compartment to the synaptosomal detergent-insoluble fraction (Figure 20G, H; Figure 23B). mGluR5 represents a key player in the modulation of synaptic activity by contributing to long-term mechanisms of synaptic plasticity. Despite the relevance of this receptor in several pathological conditions, such as Alzheimer´s Disease, Schizophrenia, Fragile X Syndrome, Rett´s Syndrom, and ASD, the modulatory mechanism underlying the recycling trafficking of mGluR5 has not been fully elucidated to date.

5.5 Tspan15 and mGluR5 interact on Rab11+ endosomes

When proteins, such as a synaptic receptor, undergo internalization from the plasma membrane into the intracellular environment, they will be transferred to the endosomal compartment. The latter is composed of a set of organelles and vesicles working as temporary sorting and storing stations. The regulation of such complex machinery is crucial for the physiological trafficking, subcellular localization, and activity level of receptors. The different endosomal organelles and vesicles can be identified by the presence of distinct members of the Rab GTPase protein family. In general, endocytic trafficking of synaptic receptors is critical for the modulation of synaptic activity and the occurrence of plasticity. While the recycling trafficking of AMPARs has been widely studied and elucidated (Correia et al., 2008; Huganir & Nicoll, 2013; Park et al., 2004; van der Sluijs & Hoogenraad, 2011), the endocytic recycling of metabotropic glutamatergic receptors, such as mGluR5 and the role in synaptic plasticity remains

still elusive (Cheng et al., 2013; Gu & Huganir, 2016; Piguel et al., 2014; Suh et al., 2010). Hence, it is crucial to identify new interaction partners and regulators of mGluR5 trafficking, as these could represent a potential therapeutic target in the future. This study proposes Tspan15 as a novel interaction partner of mGluR5. Immunostaining of Myc-tagged Tspan15 and endogenous mGluR5 indicates a moderate positive level of colocalization at the dendritic body (Figure 21A), further confirmed by live cell imaging of co-transport of mGLuR5 and Tspan15 on vesicles (Figure 21B). After the stimulation, mGluR5 is known to be desensitized, internalized and recycled back to the plasma membrane on Rab11-positive vesicles to potentially undergo a new round of activation (Scheefhals et al., 2019). Consistently with the mGluR5 subcellular redistribution in Tspan15 KO, Tspan15 and mGluR5 were found in cotransport on Rab11-positive endosomes in COS7 cells (Figure 22B) and triple co-immunoprecipitation in N2A cells (Figure 22A). This data suggest that Tspan15 and mGluR5 potentially interact during the recycling of the metabotropic receptor.

5.6 Expression of Tspan15 alters apical dendritic morphology in CA1 pyramidal neurons

mGluR5 has been identified in neurons as a main actor in the mechanisms of synaptic plasticity underlying dendritic spine weakening and maturation and dendritic shaping (Ballester-Rosado et al., 2010); (She et al., 2009) (Wijetunge et al., 2008). For this reason, a morphological analysis of CA1 pyramidal neurons was performed by Diolistic staining of hippocampal slices. CA1 pyramidal neurons mainly receive excitatory inputs from the CA3 region via the Schaffer collaterals fibers, which reach dendritic spines on both apical and basal dendrites. However, distal apical dendrites localizing at the stratum lacunose-molecular are specifically responsible for receiving further excitatory input via the perforant (temporoammonic) pathway, which represents the main cortical input to the hippocampal formation. Interestingly, abnormalities of this connection have been linked to social interaction and social contextual memory alterations (Mohammadkhani et al., 2022). Interestingly, Sholl analysis of the reconstructed neuronal arbor highlights specific morphological abnormalities for apical dendrites (Figure 18A), consistently with the phenotype previously reported for mGluR5 KO

neurons by Ballester-Rosado et al (Ballester-Rosado et al., 2010). Furthermore, analysis of apical dendritic spines showed increased density recalling the same phenotype found in mGluR5 KO mice (Figure 18B) (Chen et al., 2012). The distal shift and increased spine density at the apical level in Tspan15KO mice could be suggestive of increased synaptic activity at the perforant path and a potential impairment of social abilities, later investigated in this study.

5.7 Tspan15KO mice exhibit functional deficits of mGluR5 signaling

GPCRs, such as the mGluRs, are immediately desensitized upon activation to avoid overstimulation of the biological system. This desensitization leads to the downregulation of receptor activity and it occurs via phosphorylation performed by the recruitment of β-arrestin and G protein-coupled receptor kinase (GRK). In addition, mGluR5 is consequently internalized and transferred to early endosomes. On a functional level, the expression of Tspan15 appears to contribute to the physiological modulation of mGluR5 surface levels following activation as suggested by the immunostaining of surface mGluR5 upon DHPG agonist treatment (Figure 24). In addition, further dysregulation of mGluR5-related signaling was observed by biochemically detecting the phosphorylation levels of the effector ERK. Interestingly, western blot quantification of WT and Tspan15KO post-nuclear lysates indicates that a lack of Tspan15 expression correlates with a lower ratio of phospho-ERK/ERK, thus suggesting a potential downregulation of the mGluR5 downstream transduction pathway (Figure 26).

5.8 Tspan15KO mice show a deficiency in late mGluR5-dependent LTD sustenance

mGluR5-dependent long-term depression (LTD) represents a mechanism of synaptic plasticity occurring in different brain regions such as the hippocampus. Dysregulation of this form of LTD has been observed in correlation with different neurological disorders. mGluR5-mediated LTD takes place by triggering the phosphorylation of AMPAR followed by their subsequent internalization. In addition, mGluR5 activation leads also to the local synthesis of new proteins involved in the AMPA receptor

endocytosis and downregulation. (Lüscher et al., 1999). The dysregulation of mGluR5 signaling in the absence of Tspan15 was further confirmed by electrophysiological recordings of mGluR5-dependent LTD. Indeed, Tspan15 KO mice showed a deficiency in LTD sustainment in the last phase (Figure 25). Altogether these results indicate an impairment in mGluR5 signaling in the late phase of mGluR5-dependent LTD. In addition, they potentially suggest that in the absence of Tspan15 expression mGluR5 presents a reduced ability to perfom endocytic recycling upon initial activation, therefore remaining functionally downregulated. Unfortunately, current data do not completely explore this scenario, therefore deeper investigation of the recycling properties of mGluR5 in Tspan15KO would be beneficial to clarify the above-presented electrophysiological phenotype.

5.9 Lack of Tspan15 expression correlates with mGluR5 misplacement at the postsynapse, mimicking the FXS phenotype

At glutamatergic synapses, ionotropic glutamate receptors localize in nanodomains at the postsynaptic density (PSD) core, in proximity to the presynaptic active zone. This positioning and organization are thought to promote the strength of the synaptic response. In contrast, metabotropic glutamate receptors from group I, such as mGluR5, are abundantly confined in the perisynaptic zone, a more distant localization from the presynaptic vesicle release site. This spatial segregation allows AMPAR and NMDAR to react already to lower concentrations of released glutamate, while perisynaptic mGluRs necessitate higher concentrations of neurotransmitter. The reported mGluR5-related signaling alterations, as well the redistribution of this receptor from the intracellular membrane-enriched fraction to the synaptosomal detergent-insoluble fraction, triggered the interest to investigate if lack of Tspan15 correlates with an abnormal nanoscale organization of mGluR5 at dendritic spines (Figure 23). Interestingly, dSTORM super-resolution imaging revealed an overall depletion of mGluR5 at the surface of the postsynapses, coupled with an abnormal invasion of the post-synaptic density (PSD), similar to the phenotype observed in the context of Fragile X Syndrome (FXS). As mentioned, this pathology is also characterized by mGluR5-

mediated behavioral impairments, such as exaggerated aggressive behavior (Scheefhals et al., 2023).

5.10 Absence of Tspan15 expression correlates with exaggerated aggressive and dominant behavior

Social interactions are essential for multiple animal species to secure survival. Aggressive behavior is a form of motivated social behavior in which physical contact occurs that takes place to overcome critical situations. The main triggers for aggressive behavior are the social hierarchy ranking, competition for food, defense of offspring, and defense of territory. Engaging in a fight or not depends on a cost/benefit analysis and when this computation is altered and biased the result can lead to exaggerated and escalated aggressive behavior. In humans, several mGluR5-related neurological and psychiatric conditions are related to exaggerated aggressiveness (Table 1), as for example, Fragile X Syndrome (Zoicas & Kornhuber, 2019). In turn, mGluR5 downregulation in rodents has been extensively shown to disinhibit social investigation, with a consequent increase in social time (Aguilar-Valles et al., 2015) (Chung et al., 2015) (Burket et al., 2011) (Spooren et al., 2000) (Oberman, 2012). The current state of the art suggests therefore mGluR5 is a valuable therapeutical target to study in relation to pathological conditions related to social deficits. Given the above-mentioned similarities between the Tspan15KO and FXS model phenotypes and the shared dysregulation of mGluR5 signaling, the behavior of WT and Tspan15 KO mice was tested with a particular focus on the social sphere (Table 10). The mice exhibited comparable levels of locomotor activity, exploratory behavior, anxiety in the Open Field test and the Elevated Plus Maze, and absence of obsessive-compulsive and normal nesting activity. However, as suggested by the dysregulation of the mGluR5 pathway in the absence of Tspan15, Tspan15 KO male mice showed an increase in social time, but not social preference in the social recognition/interaction test (Figure 28), mimicking the effect of an antagonistic treatment for mGluR5. Moreover, Tspan15KO mice displayed an increased social dominant behavior in the urine marking test, where they specifically show a higher number of female-induced pheromone marks compared to WT littermates (Figure 27). In the end, Tspan15KO were observed in the home cage

environment and their social behavior versus WT littermates (social spontaneous observations) and unfamiliar intruder WT mice (Resident-Intruder test) was assessed ( ). Remarkably, the enhanced social investigation and dominant behavior of Tspan15KO mice were confirmed in the Resident-Intruder test by observing respectively an increase in the frequency of social investigations and duration of active allogroming when compared with WT littermates (D, F). Lastly, lack of expression of Tspan15 correlates with an exaggerated aggressive behavior versus both brother cagemates (A) and unfamiliar intruder mice (C), further recalling the FXS phenotype.

5.11 Speculations, conclusions, and future directions about the contribution of Tspan15 to synaptic plasticity

Interestingly, Amyloid Precursor Protein (APP) cleavage mediated by the sheddase enzyme ADAM10, the main interactor of Tspan15, is dysregulated during a critical time window for the CNS development in the FXS. This altered processing of APP is thought to contribute to FXS-related synaptic dysfunctions and eventually to the cognitive and behavioral symptoms characterizing this pathology, since the excessive concentration of soluble APP-alpha can interfere with mGluR5 signaling and subcellular localization (Pasciuto et al., 2015). As a mere speculation, the molecular and behavioral phenotype observed in the Tspan15KO mice in the present investigation may potentially result on the one hand from compromised activity levelsand substrate preference of ADAM10 with a consequent increase of soluble APP-alpha; on the other hand, it could result from reduced proximity of ADAM10 and mGluR5 since they were both shown to bind Tspan15. In conclusion, the first part of this study indicates Tspan15 as a novel binding partner of mGluR5 and the importance of this interaction for the subcellular localization of the receptor, its signaling, and impact on the behavioral sphere. Future experiments will be needed to elucidate the molecular mechanisms underlying these abnormalities and potentially provide more understanding of mGluR5-related pathological conditions.

5.12 Role of Tspan15 in the docking of cortical extracellular vesicles to target neurons

To date, several tetraspanins have been recognized as representative EV resident proteins, including CD9, CD37, CD53, CD63, CD81, and CD82 (Gurung et al., 2021). Abnormal EV regulation is a common feature shared among different pathological conditions (Xiao et al 2021). For this reason, the study and potential theranostic use of EVs have gained great interest in recent years. On the one hand, EVs could represent a vehicle to transfer nucleic acids or medical compounds to a specific recipient cell type (Zhou et al., 2022). On the other hand, diagnostics could screen for EVs as putative biomarkers at the onset of pathologies (Ollen-Bittle et al., 2022). Hence, the importance of elucidating the mechanisms regulating the interaction between EVs and the surface of target cells is evident. In addition, neuronal survival and activity can be affected by EV uptake and EVs are thought to participate in the development of neurodegenerative pathologies. Several tetraspanins have been identified as EV-resident proteins, however, the presence and role of Tspan15 in EV-mediated communication among neurons are still unclear.

5.13 Tspan15 is a resident protein of cortical extracellular vesicles

The present data indicate Tetraspanin-15 (Tspan15) as an EV protein component, as observed in EV-enriched fractions from the cell culture medium (Figure 30). Consistently, Tspan15-GFP has been observed on vesicles hosted inside the lumen of multivesicular bodies, organelles representing the upstream source of exosome biogenesis (Figure 31).

5.14 Tspan15-positive EVs can be transferred from a donor cell to a target neuron

Tetraspanins have been suggested as modulators of EV biogenesis and internalization. Indeed, Tspan8 has been recently shown to facilitate the EV transfer in endothelial cells and consequentially stimulate the molecular pathway leading to their activation (Nazarenko et al., 2010). So far, Tspan15 has not been linked to a similar

function. Therefore the role of Tspan15 in extracellular vesicle (EV)-mediated communication among neurons has been investigated.

Interestingly, Tspan15-GFP-positive extracellular vesicles interacted with in target N2A cells observed in live cell imaging and a transfer assay of conditioned media (Figure 32). Moreover, Tspan15-GFP-positive EVs were also observe in partial colocalization with the intracellular early endosome marker EEA1. (Figure 33). These results suggest that Tspan15 could play a role in EV-based intercellular communication at the level of EV docking to target cellular surfaces.

In this investigation, the Tspan15KO mouse line was used to shed light on the role of Tspan15 in EV targeting on the surface of recipient cells. At first, focusing on the importance of Tspan15 expression in the target cells, comparing WT EV contacts to recipient WT and Tspan15 KO neurons (Figure 34). In a second step, with a specular approach, the contribution of Tspan15 expression on EVs was studied, comparing WT and Tspan15-depleted EVs interactions with WT neurons ( ). The present data suggest that the expression of Tspan15 in target neurons is not affecting the interaction of EVs with the recipient cells (Figure 34H-J). On the other hand, while the lack of expression of Tspan15 in donor cells did not affect the biogenesis and the diameter of the EVs (C, B), Tspan15-depleted EVs showed a reduced level of interaction with WT target neurons (E-G).

5.15 Technical limitations of the study

As an interpretative limitation of this conclusion, it has to be recognized that it could not be ruled out whether the decreased level of interaction occurring in the case of Tspan15-depleted EVs is to be attributed to (1) the absence of Tspan15 from the membrane of EVs; (2) the lack of expression of Tspan15 in the donor cells, especially on the intraluminal vesicles of MVB; (3) a combination of the two above-mentioned scenarios.

5.16 Speculations, conclusions, and future directions for the role Tspan15 in EV-mediated neuronal communication

Tspan15 has been previously shown to be a binding partner and modulator of the shedding activity metalloprotease ADAM10 (Seipold et al., 2018). In turn, also ADAM10 is an EV resident protein and it can cleave different substrates. In particular, Tspan15 has been shown to promote specifically the ADAM10-dependent cleavage of N-cadherin, an adhesion molecule expressed in neurons, and to modulate APP shedding (**Table 2**). Therefore, future experiments could elucidate if the absence of Tspan15 can alter the physiological expression of ADAM10 on Tspan15-positive EVs and cleavage activity of the enzyme, both at the quantitative level and at the qualitative level by affecting the level and the preference of shedding among the different substrates.

This investigation suggests Tspan15 as an EV component and modulator of EV-based intercellular communication.

6 Acknowledgment

This Ph.D. has been a long and challenging journey into science, representing an opportunity for personal and professional growth and a chance to meet friendly and interesting people. In achieving this personal accomplishment, I want to express my gratitude to all the several figures who have supported me over the years and made this moment possible.

In particular, I would like to thank my supervisor Prof. Dr. Matthias Kneuseel, for providing me with the opportunity to carry out this scientific investigation and always supporting me in evolving professionally. A big thank you to my smart mentor Dr. Kira Gromova Brune, for forging me into the doctor I am now.

I thank the members of the doctoral examination committee, P.D. Sabine Hoffmeister-Ullerich, Prof. Dr. Kay Grünewald and Prof. Brune for their kind attention, time and expertise.

Thanks for helping me get back up after every fall. I would like to thank all the collaborators who made my doctoral work possible for their valuable contributions. I express my gratitude to Dr. Franco L. Lombino for his spontaneous and friendly support, not only shown at the bench. I thank Prof. Dr. Daniel Choquet, Dr. Eric Hosy, Dr. Hanna Ziegar, for welcoming me into their group and providing me with a new opportunity to grow and learn, this time in France.

Thanks to all the members of the Institute for Molecular Neurogenetics, for making me really feel part of the group, for sharing so much in and out of the lab (see chapter trip to Kos, Sicily, Lisboa, Paris, etc.). I thank Rebecca alias Rita Levi Montalcini for her expertise of scientific english and her friendly nature. And big thanks to Yvonne for being always very supportive (and patiance)! Thanks to Noelia, for starting this journey as strangers and finishing it together as friends, without losing each other. I want to sincerely thank my trusted orthopedist, Dr. Zhu, for being the best Chanchamayo I could find. I thank Herr ~~Lutzentkuken~~, ~~Luzzenküken~~, ~~Luetzzenkuk~~….I thank Felix for being not only a great collaborator, but also my (very) German friend. What would this Ph.D. have been without Ludobicia around?! Unfortunately, we have no control to be able to answer this question, she was always around and she will continue to be around.

I thank my family, Elena, Mario and Paolo for being the pivot around which my life revolves. No matter where I am, I can always see the light of home.
And a huge thank you to Silvia, for always being by my side with her love, support and kindness, treating my wounds and boosting me up.

And finally thanks to the boy who arrived here in 2019, for achieving his goal.

7 References

1. Allen Brain Mouse Atlas (https://mouse.brain-map.org)
2. Aguilar-Valles, A., Matta-Camacho, E., Khoutorsky, A., Gkogkas, C., Nader, K., Lacaille, J. C., & Sonenberg, N. (2015). Inhibition of Group I Metabotropic Glutamate Receptors Reverses Autistic-Like Phenotypes Caused by Deficiency of the Translation Repressor eIF4E Binding Protein 2. *J Neurosci*, *35*(31), 11125-11132. https://doi.org/10.1523/jneurosci.4615-14.2015
3. Allgood, S. C., & Neunuebel, M. R. (2018). The recycling endosome and bacterial pathogens. *Cell Microbiol*, *20*(7), e12857. https://doi.org/10.1111/cmi.12857
4. Aloisi, E., Le Corf, K., Dupuis, J., Zhang, P., Ginger, M., Labrousse, V., Spatuzza, M., Georg Haberl, M., Costa, L., Shigemoto, R., Tappe-Theodor, A., Drago, F., Vincenzo Piazza, P., Mulle, C., Groc, L., Ciranna, L., Catania, M. V., & Frick, A. (2017). Altered surface mGluR5 dynamics provoke synaptic NMDAR dysfunction and cognitive defects in Fmr1 knockout mice. *Nat Commun*, *8*(1), 1103. https://doi.org/10.1038/s41467-017-01191-2
5. Ballester-Rosado, C. J., Albright, M. J., Wu, C. S., Liao, C. C., Zhu, J., Xu, J., Lee, L. J., & Lu, H. C. (2010). mGluR5 in cortical excitatory neurons exerts both cell-autonomous and -nonautonomous influences on cortical somatosensory circuit formation. *J Neurosci*, *30*(50), 16896-16909. https://doi.org/10.1523/jneurosci.2462-10.2010
6. Becic, A., Leifeld, J., Shaukat, J., & Hollmann, M. (2021). Tetraspanins as Potential Modulators of Glutamatergic Synaptic Function. *Front Mol Neurosci*, *14*, 801882. https://doi.org/10.3389/fnmol.2021.801882
7. Been, L. E., Moore, K. M., Kennedy, B. C., & Meisel, R. L. (2016). Metabotropic Glutamate Receptor and Fragile X Signaling in a Female Model of Escalated Aggression. *Biol Psychiatry*, *79*(8), 685-692. https://doi.org/10.1016/j.biopsych.2015.07.021
8. Berditchevski, F., Odintsova, E., Sawada, S., & Gilbert, E. (2002). Expression of the palmitoylation-deficient CD151 weakens the association of alpha 3 beta 1 integrin with the tetraspanin-enriched microdomains and affects integrin-

dependent signaling. *J Biol Chem*, *277*(40), 36991-37000. https://doi.org/10.1074/jbc.M205265200

9. Bonnet, M., Maisonial-Besset, A., Zhu, Y., Witkowski, T., Roche, G., Boucheix, C., Greco, C., & Degoul, F. (2019). Targeting the Tetraspanins with Monoclonal Antibodies in Oncology: Focus on Tspan8/Co-029. *Cancers (Basel)*, *11*(2). https://doi.org/10.3390/cancers11020179
10. Bordi, F., & Ugolini, A. (1999). Group I metabotropic glutamate receptors: implications for brain diseases. *Prog Neurobiol*, *59*(1), 55-79. https://doi.org/10.1016/s0301-0082(98)00095-1
11. Borland, J. M., Kim, E., Swanson, S. P., Rothwell, P. E., Mermelstein, P. G., & Meisel, R. L. (2020). Effect of Aggressive Experience in Female Syrian Hamsters on Glutamate Receptor Expression in the Nucleus Accumbens. *Front Behav Neurosci*, *14*, 583395. https://doi.org/10.3389/fnbeh.2020.583395
12. Boucheix, C., & Rubinstein, E. (2001). Tetraspanins. *Cell Mol Life Sci*, *58*(9), 1189-1205. https://doi.org/10.1007/pl00000933
13. Bruce Alberts, A. J., Julian Lewis, Martin Raff, Keith Roberts, and Peter Walter. (2002). *Molecular Biology of the Cell*. Garland Science.
14. Budnik, V., Ruiz-Cañada, C., & Wendler, F. (2016). Extracellular vesicles round off communication in the nervous system. *Nat Rev Neurosci*, *17*(3), 160-172. https://doi.org/10.1038/nrn.2015.29
15. Burket, J. A., Herndon, A. L., Winebarger, E. E., Jacome, L. F., & Deutsch, S. I. (2011). Complex effects of mGluR5 antagonism on sociability and stereotypic behaviors in mice: possible implications for the pharmacotherapy of autism spectrum disorders. *Brain Res Bull*, *86*(3-4), 152-158. https://doi.org/10.1016/j.brainresbull.2011.08.001
16. Charrin, S., Jouannet, S., Boucheix, C., & Rubinstein, E. (2014). Tetraspanins at a glance. *J Cell Sci*, *127*(Pt 17), 3641-3648. https://doi.org/10.1242/jcs.154906
17. Charrin, S., le Naour, F., Silvie, O., Milhiet, P. E., Boucheix, C., & Rubinstein, E. (2009). Lateral organization of membrane proteins: tetraspanins spin their web. *Biochem J*, *420*(2), 133-154. https://doi.org/10.1042/bj20082422

18. Chen, C. C., Lu, H. C., & Brumberg, J. C. (2012). mGluR5 knockout mice display increased dendritic spine densities. *Neurosci Lett*, *524*(1), 65-68. https://doi.org/10.1016/j.neulet.2012.07.014
19. Cheng, J., Liu, W., Duffney, L. J., & Yan, Z. (2013). SNARE proteins are essential in the potentiation of NMDA receptors by group II metabotropic glutamate receptors. *J Physiol*, *591*(16), 3935-3947. https://doi.org/10.1113/jphysiol.2013.255075
20. Chung, W., Choi, S. Y., Lee, E., Park, H., Kang, J., Park, H., Choi, Y., Lee, D., Park, S. G., Kim, R., Cho, Y. S., Choi, J., Kim, M. H., Lee, J. W., Lee, S., Rhim, I., Jung, M. W., Kim, D., Bae, Y. C., & Kim, E. (2015). Social deficits in IRSp53 mutant mice improved by NMDAR and mGluR5 suppression. *Nat Neurosci*, *18*(3), 435-443. https://doi.org/10.1038/nn.3927
21. Collingridge, G. L., Isaac, J. T., & Wang, Y. T. (2004). Receptor trafficking and synaptic plasticity. *Nat Rev Neurosci*, *5*(12), 952-962. https://doi.org/10.1038/nrn1556
22. Conn, P. J., & Pin, J. P. (1997). Pharmacology and functions of metabotropic glutamate receptors. *Annu Rev Pharmacol Toxicol*, *37*, 205-237. https://doi.org/10.1146/annurev.pharmtox.37.1.205
23. Correia, S. S., Bassani, S., Brown, T. C., Lisé, M. F., Backos, D. S., El-Husseini, A., Passafaro, M., & Esteban, J. A. (2008). Motor protein-dependent transport of AMPA receptors into spines during long-term potentiation. *Nat Neurosci*, *11*(4), 457-466. https://doi.org/10.1038/nn2063
24. Dale Purves, G. J. A., David Fitzpatrick, Lawrence C Katz, Anthony-Samuel LaMantia, James O McNamara, and S Mark Williams. (2001). *Neuroscience*.
25. Dani, V. S., Chang, Q., Maffei, A., Turrigiano, G. G., Jaenisch, R., & Nelson, S. B. (2005). Reduced cortical activity due to a shift in the balance between excitation and inhibition in a mouse model of Rett syndrome. *Proc Natl Acad Sci U S A*, *102*(35), 12560-12565. https://doi.org/10.1073/pnas.0506071102
26. Deacon, R. M. (2006a). Assessing nest building in mice. *Nat Protoc*, *1*(3), 1117-1119. https://doi.org/10.1038/nprot.2006.170

27. Deacon, R. M. (2006b). Digging and marble burying in mice: simple methods for in vivo identification of biological impacts. *Nat Protoc*, *1*(1), 122-124. https://doi.org/10.1038/nprot.2006.20
28. Dhami, G. K., & Ferguson, S. S. (2006). Regulation of metabotropic glutamate receptor signaling, desensitization and endocytosis. *Pharmacol Ther*, *111*(1), 260-271. https://doi.org/10.1016/j.pharmthera.2005.01.008
29. Dryman, M. T., & Heimberg, R. G. (2018). Emotion regulation in social anxiety and depression: a systematic review of expressive suppression and cognitive reappraisal. *Clin Psychol Rev*, *65*, 17-42. https://doi.org/10.1016/j.cpr.2018.07.004
30. Eric R. Kandel, J. H. S., Thomas M. Jessell, Steven A. Siegelbaum, A. J. Hudspeth. (2012). *Principles of Neural Science* McGraw-Hill Education Ltd.
31. Fellini, L., & Morellini, F. (2013). Mice create what-where-when hippocampus-dependent memories of unique experiences. *J Neurosci*, *33*(3), 1038-1043. https://doi.org/10.1523/jneurosci.2280-12.2013
32. Freitag, S., Schachner, M., & Morellini, F. (2003). Behavioral alterations in mice deficient for the extracellular matrix glycoprotein tenascin-R. *Behav Brain Res*, *145*(1-2), 189-207. https://doi.org/10.1016/s0166-4328(03)00109-8
33. Fröhlich, D., Kuo, W. P., Frühbeis, C., Sun, J. J., Zehendner, C. M., Luhmann, H. J., Pinto, S., Toedling, J., Trotter, J., & Krämer-Albers, E. M. (2014). Multifaceted effects of oligodendroglial exosomes on neurons: impact on neuronal firing rate, signal transduction and gene regulation. *Philos Trans R Soc Lond B Biol Sci*, *369*(1652). https://doi.org/10.1098/rstb.2013.0510
34. Frye, R. E. (2018). Social Skills Deficits in Autism Spectrum Disorder: Potential Biological Origins and Progress in Developing Therapeutic Agents. *CNS Drugs*, *32*(8), 713-734. https://doi.org/10.1007/s40263-018-0556-y
35. Goncalves, J., Bartol, T. M., Camus, C., Levet, F., Menegolla, A. P., Sejnowski, T. J., Sibarita, J. B., Vivaudou, M., Choquet, D., & Hosy, E. (2020). Nanoscale co-organization and coactivation of AMPAR, NMDAR, and mGluR at excitatory synapses. *Proc Natl Acad Sci U S A*, *117*(25), 14503-14511. https://doi.org/10.1073/pnas.1922563117

36. Granger, A. J., Shi, Y., Lu, W., Cerpas, M., & Nicoll, R. A. (2013). LTP requires a reserve pool of glutamate receptors independent of subunit type. *Nature*, *493*(7433), 495-500. https://doi.org/10.1038/nature11775
37. Gu, Y., & Huganir, R. L. (2016). Identification of the SNARE complex mediating the exocytosis of NMDA receptors. *Proc Natl Acad Sci U S A*, *113*(43), 12280-12285. https://doi.org/10.1073/pnas.1614042113
38. Gurung, S., Perocheau, D., Touramanidou, L., & Baruteau, J. (2021). The exosome journey: from biogenesis to uptake and intracellular signalling. *Cell Commun Signal*, *19*(1), 47. https://doi.org/10.1186/s12964-021-00730-1
39. Haas, K. T., Lee, M., Esposito, A., & Venkitaraman, A. R. (2018). Single-molecule localization microscopy reveals molecular transactions during RAD51 filament assembly at cellular DNA damage sites. *Nucleic Acids Res*, *46*(5), 2398-2416. https://doi.org/10.1093/nar/gkx1303
40. Hagerman, R. J., Protic, D., Rajaratnam, A., Salcedo-Arellano, M. J., Aydin, E. Y., & Schneider, A. (2018). Fragile X-Associated Neuropsychiatric Disorders (FXAND). *Front Psychiatry*, *9*, 564. https://doi.org/10.3389/fpsyt.2018.00564
41. Hemler, M. E. (2005). Tetraspanin functions and associated microdomains. *Nat Rev Mol Cell Biol*, *6*(10), 801-811. https://doi.org/10.1038/nrm1736
42. Hemler, M. E. (2008). Targeting of tetraspanin proteins--potential benefits and strategies. *Nat Rev Drug Discov*, *7*(9), 747-758. https://doi.org/10.1038/nrd2659
43. Holtmaat, A., & Svoboda, K. (2009). Experience-dependent structural synaptic plasticity in the mammalian brain. *Nat Rev Neurosci*, *10*(9), 647-658. https://doi.org/10.1038/nrn2699
44. Huang, R., Sun, H., Lin, R., Zhang, J., Yin, H., Xian, S., Li, M., Wang, S., Li, Z., Qiao, Y., Jiang, M., Yan, P., Meng, T., & Huang, Z. (2022). The role of tetraspanins pan-cancer. *iScience*, *25*(8), 104777. https://doi.org/10.1016/j.isci.2022.104777
45. Huang, S., Yuan, S., Dong, M., Su, J., Yu, C., Shen, Y., Xie, X., Yu, Y., Yu, X., Chen, S., Zhang, S., Pontarotti, P., & Xu, A. (2005). The phylogenetic analysis of tetraspanins projects the evolution of cell-cell interactions from unicellular to multicellular organisms. *Genomics*, *86*(6), 674-684. https://doi.org/10.1016/j.ygeno.2005.08.004

46. Huganir, R. L., & Nicoll, R. A. (2013). AMPARs and synaptic plasticity: the last 25 years. *Neuron*, *80*(3), 704-717. https://doi.org/10.1016/j.neuron.2013.10.025
47. Jouannet, S., Saint-Pol, J., Fernandez, L., Nguyen, V., Charrin, S., Boucheix, C., Brou, C., Milhiet, P. E., & Rubinstein, E. (2016). TspanC8 tetraspanins differentially regulate the cleavage of ADAM10 substrates, Notch activation and ADAM10 membrane compartmentalization. *Cell Mol Life Sci*, *73*(9), 1895-1915. https://doi.org/10.1007/s00018-015-2111-z
48. Kitadokoro, K., Bordo, D., Galli, G., Petracca, R., Falugi, F., Abrignani, S., Grandi, G., & Bolognesi, M. (2001). CD81 extracellular domain 3D structure: insight into the tetraspanin superfamily structural motifs. *EMBO J*, *20*(1-2), 12-18. https://doi.org/10.1093/emboj/20.1.12
49. Kneussel, M., & Hausrat, T. J. (2016). Postsynaptic Neurotransmitter Receptor Reserve Pools for Synaptic Potentiation. *Trends Neurosci*, *39*(3), 170-182. https://doi.org/10.1016/j.tins.2016.01.002
50. Lachenal, G., Pernet-Gallay, K., Chivet, M., Hemming, F. J., Belly, A., Bodon, G., Blot, B., Haase, G., Goldberg, Y., & Sadoul, R. (2011). Release of exosomes from differentiated neurons and its regulation by synaptic glutamatergic activity. *Mol Cell Neurosci*, *46*(2), 409-418. https://doi.org/10.1016/j.mcn.2010.11.004
51. Levet, F., Julien, G., Galland, R., Butler, C., Beghin, A., Chazeau, A., Hoess, P., Ries, J., Giannone, G., & Sibarita, J. B. (2019). A tessellation-based colocalization analysis approach for single-molecule localization microscopy. *Nat Commun*, *10*(1), 2379. https://doi.org/10.1038/s41467-019-10007-4
52. Levy, S., & Shoham, T. (2005). Protein-protein interactions in the tetraspanin web. *Physiology (Bethesda)*, *20*, 218-224. https://doi.org/10.1152/physiol.00015.2005
53. Lüscher, C., Xia, H., Beattie, E. C., Carroll, R. C., von Zastrow, M., Malenka, R. C., & Nicoll, R. A. (1999). Role of AMPA receptor cycling in synaptic transmission and plasticity. *Neuron*, *24*(3), 649-658. https://doi.org/10.1016/s0896-6273(00)81119-8
54. Malm, T., Loppi, S., & Kanninen, K. M. (2016). Exosomes in Alzheimer's disease. *Neurochem Int*, *97*, 193-199. https://doi.org/10.1016/j.neuint.2016.04.011
55. Mohammadkhani, R., Ghahremani, R., Salehi, I., Safari, S., Karimi, S. A., & Zarei, M. (2022). Impairment in social interaction and hippocampal long-term potentiation

at perforant pathway-dentate gyrus synapses in a prenatal valproic acid-induced rat model of autism. *Brain Commun*, *4*(5), fcac221. https://doi.org/10.1093/braincomms/fcac221

56. Moretto, E., Miozzo, F., Longatti, A., Bonnet, C., Coussen, F., Jaudon, F., Cingolani, L. A., & Passafaro, M. (2023). The tetraspanin TSPAN5 regulates AMPAR exocytosis by interacting with the AP4 complex. *Elife*, *12*. https://doi.org/10.7554/eLife.76425
57. Muhia, M., Thies, E., Labonté, D., Ghiretti, A. E., Gromova, K. V., Xompero, F., Lappe-Siefke, C., Hermans-Borgmeyer, I., Kuhl, D., Schweizer, M., Ohana, O., Schwarz, J. R., Holzbaur, E. L. F., & Kneussel, M. (2016). The Kinesin KIF21B Regulates Microtubule Dynamics and Is Essential for Neuronal Morphology, Synapse Function, and Learning and Memory. *Cell Rep*, *15*(5), 968-977. https://doi.org/10.1016/j.celrep.2016.03.086
58. Muhia, M., YuanXiang, P., Sedlacik, J., Schwarz, J. R., Heisler, F. F., Gromova, K. V., Thies, E., Breiden, P., Pechmann, Y., Kreutz, M. R., & Kneussel, M. (2022). Muskelin regulates actin-dependent synaptic changes and intrinsic brain activity relevant to behavioral and cognitive processes. *Commun Biol*, *5*(1), 589. https://doi.org/10.1038/s42003-022-03446-1
59. Mulcahy, L. A., Pink, R. C., & Carter, D. R. (2014). Routes and mechanisms of extracellular vesicle uptake. *J Extracell Vesicles*, *3*. https://doi.org/10.3402/jev.v3.24641
60. Nazarenko, I., Rana, S., Baumann, A., McAlear, J., Hellwig, A., Trendelenburg, M., Lochnit, G., Preissner, K. T., & Zöller, M. (2010). Cell surface tetraspanin Tspan8 contributes to molecular pathways of exosome-induced endothelial cell activation. *Cancer Res*, *70*(4), 1668-1678. https://doi.org/10.1158/0008-5472.Can-09-2470
61. Nishiuchi, R., Sanzen, N., Nada, S., Sumida, Y., Wada, Y., Okada, M., Takagi, J., Hasegawa, H., & Sekiguchi, K. (2005). Potentiation of the ligand-binding activity of integrin alpha3beta1 via association with tetraspanin CD151. *Proc Natl Acad Sci U S A*, *102*(6), 1939-1944. https://doi.org/10.1073/pnas.0409493102
62. Noy, P. J., Yang, J., Reyat, J. S., Matthews, A. L., Charlton, A. E., Furmston, J., Rogers, D. A., Rainger, G. E., & Tomlinson, M. G. (2016). TspanC8 Tetraspanins and A Disintegrin and Metalloprotease 10 (ADAM10) Interact via Their

Extracellular Regions: EVIDENCE FOR DISTINCT BINDING MECHANISMS FOR DIFFERENT TspanC8 PROTEINS. *J Biol Chem*, *291*(7), 3145-3157. https://doi.org/10.1074/jbc.M115.703058

63. Oberman, L. M. (2012). mGluR antagonists and GABA agonists as novel pharmacological agents for the treatment of autism spectrum disorders. *Expert Opin Investig Drugs*, *21*(12), 1819-1825. https://doi.org/10.1517/13543784.2012.729819
64. Oliveira, L. M., Bermudez, M. B., Macedo, M. J. A., & Passos, I. C. (2018). Comorbid social anxiety disorder in patients with alcohol use disorder: A systematic review. *J Psychiatr Res*, *106*, 8-14. https://doi.org/10.1016/j.jpsychires.2018.09.008
65. Ollen-Bittle, N., Roseborough, A. D., Wang, W., Wu, J. D., & Whitehead, S. N. (2022). Mechanisms and Biomarker Potential of Extracellular Vesicles in Stroke. *Biology (Basel)*, *11*(8). https://doi.org/10.3390/biology11081231
66. Park, M., Penick, E. C., Edwards, J. G., Kauer, J. A., & Ehlers, M. D. (2004). Recycling endosomes supply AMPA receptors for LTP. *Science*, *305*(5692), 1972-1975. https://doi.org/10.1126/science.1102026
67. Pasciuto, E., Ahmed, T., Wahle, T., Gardoni, F., D'Andrea, L., Pacini, L., Jacquemont, S., Tassone, F., Balschun, D., Dotti, C. G., Callaerts-Vegh, Z., D'Hooge, R., Müller, U. C., Di Luca, M., De Strooper, B., & Bagni, C. (2015). Dysregulated ADAM10-Mediated Processing of APP during a Critical Time Window Leads to Synaptic Deficits in Fragile X Syndrome. *Neuron*, *87*(2), 382-398. https://doi.org/10.1016/j.neuron.2015.06.032
68. Petrini, E. M., Lu, J., Cognet, L., Lounis, B., Ehlers, M. D., & Choquet, D. (2009). Endocytic trafficking and recycling maintain a pool of mobile surface AMPA receptors required for synaptic potentiation. *Neuron*, *63*(1), 92-105. https://doi.org/10.1016/j.neuron.2009.05.025
69. Piguel, N. H., Fievre, S., Blanc, J. M., Carta, M., Moreau, M. M., Moutin, E., Pinheiro, V. L., Medina, C., Ezan, J., Lasvaux, L., Loll, F., Durand, C. M., Chang, K., Petralia, R. S., Wenthold, R. J., Stephenson, F. A., Vuillard, L., Darbon, H., Perroy, J., Mulle, C., Montcouquiol, M., Racca, C., & Sans, N. (2014).

Scribble1/AP2 complex coordinates NMDA receptor endocytic recycling. *Cell Rep*, *9*(2), 712-727. https://doi.org/10.1016/j.celrep.2014.09.017

70. Porcelli, S., Van Der Wee, N., van der Werff, S., Aghajani, M., Glennon, J. C., van Heukelum, S., Mogavero, F., Lobo, A., Olivera, F. J., Lobo, E., Posadas, M., Dukart, J., Kozak, R., Arce, E., Ikram, A., Vorstman, J., Bilderbeck, A., Saris, I., Kas, M. J., & Serretti, A. (2019). Social brain, social dysfunction and social withdrawal. *Neurosci Biobehav Rev*, *97*, 10-33. https://doi.org/10.1016/j.neubiorev.2018.09.012
71. Prox, J., Willenbrock, M., Weber, S., Lehmann, T., Schmidt-Arras, D., Schwanbeck, R., Saftig, P., & Schwake, M. (2012). Tetraspanin15 regulates cellular trafficking and activity of the ectodomain sheddase ADAM10. *Cell Mol Life Sci*, *69*(17), 2919-2932. https://doi.org/10.1007/s00018-012-0960-2
72. Risher, W. C., Ustunkaya, T., Singh Alvarado, J., & Eroglu, C. (2014). Rapid Golgi analysis method for efficient and unbiased classification of dendritic spines. *PLoS One*, *9*(9), e107591. https://doi.org/10.1371/journal.pone.0107591
73. Scheefhals, N., Catsburg, L. A. E., Westerveld, M. L., Blanpied, T. A., Hoogenraad, C. C., & MacGillavry, H. D. (2019). Shank Proteins Couple the Endocytic Zone to the Postsynaptic Density to Control Trafficking and Signaling of Metabotropic Glutamate Receptor 5. *Cell Rep*, *29*(2), 258-269.e258. https://doi.org/10.1016/j.celrep.2019.08.102
74. Scheefhals, N., & MacGillavry, H. D. (2018). Functional organization of postsynaptic glutamate receptors. *Mol Cell Neurosci*, *91*, 82-94. https://doi.org/10.1016/j.mcn.2018.05.002
75. Scheefhals, N., Westra, M., & MacGillavry, H. D. (2023). mGluR5 is transiently confined in perisynaptic nanodomains to shape synaptic function. *Nat Commun*, *14*(1), 244. https://doi.org/10.1038/s41467-022-35680-w
76. Schnatz, A., Muller, C., Brahmer, A., & Kramer-Albers, E. M. (2021). Extracellular Vesicles in neural cell interaction and CNS homeostasis. *FASEB Bioadv*, *3*(8), 577-592. https://doi.org/10.1096/fba.2021-00035
77. Schob, C., Morellini, F., Ohana, O., Bakota, L., Hrynchak, M. V., Brandt, R., Brockmann, M. D., Cichon, N., Hartung, H., Hanganu-Opatz, I. L., Kraus, V., Scharf, S., Herrmans-Borgmeyer, I., Schweizer, M., Kuhl, D., Wöhr, M., Vörckel,

K. J., Calzada-Wack, J., Fuchs, H., Gailus-Durner, V., Hrabě de Angelis, M., Garner, C. C., Kreienkamp, H. J., & Kindler, S. (2019). Cognitive impairment and autistic-like behaviour in SAPAP4-deficient mice. *Transl Psychiatry*, *9*(1), 7. https://doi.org/10.1038/s41398-018-0327-z

78. Seigneuret, M., Delaguillaumie, A., Lagaudrière-Gesbert, C., & Conjeaud, H. (2001). Structure of the tetraspanin main extracellular domain. A partially conserved fold with a structurally variable domain insertion. *J Biol Chem*, *276*(43), 40055-40064. https://doi.org/10.1074/jbc.M105557200
79. Seipold, L., Altmeppen, H., Koudelka, T., Tholey, A., Kasparek, P., Sedlacek, R., Schweizer, M., Bär, J., Mikhaylova, M., Glatzel, M., & Saftig, P. (2018). In vivo regulation of the A disintegrin and metalloproteinase 10 (ADAM10) by the tetraspanin 15. *Cell Mol Life Sci*, *75*(17), 3251-3267. https://doi.org/10.1007/s00018-018-2791-2
80. She, W. C., Quairiaux, C., Albright, M. J., Wang, Y. C., Sanchez, D. E., Chang, P. S., Welker, E., & Lu, H. C. (2009). Roles of mGluR5 in synaptic function and plasticity of the mouse thalamocortical pathway. *Eur J Neurosci*, *29*(7), 1379-1396. https://doi.org/10.1111/j.1460-9568.2009.06696.x
81. Sheff, D. R., Daro, E. A., Hull, M., & Mellman, I. (1999). The receptor recycling pathway contains two distinct populations of early endosomes with different sorting functions. *J Cell Biol*, *145*(1), 123-139. https://doi.org/10.1083/jcb.145.1.123
82. Spooren, W. P., Vassout, A., Neijt, H. C., Kuhn, R., Gasparini, F., Roux, S., Porsolt, R. D., & Gentsch, C. (2000). Anxiolytic-like effects of the prototypical metabotropic glutamate receptor 5 antagonist 2-methyl-6-(phenylethynyl)pyridine in rodents. *J Pharmacol Exp Ther*, *295*(3), 1267-1275.
83. Su, L. D., Wang, N., Han, J., & Shen, Y. (2022). Group 1 Metabotropic Glutamate Receptors in Neurological and Psychiatric Diseases: Mechanisms and Prospective. *Neuroscientist*, *28*(5), 453-468. https://doi.org/10.1177/10738584211021018
84. Suh, Y. H., Terashima, A., Petralia, R. S., Wenthold, R. J., Isaac, J. T., Roche, K. W., & Roche, P. A. (2010). A neuronal role for SNAP-23 in postsynaptic glutamate receptor trafficking. *Nat Neurosci*, *13*(3), 338-343. https://doi.org/10.1038/nn.2488

85. Teng, F., & Fussenegger, M. (2020). Shedding Light on Extracellular Vesicle Biogenesis and Bioengineering. *Adv Sci (Weinh)*, *8*(1), 2003505. https://doi.org/10.1002/advs.202003505
86. Termini, C. M., & Gillette, J. M. (2017). Tetraspanins Function as Regulators of Cellular Signaling. *Front Cell Dev Biol*, *5*, 34. https://doi.org/10.3389/fcell.2017.00034
87. Théry, C., Amigorena, S., Raposo, G., & Clayton, A. (2006). Isolation and characterization of exosomes from cell culture supernatants and biological fluids. *Curr Protoc Cell Biol*, *Chapter 3*, Unit 3.22. https://doi.org/10.1002/0471143030.cb0322s30
88. Thiede-Stan, N. K., Tews, B., Albrecht, D., Ristic, Z., Ewers, H., & Schwab, M. E. (2015). Tetraspanin-3 is an organizer of the multi-subunit Nogo-A signaling complex. *J Cell Sci*, *128*(19), 3583-3596. https://doi.org/10.1242/jcs.167981
89. van der Sluijs, P., & Hoogenraad, C. C. (2011). New insights in endosomal dynamics and AMPA receptor trafficking. *Semin Cell Dev Biol*, *22*(5), 499-505. https://doi.org/10.1016/j.semcdb.2011.06.008
90. van Niel, G., D'Angelo, G., & Raposo, G. (2018). Shedding light on the cell biology of extracellular vesicles. *Nat Rev Mol Cell Biol*, *19*(4), 213-228. https://doi.org/10.1038/nrm.2017.125
91. van Niel, G., Porto-Carreiro, I., Simoes, S., & Raposo, G. (2006). Exosomes: a common pathway for a specialized function. *J Biochem*, *140*(1), 13-21. https://doi.org/10.1093/jb/mvj128
92. Vilcaes, A. A., Chanaday, N. L., & Kavalali, E. T. (2021). Interneuronal exchange and functional integration of synaptobrevin via extracellular vesicles. *Neuron*, *109*(6), 971-983.e975. https://doi.org/10.1016/j.neuron.2021.01.007
93. Wijetunge, L. S., Till, S. M., Gillingwater, T. H., Ingham, C. A., & Kind, P. C. (2008). mGluR5 regulates glutamate-dependent development of the mouse somatosensory cortex. *J Neurosci*, *28*(49), 13028-13037. https://doi.org/10.1523/jneurosci.2600-08.2008
94. Willard, S. S., & Koochekpour, S. (2013). Glutamate, glutamate receptors, and downstream signaling pathways. *Int J Biol Sci*, *9*(9), 948-959. https://doi.org/10.7150/ijbs.6426

95. Yang, X., Claas, C., Kraeft, S. K., Chen, L. B., Wang, Z., Kreidberg, J. A., & Hemler, M. E. (2002). Palmitoylation of tetraspanin proteins: modulation of CD151 lateral interactions, subcellular distribution, and integrin-dependent cell morphology. *Mol Biol Cell*, *13*(3), 767-781. https://doi.org/10.1091/mbc.01-05-0275
96. Yauch, R. L., & Hemler, M. E. (2000). Specific interactions among transmembrane 4 superfamily (TM4SF) proteins and phosphoinositide 4-kinase. *Biochem J*, *351 Pt 3*(Pt 3), 629-637.
97. Zhang, L., & Wrana, J. L. (2014). The emerging role of exosomes in Wnt secretion and transport. *Curr Opin Genet Dev*, *27*, 14-19. https://doi.org/10.1016/j.gde.2014.03.006
98. Zhou, X., Miao, Y., Wang, Y., He, S., Guo, L., Mao, J., Chen, M., Yang, Y., Zhang, X., & Gan, Y. (2022). Tumour-derived extracellular vesicle membrane hybrid lipid nanovesicles enhance siRNA delivery by tumour-homing and intracellular freeway transportation. *J Extracell Vesicles*, *11*(3), e12198. https://doi.org/10.1002/jev2.12198
99. Zoicas, I., & Kornhuber, J. (2019). The Role of Metabotropic Glutamate Receptors in Social Behavior in Rodents. *Int J Mol Sci*, *20*(6). https://doi.org/10.3390/ijms20061412

8 Appendix

List 5 - Hazardous substances according to the GHS

REAGENT	CAT.	PROVIDER	GHS	HAZARD STATEMENT (H)	PRECAUTIONARY STATEMENT (P)
ACRYLAMIDE/BIS-ACRYLAMIDE	A2917	Sigma Aldrich	GHS06 GHS08	H301, H312, H332, H315, H317, H319, H340, H350, H361f, H372	P201, P280, P302, P352, P304, P340, P305, P351, P338, P308, P310
AMMONIUM PERSULFATE (APS)	9592.1	Carl Roth GmbH and Co. KG,	GHS03 GHS07 GHS08	H272, H302 H315, H317 H319, H334, H335	P261, P280 P302/352 P305/351/338 P332/313 P337/313
AMPICILLIN SODIUM SALT	K029.1	Carl Roth GmbH and Co. KG,	GHS08	H317, H334	P261, P280 P302/352 P342/311 P305/351/338,P310
1,4-DITHIOTHREIT (DTT)	6908.2	Carl Roth GmbH and Co. KG,	GHS07	H302, H315 H319, H335, H412	P260, P270 P305/351/338 P337/313
3,3′-DIAMINOBENZIDINE TETRAHYDROCHLORIDE HYDRATE	D5637	Sigma-Aldrich	GHS07 GHS08	H302, H319, H341, H350	P202, P264,. P270, P312, P305,P351, P338, P308,P313
GLUTARALDEHYDE (GA)	G5882	Sigma-Aldrich	GHS05 GHS07 GHS08 GHS09	H302 H332 H317 H334 H335 H410	P273 P280 P301 P312 P303 P361 P353 P304 P340 P310 P305 P351 P338
ETHANOL	9065.4	Carl Roth GmbH and Co. KG	GHS02 GHS07	H225 H319	P210 P233 P305/351/338
ETHANOL DENATURED	2211-5L	Chemsolute	GHS02 GHS07	H225 H319	P210 P240 P241 P260 P280 P303/361/353 P305/351/338 P501
38-DIAMINO-5-ETHYL-6-PHENYLPHENANTHRIDIN-5-IUM BROMIDE	2218.3	Carl Roth GmbH and Co. KG	GHS08	H341	P201 P280 P308 P313
DAB	D5637	Sigma-Aldrich	GHS07 GHS08	H302 H319 H341 H350	P202 P264. P270 P312 P305P351 P338 P308P313
HYDROCHLORIC ACID	4625.1	Carl Roth GmbH and Co. KG	GHS05 GHS07	H290 H314 H318H335	P280 P303 P361 P353 P305 P351 P338 P310
ISOPROPANOL	6752.2	Carl Roth GmbH and Co. KG	GHS02 GHS07	H225 H319 H336	P210 P233 P305/351/338
KANAMYCIN A	T832.3	Carl Roth GmbH and Co. KG	GHS08	H360	P201 P202 P280 P308+P313
METHANOL	P717.1	Carl Roth GmbH and Co. KG	GHS02 GHS06 GHS08	H225 H301 H311 H331 H370	P201 P233 P280 P301 P310 P303 P361 P353 P304 P340 P311
PARAFORMALDEHYDE (PFA)	335.3	Carl Roth GmbH and Co. KG	GHS02 GHS05 GHS07 GHS08	H228 H302 H332 H315 H317 H318 H335 H350	P201 P210 P280 P302 P353 P305 P351 P338
PHENYLMETHYLSULFONYL FLUORIDE (PMSF)	6367.1	Carl Roth GmbH and Co. KG	GHS05 GHS06	H301 H314	P260 P280 P301 P310 P330 P303 P361 P353 P304 P340 P310 P305 P351 P338
2-MERCAPTOETHANOL	M3148-25M	Sigma-Aldrich	GHS05 GHS06 GHS08 GHS09	H301 H331 H310 H315 H317 H318 H361d H373 H410	P273 P280 P301 P310 P302 P352 P310 P304 P340 P311 P305 P351 P338
SODIUM DODECYL SULFATE	L4509	Sigma Aldrich	GHS02 GHS05 GHS07	H228 H302 H332 H315 H318 H335 H412	P210 P261 P280 P301 P312 P330 P305 P351 P338 P310 P370 P378
NNN'N'-TETRAMETHYL ETHYLENEDIAMINE (TEMED)	T9821	Sigma Aldrich	GHS02 GHS05 GHS07	H225 H332 H302 H314	P210 P280 P301 P330 P331 P303 P361 P340 P304 P353 P312 P305 P351 P338
TRITON X-100	3051.2	Carl Roth GmbH and Co. KG	GHS05 GHS07 GHS09	H302 H318 H410	P273 P280 P302/352 P305/351/338 P313

9 Declaration on Oath:

Hiermit erkläre ich an Eides statt, dass ich die vorliegende Dissertationsschrift selbst verfasst und keine anderen als die angegebenen Quellen und Hilfsmittel benutzt habe.

I hereby declare on oath that this doctoral dissertation is written independently and solely by my own based on the original work of my PhD and has not been used other than the acknowledged resources and aids.

Location and Date **Signature**